UNIVERSITÀ DEGLI STUDI DI PALERMO
Corso di DOTTORATO DI RICERCA in SCIENZE FISICHE
Curriculum in Fisica Statistica e Interdisciplinare – Internazionale
Dipartimento di Fisica e Chimica

SSD: Fis02

ANOMALOUS DIFFUSION AND NONLINEAR RELAXATION PHENOMENA IN STOCHASTIC MODELS OF INTERDISCIPLINARY PHYSICS

DOTTORANDO
ANNA A. KHARCHEVA

IL COORDINATORE
G. MASSIMO PALMA

IL TUTOR
BERNARDO SPAGNOLO

CO-TUTOR
ALEXANDER A. DUBKOV

XXXII CICLO
2019

Abstract

The study of nonlinear dynamical systems in the presence of both Gaussian and non-Gaussian noise sources is the topic of this research work. In particular, after shortly present new theoretical results for statistical characteristics in the framework of Markovian theory, we analyse four different physical systems in the presence of Lévy noise source. (a) The residence time problem of a particle subject to a non-Gaussian noise source in arbitrary potential profile was analyzed and the exact analytical results for the statistical characteristics of the residence time for anomalous diffusion in the form of Lévy flights in fully unstable potential profile was obtained. Noise enhanced stability phenomenon was found in the system investigated. (b) The correlation time of the particle coordinate as a function of the height of potential barrier, the position of potential wells and noise intensity was investigated in the case of confined steady-state Lévy flights with Lévy index $\alpha = 1$, that is Cauchy noise, in the symmetric bistable quartic potential. (c) The stationary spectral characteristics of superdiffusion of Lévy flights in one-dimensional confinement potential profiles were investigated both theoretically and numerically. Specifically, for Cauchy stable noise we calculated the steady-state probability density function for an infinitely deep rectangular potential well and for a symmetric steep potential well of the type $U(x) \propto x^{2m}$. (d) For two-dimensional diffusion the general Kolmogorov equation for the joint

probability density function of particle coordinates was obtained by functional methods directly from two Langevin equations with statistically independent non-Gaussian noise sources. We compared the properties of Brownian diffusion and Lévy flights in parabolic potential with radial symmetry.

Afterwards, we analyzed the nonlinear relaxation in the presence of Gaussian noise for the stochastic switching dynamics of the memristors. We have studied three different models. (a) We started from consideration of the simplest model of resistive switching. (b) Further, the charge-controlled and the current-controlled ideal Chua memristors with external Gaussian noise were investigated. For both cases we have obtained exact analytical expressions for the probability density function of the charge flowing through the memristor and of the memristance. (c) Moreover, we proposed a stochastic macroscopic model of a memristor, based on a generalization of known approaches and experimental results. Steady-state concentration of defects for different boundary conditions was found. Also we analysed how the concentration of defects is changed with time under arbitrary values of external voltage, noise intensity, effective diffusion coefficient and other parameters. An examination of the results was performed, the possible implications of this work and the future development of this study were outlined.

Contents

List of Figures

List of Tables

Chapter 1

Introduction

1.1 Motivations

In the theory of non-equilibrium systems, where the macrovariables obey some nonlinear equations of motion, noise plays an important role. Only in the presence of noise, in multistable systems, the generalized Brownian particle can surmount potential barriers and is thus able to explore the whole potential landscape thereby attaining different macro states. For this reason the study of noise-driven nonlinear dynamical systems with subsequent interdisciplinary applications is attracting rapidly growing interest. Obtaining rigorous analytical results in this area faces with serious difficulties, since both the studied non-equilibrium systems are nonlinear, and it should be taken into account that the sources of fluctuations usually have non-Gaussian statistics, for example in condensed matter systems, in sensory and biological systems [1; 2]. The solution of such problems, along with the general apparatus of the Markovian theory of random processes, requires using the special mathematical methods such as fractional calculus, functional technique for splitting correlation averages, method of the inverse differential operator, etc. [2; 3; 4; 5]. Despite a great interest in the study of multistability

and metastability, the problem connected with the detailed understanding of the processes taking place in the nonlinear dynamical systems under noise and its theoretical description still remains an open problem.

1.2 Context of the Study

In this thesis, in the framework of nonlinear relaxation phenomena in the presence of Gaussian and non-Gaussian noise sources, I investigate two general problem of staticstical physics: (i) anomalous diffusion in nonlinear potential profiles and (ii) stochastic dynamic of resistive switching mechanism in memristive systems.

(i) In a number of experiments, the phenomenon of anomalous diffusion was revealed [6]. Anomalous diffusion differs from the usual Brownian motion by a faster or slower scattering of the particles. Slow diffusion, called subdiffusion, is observed in substances with complex geometries (turbid crystals and glasses, amorphous semiconductors etc.). Accelerated diffusion or superdiffusion occurs in many condensed matter systems, such as diffusion in graphene, in population dynamics and many biological systems, in atmospheric turbulence and chaotic dynamics [7]. The phenomenon of anomalous diffusion can be described using the fractional differentiation apparatus and the related fractional Fokker-Planck equation. This equation can be obtained by various methods: from Langevin equation [3], from continuous time random walk (CTRW) model [8], from a fractal generalization of the Kolmogorov–Feller equation [9], from a dichotomous model with a special probabilistic time distribution between switches [10], from the Taylor series decomposition in the neighborhood of a point using fractional derivatives [11] etc.

Special attention in recent publications in this area has been given to anomalous diffusion in the form of Lévy flights, that is Lévy processes characterized

by extremely large jumps [12]. The infinite variance of Lévy flights creates some problems in understanding of the physical meaning of these processes. However, recently Lévy diffusion has been found in many physical, chemical, biological and even financial systems. For example, a similar kind of superdiffusion is observed in such natural phenomena such as phonon transport in semiconductor [13], plasma [14], fluid dynamics [15; 16], optics [17; 18; 19], animal foraging [20; 21], the long-term climate change [22] and the human mobility [23; 24].

The study of relaxation processes in nonlinear dynamical systems subjected to the Lévy noise is of permanent interest. It is interesting to study both transient characteristics (mean first passage time (MFPT), average time of the first arrival, residence time in a given area) and steady-state statistical characteristics (probability density function, correlation time, correlation function, spectral power density).

It was established in paper [25] that the external potentials of the form $|x|^c\,(c > 2)$ confine anomalous diffusion in the form of Lévy flights and lead to a finite variance if $c > 4 - \alpha$. Obviously, moments of higher order still diverge.

Currently, there is a small amount of exact results for statistical characteristics of confined Lévy flights in different potentials, mostly for the probability density functions [14; 26; 27; 28; 29; 30] and spectral-correlation characteristics [31; 32] in a steady-state. The authors of paper [33] established that the probability density function (PDF) in superharmonic external potential of power c bifurcates from the initial monomodal to a stationary bimodal state, also there exists a transient trimodal state if $c > 4$. Papers [34; 35] have verified that the stationary states in symmetric single-well potentials can be characterized by more than two modal values. It should be noted that in contrast to numerical modeling the analytical results are obtained for the limited case of Cauchy noise with Lévy index $\alpha = 1$.

Moreover, the transient dynamics of this type of anomalous diffusion is insuf-

ficiently studied from analytical point of view and there are only a small number of exact results for different time characteristics of Lévy flights in confined potential profiles [25; 31; 36]. Most publications contain only the results of numerical simulation (see, for example, [37; 38; 39; 40; 41; 42]). They all relate mostly to the barrier crossing problem for Lévy flights and indicate that the mean time of transition is inversely proportional to the noise intensity parameter.

The escape problem from the metastable state in the case of Brownian diffusion was first investigated by Kramers [43]. According to the Kramers formula, the characteristic transition time of the particle through the potential barrier has exponential dependence on the ratio of the barrier height ΔU to the noise intensity D

$$\tau = C\,(D)\; e^{\Delta U/D}.$$

In the case of anomalous diffusion in the form of Lévy flights the main tools to investigate the barrier crossing problem for Lévy flights are the first passage times, crossing times, arrival times and residence times [26; 32; 44; 45]. Due to the fact that free Lévy flights represent a special class of Markovian processes with infinite variance, time analysis faces some difficulties [6; 46]. In addition, the conditions of absorbing and reflecting boundaries, as for Brownian diffusion, become inapplicable due to the fact that superdiffusion motion is characterized by the presence of jumps, and the particle can instantly reach the boundary from an arbitrary position.

The analytical investigation of correlation and spectral properties of steady-state Lévy flights in confinement potential profiles remains a current problem. Investigations of spectra are useful to observe and analyze the interplay between fluctuations, relaxation and nonlinearity which are inherent to real physical systems. The stationary spectral power density of the particle coordinate in the infinitely deep rectangular potential well was found in [47].

(ii) Afterwards, the nonlinear relaxation in the presence of Gaussian noise for the stochastic switching dynamics of the memory devices (the memristors) has been considered.

Memristors are elements of electric circuits able to change resistance depending on the applied electrical stimulation in an analog way. These devices attract nowadays great attention as one of the most perspective candidates for next-generation nonvolatile random access memory. This is due to its excellent size scalability down to nanometers, fast switching, low power, and simple structure [48; 49; 50; 51; 52; 53; 54]. Within the context of nanotechnologies, the production of nanostructures by diffusion is a subject largely investigated [55; 56; 57]. Meanwhile, the observed stochasticity in many experiments has emerged as an important inherent property of memristors. By stochasticity of a memristive system, we mean the inherent fluctuations in structure, chemical reaction, physical values and switching times, which can occur over multiple lengths and time scales during the switching events.

The stochasticity has been perceived across a range of non-volatile memory technologies such as phase-change memory [58; 59], resistive random access memory (ReRAM) [60; 61], electrochemical metallization memory [62], conductive bridge random access memory [63], and among oxide-based memristive materials [54; 64; 65; 66]. On the other hand, the non-deterministic behavior of circuit elements is the common feature of nanoelectronics and gives the ground for the newly established field of study named as stochastic electronics [67; 68]. With extensive miniaturization, the circuit elements are increasingly diverting away from their deterministic behavior and the effect of the fluctuations, which in the classical theory have been considered as a small disturbing factor, cannot be neglected at nanoscales [69]. This stochastic behaviour highly mimics the biological medium within the brain. Therefore, using memristor as a basic element of future

neural computers looks to be even more promising [54; 60; 70; 71; 72; 73; 74].

Four different approaches for the construction of the resistive swiching model exist: dynamical, microstructural, thermodynamical and stochastic.

The dynamical approach is based on rather simple dynamic equations that catch the key physical properties of memristor behavior. The models used in references [49; 75; 76; 77; 78; 79] and the model of conductive filament (CF) growth in [80] can be attributed to this approach. These models usually involve at least two equations: one is the Ohmic-type relationship between voltage and current and the second is a first-order differential equation for a state variable. The stochasticity is not taken into account by dynamic models, while it appears in the system due to many reasons including uncertainty of the model itself. The uncertainty of the model arises because in the dynamic approach one uses only the basic properties of the memristive system for the model construction and omits some other details. The selected basic properties are mainly defined by the choice of the internal state variable which is not observed from external electrical behavior [78]. There are models of memristive systems described by different state variables such as doping ratio [78], the width of doping region [77], the concentration of vacancies in the gap region [81], the thickness of CF [80], tunneling barrier width [82] etc.

The microstructural approach provides more accurate models for all physical processes taking place at the microlevel [83; 84; 85]. While the dynamic approach provides a practical fit of an abstract mathematical formulation with generalized experimental data of switching processes, the microstructure models aimed to precisely meet the physical dynamics of fabricated devices. In this case the mathematical complexity growths significantly, the model includes a large number of various differential equations and can be analysed only by numerical simulation.

The thermodynamic models include fluctuations in a natural way. In this approach, the state of a memristive system also can be described by an internal state variable, the system parameter, the representative or configurational coordinate, etc. At the equilibrium, the thermodynamic models provide well-defined Boltzmann probability distribution of the internal state variable. The evolution of nonequilibrium system is often described by the Fokker-Planck equation (FPE) for the probability distribution of the state variable in the field of thermodynamic force, defined by the profile of the free energy [86]. The FPE takes into account for the fluctuations and the nonequilibrium distribution with time relaxes to the equilibrium Boltzmann one. If there is a constant flow, the system can relax to a nonequilibrium steady state (NESS) [87; 88; 89].

In the framework of the stochastic approach, the mathematical models involve the random forces. Similar to the dynamic approach the stochastic models are based on at least two equations: an Ohmic-type relationship and a first-order differential equation but with the noise source [68; 90; 91; 92]. On the one hand, the thermodynamic and stochastic approaches may have a common base because the first order Langevin equation corresponds to the FPE. On the other hand, the stochastic model can be constructed by adding the random force to the dynamic one [68; 82].

Nowadays, we face with a lack of stochastic models of memristors. First of all, it is important to understand what is the equilibrium or steady-state of the memristive system for a set of external parameters, and analyze the related time characteristics such as the relaxation time to the steady-state, the transition time to another equilibrium state and the lifetime of metastable states under the influence of noise. The statistics of switching times and the appropriate probability distributions were investigated in [68; 82; 93; 94] and some common properties for the mean switching time values were revealed for different systems investi-

gated. It was established that internal and external noise plays a positive role in switching dynamics. In fact, in [95] has shown that internal noise helps increase the contrast ratio between low and high resistive states, and in the [96] the authors experimentally observed, in a memristor system, a phenomenon similar to stochastic resonance [97; 98; 99] with a beneficial role of noise in resistive switching. In particular, they studied the effect of external noise on the resistive switching of a memristor system and found an optimal noise amplitude that maximizes the contrast between high and low resistive states. However, basic stochastic properties, such as the distribution of the balance of the parameters, the relaxation or the transition time have not been investigated.

1.3 Objectives and Contributions

Chapter 2 is devoted to analysis of the nonlinear dynamical systems subjected to Lévy noise source. First of all, we present general apparatus of the Markovian theory, including new theoretical results for calculating of the transient and the steady-state characteristics. Further we investigate: (i) the noise-enhanced stability phenomenon (NES) in fully unstable system, namely in the symmetric inverse parabolic potential with two sinks; (ii) the steady-state probabilistic and time characteristics in a bistable quartic potential; (iii) the stationary correlation characteristics of Lévy flights in one-dimensional confined potentials; (iv) the probabilistic characteristics of the different types of the diffusion on the plane. It is worthwhile to note that all systems considered, except system (i), are characterised by confined potential profiles.

As far as the memristors concerned, for investigating the properties of stochasticity of memristors and understanding how it influences the system it is important to construct the appropriate mathematical model. This model should catch

the fundamental balance laws that govern memristor behavior and include information about stochastic properties. Chapter 3 is dedicated to the investigation of the basic model for stochasticity of memristors and thereby providing the ground for understanding how the intrinsic fluctuations can limit or provide new advantages for emerging applications. In particular, two models of an ideal Chua memristor with the external Gaussian noise were considered and a stochastic macroscopic model of a memristive system based on a generalization of known approaches and experimental results has been proposed.

The main part of the results presented in the thesis was obtained personally by the author. In most of the joint works, the author performed analytical calculations. Formulation of problems, development of approaches and interpretation of the results were carried out jointly with co-authors of scientific papers published.

1.4 Dissemination of Results

The main results of the work were presented in the form of oral and poster presentations at six Russian and seven International scientific conferences and schools as follows

- XX-XXIII Scientific conferences on Radiophysics (N. Novgorod, Lobachevsky State University);
- XX-XXII Sessions of young scientists (Natural and Mathematical Sciences) (N. Novgorod);
- Summer school on Lévy processes (Lille, France, 2016);
- International conference on Statistical Physics Sigma Phi-2017 (Corfu, Greece, 2017);

- Summer School on Stochastic Processes with Applications to Physics and Biophysics (Acre, Israel, 2017);
- International conference "New trends in nonequilibrium statistical mechanics: classical and quantum systems" (Erice, Italy, 2018);
- Special session "Stochastic Multistable Systems" at the 2nd International Workshop "From ReRAM and Memristors to new Computing Paradigms (MEM-Q) (Rethymno, Greece, 2018);
- 25rd International Conference on Noise and Fluctuations (Neuchatel, Switzerland, 2019);
- International conference "New Trends in Non-equilibrium Stochastic Multistable Systems and Memristors (NES 2019)" (Erice, Italy, 2019).

The thesis materials are published in 7 printed works, including 4 papers in the International Scientific journals [A2, A3, A6, A7] and 3 proceedings of conferences [A1, A4, A5].

Chapter 2

Statistical characteristics of diffusions

This chapter is focused on the analysis of the statistical characteristics of anomalous diffusion in the form of Lévy flights. In section 2.1 the general relations of the Markovian theory for the calculation of the transient and the steady-state characteristics are presented. Section 2.2 is devoted to the noise-enhanced stability phenomenon (NES) in fully unstable system, namely in the symmetric inverse parabolic potential with two sinks. In section 2.3 the steady-state probabilistic and temporal characteristics in a bistable quartic potential are investigated. The stationary correlation characteristics of Lévy flights in one-dimensional confined potentials are studied theoretically and numerically in section 2.4. In section 2.5 we conduct a comparative analysis of the probabilistic characteristics of Brownian motion and anomalous diffusion on the plane.

2.1 General relations of Markovian theory

This opening section provides a basic apparatus of the Markovian theory for the calculation of the transient and the steady-state characteristics. It presents not only the previous studies regarding statistical analysis but also new results, which constitute the starting point of this research work.

We consider an arbitrary homogeneous Markovian random process $x(t)$ with the probability density of transitions $P\left(x,t|\,x_0,t_0\right)$ which depends only on the time difference $\tau = t-t_0 \geq 0$. The conditional probability density $P(x,t|x_0,t_0) = P(x,t-t_0|x_0,0)$ obeys the Kolmogorov forward equation [100]

$$\frac{\partial P\left(x,t-t_0|\,x_0,0\right)}{\partial t} = \hat{L}\left(x\right) P\left(x,t-t_0|\,x_0,0\right), \tag{2.1}$$

where $\hat{L}\left(x\right)$ is the kinetic operator, which does not depend on time.

Meanwhile, the Kolmogorov backward equation for the transition probability density reads as

$$-\frac{\partial P\left(x,t-t_0|\,x_0,0\right)}{\partial t_0} = \hat{L}^{+}\left(x_0\right) P\left(x,t-t_0|\,x_0,0\right), \tag{2.2}$$

where $\hat{L}^{+}\left(x_0\right)$ is the adjoint kinetic operator.

According to the definition, if the random process $x(t)$ initially starts from the value x_0 at $t=0$, the residence time $T(x_0)$ in the given domain G for the infinite observation time reads [32]

$$T(x_0) = \int_0^{\infty} \mathbb{1}_G\left(x(t)\right) dt, \tag{2.3}$$

where $\mathbb{1}_G(y)$ is the indicator of the domain G, determined as

$$\mathbb{1}_G(y) = \begin{cases} 1, & y \in G, \\ 0, & \text{otherwise.} \end{cases} \tag{2.4}$$

Averaging both parts of equation (2.3), we find the mean residence time in the domain G

$$\langle T(x_0) \rangle = \int_0^\infty \Pr(t, x_0) dt = \int_0^\infty dt \int_G P\left(x, t \middle| x_0, 0\right) dx, \tag{2.5}$$

where $Pr(t, x_0)$ is the probability to find the particle in the domain G at the time t. We suppose that all the integrals in time in Eq. (2.5) are convergent. It means that the probability $Pr(t, x_0)$ and the conditional probability density $P\left(x, t \middle| x_0, 0\right)$ tend to zero fast enough when $t \to \infty$, and the Markovian process $x(t)$ describes a nonlinear system without steady state. Changing the order of integration, we can write equation (2.5) in the following form

$$\langle T(x_0) \rangle = \int_G Y\left(x, x_0\right) dx, \tag{2.6}$$

where

$$Y\left(x, x_0\right) = \int_0^\infty P\left(x, t \middle| x_0, 0\right) dt. \tag{2.7}$$

From definition (2.3) the second moment of the residence time can be calculated as

$$\begin{aligned} \left\langle T^2(x_0) \right\rangle &= \int_0^\infty dt \int_0^\infty d\tau \left\langle \mathbb{1}_G\left(x(t)\right) \mathbb{1}_G\left(x(\tau)\right) \right\rangle \\ &= \int_0^\infty dt \int_0^\infty d\tau \int_{G \times G} P\left(x, t; y, \tau \middle| x_0, 0\right) dx\, dy. \end{aligned}$$

Using Markovian property of the random process $x(t)$

$$P\left(x,t_2;y,t_1|\,x_0,t_0\right)=P\left(x,t_2-t_1|\,y,0\right)P\left(y,t_1-t_0|\,x_0,0\right)$$

where $t_0<t_1<t_2$, we have

$$\begin{aligned}\left\langle T^2(x_0)\right\rangle=\int_0^\infty dt\int_t^\infty d\tau\int_G dx\int_G dy\,P\left(x,t|\,x_0,0\right)\\ \times P\left(y,\tau-t|\,x,0\right)+\int_0^\infty d\tau\int_\tau^\infty dt\int_G dx\\ \times\int_G dy\,P\left(y,\tau|\,x_0,0\right)P\left(x,t-\tau|\,y,0\right).\end{aligned}$$

Changing variables under the integrals and taking into account equations (2.6) and (2.7), we finally find

$$\left\langle T^2(x_0)\right\rangle=2\int_G Y\left(x,x_0\right)dx\int_G Y\left(y,x\right)dy=2\int_G Y\left(x,x_0\right)\left\langle T(x)\right\rangle dx. \tag{2.8}$$

The variance of the residence time can be calculated as

$$\mathrm{Var}\left(x_0\right)=\left\langle T^2(x_0)\right\rangle-\left\langle T(x_0)\right\rangle^2. \tag{2.9}$$

Similarly, the n-th moment of the residence time (2.3) can be written as

$$\left\langle T^n(x_0)\right\rangle=n\int_G Y\left(x,x_0\right)\left\langle T^{n-1}(x)\right\rangle dx. \tag{2.10}$$

Now we derive a closed equation for the characteristic function of the residence time. According to the definition, we have

$$\theta\left(k,x_0\right)=\left\langle e^{ikT(x_0)}\right\rangle=1+\sum_{n=1}^{\infty}\frac{(ik)^n}{n!}\left\langle T^n(x_0)\right\rangle. \tag{2.11}$$

Substitution of equation (2.10) in equation (2.11) gives

$$\theta\left(k,x_0\right)=1+\sum_{n=1}^{\infty}\frac{(ik)^n}{(n-1)!}\int_G Y\left(x,x_0\right)\left\langle T^{n-1}(x)\right\rangle dx$$
$$=1+ik\int_G Y\left(x,x_0\right)\sum_{m=0}^{\infty}\frac{(ik)^m}{m!}\left\langle T^m(x)\right\rangle dx. \tag{2.12}$$

Thus, from equations (2.11) and (2.12) we arrive at the following integral equation for the characteristic function of the residence time

$$\theta\left(k,x_0\right)=1+ik\int_G Y\left(x,x_0\right)\theta\left(k,x\right)dx. \tag{2.13}$$

The integro-differential equation for the probability density function $W_{x_0}\left(\tau\right)=(1/2\pi)\int_{-\infty}^{\infty}\theta(k,x_0)e^{-ikt}dk$ of the residence time (2.3) can be obtained by inverse Fourier transform of equation (2.13)

$$W_{x_0}\left(t\right)=\delta\left(t\right)-\frac{d}{dt}\int_G Y\left(x,x_0\right)W_x\left(t\right)dx. \tag{2.14}$$

Equations (2.13) and (2.14) describe the full statistics of the residence time and are valid for an arbitrary homogeneous Markovian random process $x(t)$. These results are new and represent a contribution to the Markovian theory of stochastic processes. Unfortunately, equations (2.13) and (2.14) can be solved only in some simple cases.

Further the formulas to perform calculations of the statistical characteristics of the stationary Markovian processes are given.

The correlation function of a stationary Markovian process can be calculated by definition

$$K[\tau]=\left\langle x(t)x(t+\tau)\right\rangle_{st}=\int_{-\infty}^{+\infty}x_0P_{st}(x_0)dx_0\int_{-\infty}^{+\infty}xP(x,\tau|x_0,0)dx. \tag{2.15}$$

Here the angular brackets with the subscript st denote averaging over the steady-state probability distribution $P_{st}(x)$, which satisfies Kolmogorov equation (see equation (2.1))

$$\hat{L}(x)P_{st}(x) = 0. \tag{2.16}$$

Using the obvious initial condition $P(x,0|x_0,0) = \delta(x - x_0)$, we write the solution of the equation (2.2) in the formal operator form

$$P(x,\tau|x_0,0) = e^{\hat{L}^+(x_0)\tau}\delta(x - x_0). \tag{2.17}$$

Substituting equation (2.17) in equation (2.15), we arrive at [101]

$$K[\tau] = \left\langle x\, e^{\hat{L}^+(x)\tau} x \right\rangle_{st}. \tag{2.18}$$

Based on equation (2.18), the correlation function can be represented by the following series [102]

$$K[\tau] = \langle x \rangle_{st}^2 + \sum_{n=1}^{\infty} \alpha_n^2\, e^{-\lambda_n \tau}, \tag{2.19}$$

where $\alpha_n = \langle x\psi_n(x)\rangle_{st}$, $\psi_n(x)$ and λ_n are the eigenfunctions and positive eigenvalues of the adjoint kinetic operator $\hat{L}^+(x)$, respectively, which obey the following equation

$$\hat{L}^+(x)\psi_n(x) = -\lambda_n\psi_n(x). \tag{2.20}$$

The correlation time of a stationary random process $x(t)$ can be defined as the width of equivalent rectangle (see, e.g. [103] and figure 2.1)

$$\tau_c = \frac{1}{\langle x,x\rangle}\int_0^{\infty} \left(K[\tau] - \langle x\rangle^2\right) d\tau, \tag{2.21}$$

where $K[\tau] = \langle x(t)x(t+\tau)\rangle$ is the correlation function of $x(t)$ changed from $K[0] = \langle x^2\rangle$ to $K[\infty] = \langle x\rangle^2$, and $\langle x,x\rangle = \langle x^2\rangle - \langle x\rangle^2$ is the variance. As

seen from equation (2.19), the correlation function of an arbitrary stationary Markovian process is non-negative and monotonically decreasing, as shown in figure 2.1. This fact indicates the applicability of definition (2.21) in this case if the integral in equation (2.21) converges.

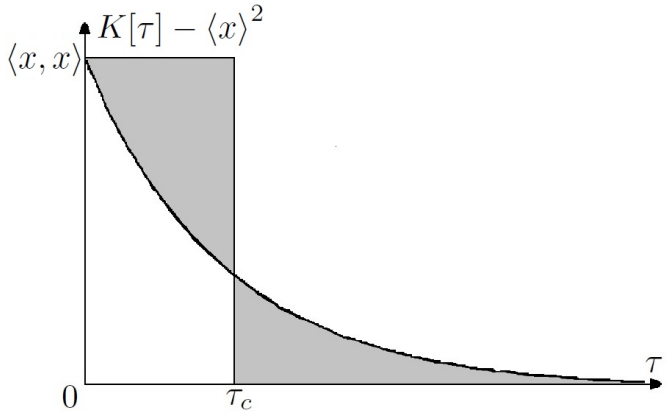

Figure 2.1: Illustration to the definition (2.21) of the correlation time τ_c. The shaded areas should be equal.

Let us show that the calculation of the correlation time of a stationary Markovian process by the formula (2.21) can be performed accurately without finding the probability density of transitions in some cases. Substituting equation (2.18) in equation (2.21) and execute integration, we arrive at

$$\tau_c = -\frac{1}{\langle x, x \rangle_{st}} \left\langle x, \frac{1}{\hat{L}^+(x)}\, x \right\rangle_{st}, \tag{2.22}$$

where $\langle f(x), g(x) \rangle = \langle f(x) g(x) \rangle - \langle f(x) \rangle \langle g(x) \rangle$. It should be noted that result (2.22) in the particular case of $\langle x \rangle_{st} = 0$ was previously obtained in paper [104]. Using the definition of the adjoint kinetic operator $\hat{L}^+(x)$

$$\int_{-\infty}^{\infty} f(x)\, \hat{L}(x) g(x)\, dx = \int_{-\infty}^{\infty} g(x)\, \hat{L}^+(x) f(x)\, dx, \tag{2.23}$$

from equation (2.22) we obtain

$$\tau_c = \frac{1}{\langle x, x\rangle_{st}} \int_{-\infty}^{\infty} x \, \frac{1}{\hat{L}(x)} \left(\langle x\rangle_{st} - x\right) P_{st}(x)\, dx. \tag{2.24}$$

As seen from formula (2.24), we have to find a particular solution $\phi(x)$ of the following integro–differential equation

$$\hat{L}(x)\phi\left(x\right) = \left(\langle x\rangle_{st} - x\right) P_{st}\left(x\right) \tag{2.25}$$

and then calculate the correlation time as

$$\tau_c = \frac{1}{\langle x, x\rangle_{st}} \int_{-\infty}^{\infty} x\phi\left(x\right) dx. \tag{2.26}$$

For discontinuous Markovian process $x(t)$ the Kolmogorov equation for PDF becomes integro-differential [3] and to solve equation (2.25) the Fourier transform is usually used. In this sense, the correlation time τ_c in equation (2.26) is conveniently expressed in terms of the function $\tilde{\phi}(k)$ which is the Fourier image of the function $\phi\left(x\right)$

$$\tilde{\phi}\left(k\right) = \int_{-\infty}^{\infty} \phi\left(x\right) e^{ikx} dx. \tag{2.27}$$

Using the first remarkable limit we write the formula (2.26) in more simple form (see [31])

$$\begin{aligned} \tau_c &= \frac{1}{\langle x, x\rangle_{st}} \int_{-\infty}^{\infty} \phi\left(x\right) \lim_{k\to 0} \frac{\sin kx}{k}\, dx \\ &= \frac{1}{\langle x, x\rangle_{st}} \lim_{k\to 0} \frac{\varphi(k) - \varphi(0)}{k}\, dx = \frac{\varphi'\left(0\right)}{\langle x, x\rangle_{st}}, \end{aligned} \tag{2.28}$$

where, in accordance with equation (2.27),

$$\varphi(k) = \int_{-\infty}^{+\infty} \phi(x) \sin kx dx = \mathrm{Im}\{\tilde{\phi}(k)\}. \tag{2.29}$$

Thus, in order to find the correlation time after Fourier transform of equation (2.25) we should obtain an equation for the imaginary part of the function $\tilde{\phi}(k)$, solve it and then substitute the result in equation (2.28).

Based on the general operator formula (2.18) for the correlation function $K[\tau]$ of stationary Markovian process $x(t)$, its spectral characteristics can be found. According to the Wiener–Khinchin theorem, one can calculate the spectral power density as

$$S(\omega) = \int_{-\infty}^{\infty} K[\tau] \cos \omega\tau d\tau = 2\mathrm{Re}\left\{\int_0^{\infty} K[\tau] e^{i\omega\tau} d\tau\right\} = 2\,\mathrm{Re}\left\{\tilde{K}[i\omega]\right\}, \tag{2.30}$$

where $\tilde{K}[p]$ is the Laplace transform of $K[\tau]$ and $\mathrm{Re}\{\tilde{K}[i\omega]\}$ denotes the real part of expression. According to equation (2.18) function $\tilde{K}[p]$ reads

$$\tilde{K}[p] = \left\langle x \frac{1}{p - \hat{L}^+(x)} x \right\rangle_{st}. \tag{2.31}$$

As seen from equation (2.31), we have to solve the following integro–differential equation for the auxiliary function $\varphi_p(x)$

$$\hat{L}^+(x)\varphi_p(x) - p\varphi_p(x) = -x \tag{2.32}$$

and then calculate the average

$$\tilde{K}[p] = \langle x\varphi_p(x)\rangle_{st}. \tag{2.33}$$

In the framework of this study we consider two models of Markovian random processes frequently used in calculations.

The overdamped motion under non-Gaussian white noise $\xi(t)$ in an arbitrary potential $U(x)$ is governed by the following Langevin equation

$$\frac{dx}{dt} = -U'(x) + \xi(t), \tag{2.34}$$

where $x(t)$ is the coordinate of a particle.

The corresponding Kolmogorovs equation for probability density of the Markovian process $x(t)$ was obtained in [3] and reads as

$$\frac{\partial P}{\partial t} = \frac{\partial}{\partial x}[U'(x)P] + \int_{-\infty}^{+\infty} \frac{\rho(z)}{z^2}\left[\exp\left\{-z\frac{\partial}{\partial x}\right\} - 1 + \sin z\frac{\partial}{\partial x}\right] dzP, \tag{2.35}$$

where $\rho(z) \geq 0$ is the kernel function.

In particular, the corresponding kernel function for a white Gaussian noise $\xi(t)$ with zero mean and the intensity $2D$ is $\rho(x) = 2D\delta(x)$. Therefore, we obtain from equation (2.35) the ordinary Fokker–Planck equation

$$\frac{\partial P}{\partial t} = \frac{\partial}{\partial x}[U'(x)P] + D\frac{\partial^2 P}{\partial x^2}. \tag{2.36}$$

Meanwhile, for non-Gaussian driving force $\xi(t)$ with symmetric α-stable Lévy distribution (Lévy index $0 < \alpha < 2$), the kernel function is $\rho(x) = Q_\alpha|x|^{1-\alpha}$. As a result, equation (2.35) transforms to the fractional Fokker-Planck equation

$$\frac{\partial P}{\partial t} = \frac{\partial}{\partial x}[U'(x)P] + D_\alpha\frac{\partial^\alpha P}{\partial|x|^\alpha} \tag{2.37}$$

with the fractional space derivative

$$D_\alpha\frac{\partial^\alpha P(x,t)}{\partial|x|^\alpha} = Q_\alpha\int_{-\infty}^{+\infty}\frac{P(x-z,t) - P(x,t)}{|z|^{1+\alpha}}dz. \tag{2.38}$$

Here: D_α is the noise intensity parameter and

$$Q_\alpha = \frac{D_\alpha \Gamma(\alpha+1)\sin(\pi\alpha/2)}{\pi}.$$

Equation (2.37) describes the anomalous diffusion in the form of Lévy flights.

2.2 NES effect for Lévy flights in inverse parabolic potential

Further we investigate the mean residence time of a particle in given area in the case of Lévy flight superdiffusion in the unstable parabolic potential $U(x) = -bx^2/2$ ($b > 0$), see figure 2.2.

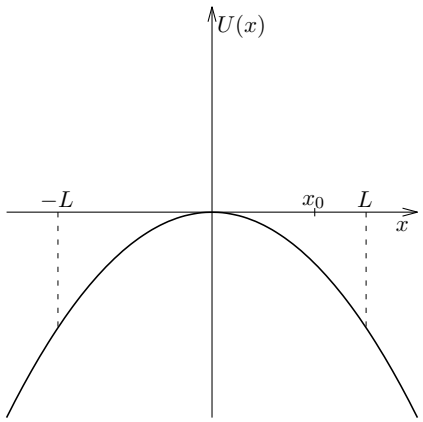

Figure 2.2: The inverse parabolic potential.

Substituting the parabolic potential in the Langevin equation (2.34) with Lévy noise source $\xi_\alpha(t)$, we arrive at the following linear differential equation

$$\frac{dx}{dt} = bx + \xi_\alpha(t). \tag{2.39}$$

Solution of the above equation can be written in explicit form

$$x(t) = x_0 e^{bt} + \int_0^t e^{b(t-\tau)} \xi_\alpha(\tau) d\tau, \tag{2.40}$$

where x_0 is the initial position of a particle. Using the exact solution (2.40), we

can find the characteristic function of the particle position x by the definition

$$\vartheta\left(k,t\right)=\left\langle e^{ikx(t)}\right\rangle . \tag{2.41}$$

Substituting $x(t)$ from equation (2.40) in equation (2.41), we get

$$\vartheta\left(k,t\right)=e^{ikx_0e^{bt}}\left\langle \exp\left\{ik\int_0^t e^{b(t-\tau)}\xi_\alpha(\tau)d\tau\right\}\right\rangle . \tag{2.42}$$

To calculate the average in equation (2.42) we use the expression for the characteristic functional of symmetric white α-stable noise with the intensity parameter $D_\alpha=\sigma^\alpha$ (see the formula (4) in [27] and also the general result (8) in [3])

$$\left\langle \exp\left\{i\int_0^t u(\tau)\,\xi_\alpha(\tau)d\tau\right\}\right\rangle =\exp\left\{-\int_0^t\left|\sigma u(\tau)\right|^\alpha d\tau\right\}, \tag{2.43}$$

where $u(t)$ is an arbitrary deterministic function.

Replacing in equation (2.43) $u(\tau)$ with $ke^{b(t-\tau)}$ and substituting in equation (2.42), we finally arrive at

$$\vartheta\left(k,t\right)=\exp\left\{ikx_0\,e^{bt}-\frac{\sigma^\alpha\left|k\right|^\alpha}{\alpha b}\left(e^{\alpha bt}-1\right)\right\}. \tag{2.44}$$

Further, we analyze the residence time of a particle in the symmetric interval $(-L,L)$, for $x_0\in(-L,L)$. Applying the inverse Fourier transform to equation (2.44), we find the conditional probability density $P\left(x,t|\,x_0,0\right)$ and then the probability to find a particle in the interval $(-L,L)$

$$\begin{aligned}\Pr\left(t,x_0\right)=\int_{-L}^{L}P\left(x,t|\,x_0,0\right)dx=\frac{2}{\pi}\int_0^\infty\frac{\sin kL}{k}\cos\left(kx_0\,e^{bt}\right)\\ \times\exp\left\{-\frac{\left(\sigma k\right)^\alpha\left(e^{\alpha bt}-1\right)}{\alpha b}\right\}dk.\end{aligned} \tag{2.45}$$

In the limit of $t \to \infty$ the main contribution to the integral (2.45) comes from the region close to zero in k so that, using the approximation $\sin kL \simeq kL$ and $exp^{\alpha bt} >> 1$, we obtain

$$\Pr(t, x_0) \simeq \frac{2L}{\pi} \int_0^\infty \cos\left(kx_0\, e^{bt}\right) \exp\left\{-\frac{\left(\sigma k\, e^{bt}\right)^\alpha}{\alpha b}\right\} dk$$

or, after setting $q = ke^{bt}$,

$$\Pr(t, x_0) \simeq \frac{2L}{\pi}\, e^{-bt} \int_0^\infty \cos(qx_0) \exp\left\{-\frac{(\sigma q)^\alpha}{\alpha b}\right\} dq. \tag{2.46}$$

Thus, the integral in equation (2.5) converges. Moreover, all the moments of the residence time (2.3) are finite.

Substituting equation (2.45) in equation (2.5), after some rearrangements we obtain the following exact formula for the mean residence time

$$\langle T(x_0)\rangle = \frac{2}{\pi b} \int_0^\infty \frac{\cos(qx_0)}{q} \exp\left\{-\frac{(\sigma q)^\alpha}{\alpha b}\right\} dq \times \int_0^q \frac{\sin kL}{k} \exp\left\{\frac{(\sigma k)^\alpha}{\alpha b}\right\} dk \tag{2.47}$$

or

$$\langle T(x_0)\rangle = \frac{2}{\pi b} \int_0^\infty \frac{\sin kL}{k} \exp\left\{\frac{(\sigma k)^\alpha}{\alpha b}\right\} dk \cdot \int_k^\infty \frac{\cos(qx_0)}{q} \exp\left\{-\frac{(\sigma q)^\alpha}{\alpha b}\right\} dq, \tag{2.48}$$

which gives the average residence time as a function of the initial conditions, the parameters of the system and of Lévy noise source. This is, together with equations (2.13) and (2.14), the main result of this section.

Let us check result (2.47) in the absence of the noise $\xi_\alpha(t)$. Putting $\sigma = 0$ in equation (2.47), we arrive at

$$T_{dyn} = \frac{2}{\pi b} \int_0^\infty \frac{\cos(qx_0)}{q}\, dq \int_0^q \frac{\sin kL}{k}\, dk = \frac{2}{\pi b} \int_0^\infty \frac{\cos(qx_0)\,\mathrm{si}(qL)}{q}\, dq, \tag{2.49}$$

where $\mathrm{si}(x)$ is the sine integral function. Using the auxiliary integral ($\alpha, \beta > 0$)

$$\int_0^\infty \frac{\cos(\beta x)\,\mathrm{si}(\alpha x)}{x}\,dx = \begin{cases} (\pi/2)\ln(\alpha/\beta), & \alpha > \beta, \\ 0, & \alpha < \beta \end{cases}$$

and taking into account that $|x_0| < L$, we find the dynamical (deterministic) residence time

$$T_{dyn} = \frac{1}{b}\,\ln\frac{L}{|x_0|}\,. \tag{2.50}$$

At the same time, the direct integration of equation (2.39) without noise, but with separable variables

$$\int_{x_0}^{L}\frac{dx}{x} = \int_0^{T_{dyn}} b\,dt,$$

gives the same result.

Let us show that for the Cauchy stable noise with $\alpha = 1$ we can write equation (2.47) in the form of single integral. Substituting $\alpha = 1$ in equation (2.47) and changing the order of integration, we arrive at

$$\langle T(x_0)\rangle = \frac{2}{\pi b}\int_0^\infty \frac{\sin kL}{k}\,e^{\sigma k/b}dk \int_k^\infty \frac{\cos(qx_0)}{q}\,e^{-\sigma q/b}dq. \tag{2.51}$$

Differentiating equation (2.51) with respect to the parameter x_0 and calculating the internal integral, we get

$$\frac{d\langle T(x_0)\rangle}{dx_0} = -\frac{2}{\pi}\int_0^\infty \frac{(bx_0\cos kx_0 + \sigma\sin kx_0)\sin kL}{k\,(\sigma^2 + b^2x_0^2)}\,dk. \tag{2.52}$$

Using Dirichlet

$$\int_0^\infty \frac{\sin\alpha x}{x}\,dx = \frac{\pi}{2}\,\mathrm{sgn}(\alpha)$$

and Frullani formulae

$$\int_0^\infty \frac{\cos ax - \cos bx}{x}\, dx = \ln\left|\frac{b}{a}\right|,$$

where $\mathrm{sgn}\,(x)$ is the sign function, we obtain from equation (2.52)

$$\frac{d\,\langle T(x_0)\rangle}{dx_0} = \frac{\frac{\sigma}{\pi}\ln\left|\frac{L-x_0}{L+x_0}\right| - bx_0 1\,(L-x_0)}{\sigma^2 + b^2 x_0^2}\,, \tag{2.53}$$

where $1(x)$ is the step function. According to equation (2.47),

$$\lim_{x_0\to\infty} \langle T(x_0)\rangle = 0.$$

As a consequence, we find from equation (2.53)

$$\langle T(x_0)\rangle = \int_{x_0}^\infty \left[bz1\,(L-z) + \frac{\sigma}{\pi}\ln\left|\frac{L+z}{L-z}\right|\right]\, \frac{dz}{\sigma^2 + b^2 z^2}$$

or

$$\langle T(x_0)\rangle = \frac{1}{2b}\ln\frac{\sigma^2 + b^2L^2}{\sigma^2 + b^2x_0^2} + \frac{\sigma}{\pi}\int_{x_0}^\infty \ln\left|\frac{L+z}{L-z}\right| \frac{dz}{\sigma^2 + b^2z^2}\,, \tag{2.54}$$

where $|x_0| < L$. Of course, in the case $\sigma = 0$ equation (2.54) coincides with equation (2.50).

The plot of the normalized mean residence time $\tau(x_0) = \langle T(x_0)\rangle / T_{dyn}$ as a function of the scale parameter σ (noise intensity) for $L = 1$, with various initial conditions and different values of the Lévy index α is shown in figure 2.3.

Points correspond to the Monte Carlo simulation of the Langevin equation (2.39) while solid lines present numerical integration of exact formula (2.47). The algorithm used in this work to simulate Lévy noise sources is that proposed by Weron [105] for the implementation of the Chambers method [106]. Monte Carlo simulations nicely corroborate exact results.

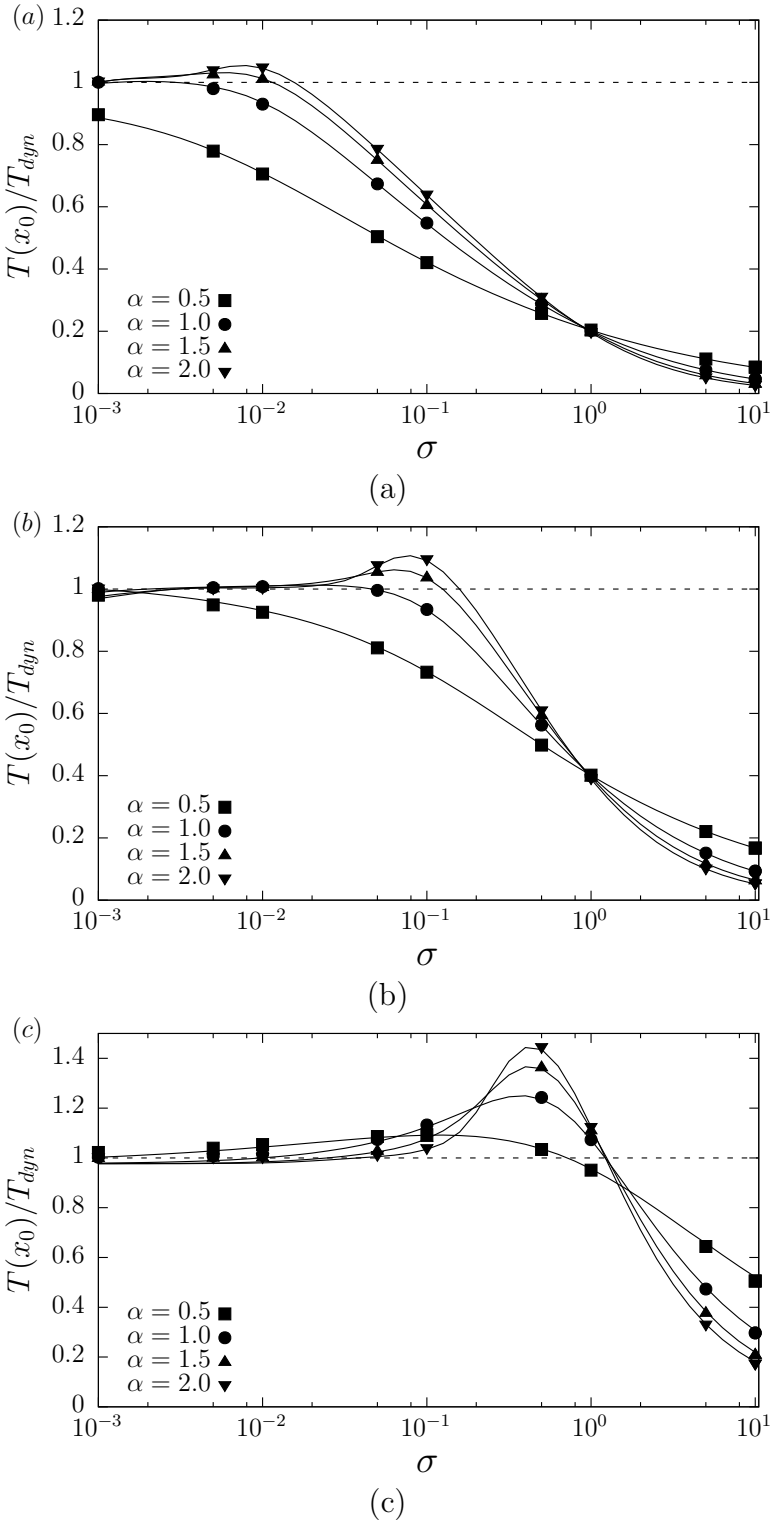

Figure 2.3: Normalized mean residence $\langle T(x_0)\rangle/T_{dyn}$ time as a function of the scale parameter σ (noise intensity) for $L = 1$, various initial initial positions of a particle (a) $x_0 = 0.01$, (b) $x_0 = 0.1$, (c) $x_0 = 0.5$, and different values of the Lévy index α, namely $\alpha = 0.5, 1.0, 1.5, 2.0$. Error bars, which are standard deviations of the mean, are within the symbol size.

In all panels of figure 2.3, one can observe a nonmonotonic behavior, with a maximum, of the normalized average residence time of the particle in the interval $(-L, L)$ as a function of the scale parameter σ (noise intensity). This is a signature of the noise enhanced stability (NES) phenomenon because the noise increases the average lifetime of the particle in a defined region of the potential profile [107; 108; 109; 110; 111; 112], and confirms its first observation in metastable states of short and long Josephson junctions [113; 114]. The NES phenomenon increases as the Lévy index increases and the initial position of the particle approaches the boundary of the interval. Moreover, increasing the value of the x_0, the value of the scale parameter σ for which we have the maximum increases too. This is due to the increase in the height of the potential barrier as the value of x_0 increases. The particle "needs" larger noise intensity to overcome the potential barrier during its stay in the defined interval, that is when $x(t) \in (-L, L)$. The decreasing of the NES effect with decreasing Lévy index is due to the peculiarity of fat tails in the distribution of Lévy noise. In fact, with low values of the α index it is easier for the particle to overcome the barrier of the unstable parabolic potential from one side to the other one and to reach the boundaries of the interval $(-L, L)$ more quickly compared to normal Brownian diffusion.

Figure 2.4 shows the dependence of the mean squared residence time versus the scale parameter σ for various initial conditions and different values of the Lévy index α. Points correspond to the Monte Carlo simulation of the Langevin equation (2.39), while lines simply connect these points. The mean squared residence time $\langle T^2(x_0)\rangle$ displays the same nonmonotonic behavior on the scale parameter as the normalized mean residence time.

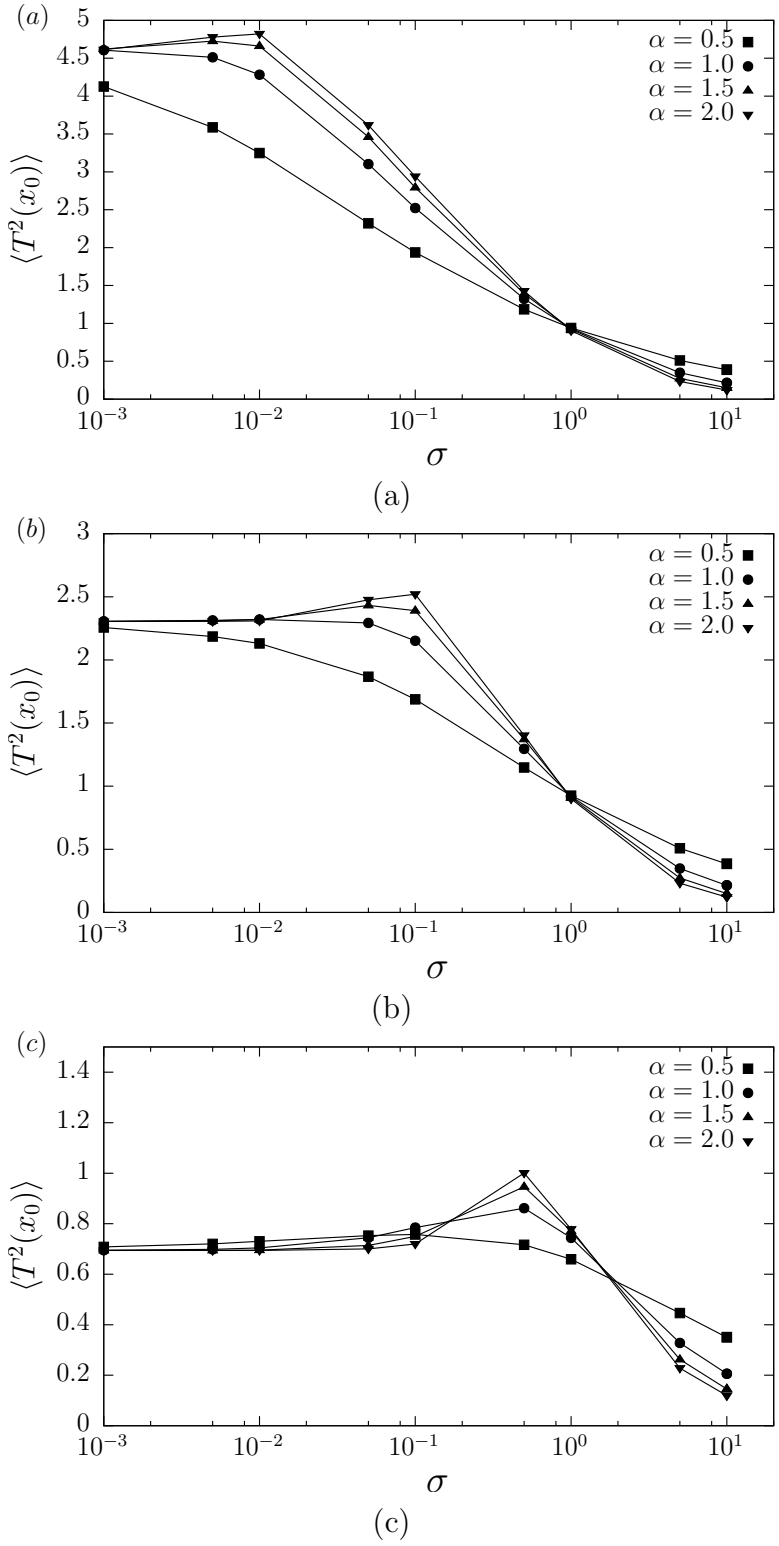

Figure 2.4: Mean squared residence time $\langle T^2(x_0)\rangle$ for $L = 1$ for various initial positions of a particle: (a) $x_0 = 0.01$, (b) $x_0 = 0.1$, (c) $x_0 = 0.5$, and different values of the Lévy index α, namely $\alpha = 0.5, 1.0, 1.5, 2.0$.

2.3 Barrier crossing event for Lévy flights in bistable potential

Further, we examine the steady-state Lévy flights in the asymmetric bistable quartic potential

$$U(x) = \gamma \left(\frac{x^4}{4} - \frac{ax^2}{2} - bx \right), \tag{2.55}$$

where γ is the potential steepness and b is the asymmetry parameter ($a, b, \gamma > 0$).

2.3.1 Steady-state probability density function

Asymptotically ($t \to \infty$), after the Fourier transform of the fractional Fokker-Planck equation (2.37), we obtain

$$U' \left(\frac{d}{d(ik)} \right) \vartheta_{st} - iD_\alpha |k|^{\alpha-1} \mathrm{sgn}(k)\, \vartheta_{st} = 0, \tag{2.56}$$

where $\vartheta_{st}(k)$ is the steady-state characteristic function of the particle position $x(t)$ which is the Fourier transform of the steady-state probability density function (PDF) $P_{st}(x)$

$$\vartheta_{st}(k) = \left\langle e^{ikx} \right\rangle_{st} = \int_{-\infty}^{\infty} e^{ikx} P_{st}(x) dx. \tag{2.57}$$

For asymmetric quartic potential (2.55) equation (2.56) becomes a homogeneous differential equation of the third order

$$\frac{d^3\vartheta_{st}}{dk^3} + a\frac{d\vartheta_{st}}{dk} + \left[ib - \beta_\alpha |k|^{\alpha-1} \mathrm{sgn}(k) \right] \vartheta_{st} = 0, \tag{2.58}$$

where $\beta_\alpha = D_\alpha/\gamma$. Equation (2.58) can be solved analytically only in the case of driving Cauchy noise ($\alpha = 1$), when it takes the form

$$\frac{d^3\vartheta_{st}}{dk^3} + a\frac{d\vartheta_{st}}{dk} + \left[ib - \beta_1 \,\mathrm{sgn}(k) \right] \vartheta_{st} = 0. \tag{2.59}$$

In principle, we should consider both positive and negative values of k. Looking for the solution in the form $\vartheta_{st}(k) = Ce^{zk}$, for $k > 0$ we arrive from equation (2.59) at the characteristic equation

$$z^3 + az + (ib - \beta_1) = 0. \tag{2.60}$$

By studying cubic equation (2.60), we find that it has three complex roots, two of which (z_1 and z_2) have negative real part and one (z_3) – positive.

The general solution of equation (2.59) can be written in the form $\vartheta_{st}(k) = C_1e^{z_1k} + C_2e^{z_2k} + C_3e^{z_3k}$. Since $\vartheta_{st}(k) \to 0$ as $k \to \infty$, the coefficient C_3 is zero and the steady-state characteristic function for positive values of k reads

$$\vartheta_{st}(k) = C_1e^{z_1k} + C_2e^{z_2k}. \tag{2.61}$$

According to the relation $\vartheta_{st}(-k) = \vartheta^*_{st}(k)$, which follows from definition (2.57) of $\vartheta_{st}(k)$, for $k < 0$ we get

$$\vartheta_{st}(k) = C^*_1e^{-z^*_1k} + C^*_2e^{-z^*_2k}, \tag{2.62}$$

where the symbol * denotes complex conjugation.

The two unknown complex coefficients C_1 and C_2 are determined from the normalization condition $\vartheta_{st}(0) = 1$ and conditions of continuity for the first and second derivatives in the point $k = 0$, i. e.

$$\frac{d\vartheta_{st}(0^+)}{dk} = \frac{d\vartheta_{st}(0^-)}{dk}, \quad \frac{d^2\vartheta_{st}(0^+)}{dk^2} = \frac{d^2\vartheta_{st}(0^-)}{dk^2}. \tag{2.63}$$

Finally, from these conditions, we find $C_1 = a_1 + ib_1$ and $C_2 = a_2 + ib_2$, where

$$\begin{aligned} a_1 &= \frac{x_2}{x_1 + x_2}\left[1 - \frac{2x_1\,(x_1 - x_2)}{(y_2 - y_1)^2 + (x_2 - x_1)^2}\right], \\ a_2 &= 1 - a_1, \\ b_1 &= \frac{2x_1x_2(y_2 - y_1)}{(x_1 + x_2)\left[(y_2 - y_1)^2 + (x_2 - x_1)^2\right]}, \\ b_2 &= -b_1 \end{aligned} \tag{2.64}$$

and $z_k = -x_k + iy_k$ $(k = 1, 2)$ are the complex roots of equation (2.60) with negative real parts ($x_k > 0$).

Making the inverse Fourier transform, we get the stationary PDF in the case of $\alpha = 1$

$$\begin{aligned} P_{st}(x) &= \frac{1}{2\pi}\int_{-\infty}^{+\infty} \vartheta_{st}(k)e^{-ikx}dk = \frac{1}{\pi}\,\mathrm{Re}\left\{\frac{C_1}{ix - z_1} + \frac{C_2}{ix - z_2}\right\} \\ &= \frac{1}{\pi}\left\{\frac{b_1(x - y_1) + a_1x_1}{(x - y_1)^2 + x_1^2} + \frac{b_2(x - y_2) + a_2x_2}{(x - y_2)^2 + x_2^2}\right\}. \end{aligned} \tag{2.65}$$

The validity of formula (2.65) can be confirmed by comparing with the exact results recently obtained in paper [28] for the symmetric case ($b = 0$).

The potential profile considered and the shapes of the stationary PDFs (2.65), for different values of the noise intensity parameter D_1, are depicted in figure 2.5. For the considered potential, parameters $a = 7$ and $b = 6$, the minima of potential profile are located at the points -2 and 3. As for the symmetric bistable potential, the positions of the minima of the potential and the maxima of the stationary probability distribution do not coincide, as occurs for Brownian diffusion. In [28] it was shown that the distance between the maxima $P_{st}(x)$ and the minima $U(x)$ increases indefinitely with increasing parameter D_1, characterizing the intensity of the noise (and consequently the flight length increases) and decreases with

increasing height of the potential barrier.

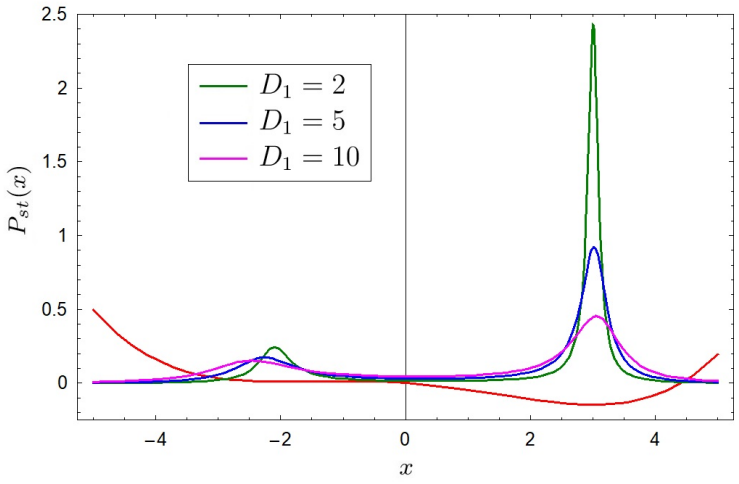

Figure 2.5: Asymmetric bistable quartic potential $U(x)$ (red curve) and stationary PDF $P_{st}(x)$ of the particle position for different values of D_1. The other parameters are: $\gamma = 1$, $a = 7$ and $b = 6$.

The stationary PDFs (2.65) for different values of the asymmetry parameter b are shown in figure 2.6. Here, the maxima shift to the right and to the left with respect to the positions of minima of potential with increasing the asymmetry parameter b. While the left maximum decreases and becomes wider, the right one increases and narrows.

The presence of two maxima or bimodality in the stationary probability distribution is a feature of Lévy flight superdiffusion. In the case of a monostable symmetric potential, i.e. in the absence of a potential barrier, due to the rapid diffusion caused by Lévy flights, the particle very quickly reaches areas near the "walls" of the potential on the left or right with respect to the reference point $x = 0$. Then the particle diffuses around this position until a new flight moves it in the opposite direction and it reaches another "wall" of potential. As a result, the particle spends most of its time in some symmetric regions with respect to the equilibrium state of the system $x = 0$, as opposed to Brownian diffusion in

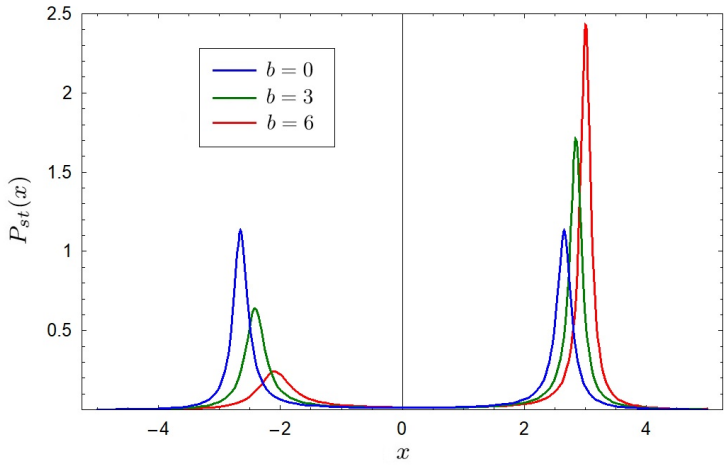

Figure 2.6: Stationary PDF $P_{st}(x)$ for different values of the asymmetry parameter b of the potential. The values of the other parameters are: $\gamma = 1$, $D_1 = 2$ and $a = 7$. The case $b = 0$ corresponds to the symmetric bistable potential.

a monostable potential profile. These symmetric regions are located near the maxima of the bimodal steady-state probability distribution.

In the case of a bistable potential with Gaussian noise, the Brownian particle spends most of its time in the vicinity of local potential minima. In the superdiffusion case, the particle reaches one of the external "walls" of the potential barrier, therefore the potential force brings the particle back into a state of equilibrium. Since the system has two potential minima, the maxima of the probability distribution (PD) move with respect to apart with respect to the maxima of PD for the monostable potential. On other words, these maxima are between the minima and the "walls" of the potential profile and are narrower.

2.3.2 Calculation of correlation time

In this subsection we find the correlation time of steady-state Lévy flights in the symmetric bistable potential, which is determined by the transitions of a particle from one stable state to another, and therefore has an obvious analogy with the

Kramers' time.

Substituting the functional kinetic operator of equation (2.37) into equation (2.25), we get

$$D_\alpha \frac{d^\alpha \phi}{d|x|^\alpha} + \frac{d}{dx}\left[U'(x)\phi\right] = \left(\langle x\rangle_{st} - x\right) P_{st}(x). \tag{2.66}$$

After Fourier transform of equation (2.66) we obtain

$$ikU'\left(\frac{d}{idk}\right)\tilde{\phi} + D_\alpha |k|^\alpha \tilde{\phi} = -\left(\langle x\rangle_{st} + i\frac{d}{dk}\right)\vartheta_{st}(k). \tag{2.67}$$

For $b = 0$ quartic potential (2.55) becomes symmetric and can be written in the following form

$$U(x) = \Delta U\left(1 - \frac{x^2}{a^2}\right)^2, \tag{2.68}$$

where ΔU is the height of a potential barrier separating the two stable states located at the points $\pm a$.

In such a case $\langle x\rangle_{st} = 0$ and equation (2.67) becomes inhomogeneous differential equation of the third order

$$\frac{d^3\tilde{\phi}}{dk^3} + a\frac{d\tilde{\phi}}{dk} - \frac{D_\alpha}{\gamma}|k|^{\alpha-1}\mathrm{sgn}(k)\,\tilde{\phi} = \frac{i}{k\gamma}\frac{d\vartheta_{st}(k)}{dk}, \tag{2.69}$$

where $\gamma = 4\Delta U/a^4$. According to formula (2.28), we have to find only the imaginary part of solution of equation (2.69). Because of the odd function $\varphi(k)$, deriving from the properties of the sine-Fourier transform and the symmetry of the steady-state characteristic function $\vartheta_{st}(k)$, deriving from the symmetry of the potential considered, we can analyze only the case $k \geq 0$, that is to find a particular solution of the following equation

$$\frac{d^3\varphi}{dk^3} + a^2\frac{d\varphi}{dk} - \frac{D_\alpha}{\gamma}k^{\alpha-1}\varphi = \frac{1}{k\gamma}\frac{d\vartheta_{st}(k)}{dk}. \tag{2.70}$$

Equation (2.70) can be solved analytically only in the case of driving noise with the stable Cauchy distribution ($\alpha = 1$). In this case equation (2.70) becomes

$$\frac{d^3\varphi}{dk^3} + a^2\frac{d\varphi}{dk} - \frac{D_1}{\gamma}\varphi = \frac{1}{k\gamma}\frac{d\vartheta_{st}(k)}{dk}, \tag{2.71}$$

where the steady-state characteristic function $\vartheta_{st}(k)$ in the right side of equation has been recently found in the paper [28] and reads

$$\vartheta_{st}(k) = \frac{1}{z - z^*}\left(ze^{z^*|k|} - z^*e^{z|k|}\right). \tag{2.72}$$

Here: z, z^* and $z_3 = p - q$ are three roots of the characteristic cubic equation: $z^3 + a^2z - D_1/\gamma = 0$ for homogeneous differential equation (2.71); $z = -(p - q)/2 + i\sqrt{3}\,(p + q)/2$; z^* and z are complex conjugate, and

$$p = \left(\sqrt{\left(\frac{a^2}{3}\right)^3 + \left(\frac{D_1}{2\gamma}\right)^2} + \frac{D_1}{2\gamma}\right)^{1/3}, \tag{2.73}$$

$$q = \left(\sqrt{\left(\frac{a^2}{3}\right)^3 + \left(\frac{D_1}{2\gamma}\right)^2} - \frac{D_1}{2\gamma}\right)^{1/3} \qquad (p > q).$$

Substitution of equation (2.72) into equation (2.71) gives

$$\frac{d^3\varphi}{dk^3} + a^2\frac{d\varphi}{dk} - \frac{D_1}{\gamma}\varphi = \frac{|z|^2}{k\gamma\,(z - z^*)}\left(e^{z^*k} - e^{zk}\right). \tag{2.74}$$

The general solution of linear differential equation (2.74) can be found by the method of the inverse operator and has the form

$$\varphi(k) = C_1\, e^{zk} + C_2\, e^{z^* k} + C_3\, e^{z_3 k} \tag{2.75}$$
$$+ \frac{|z|^2}{\gamma\,(z - z^*)} \left(\frac{1}{z - z_3}\, e^{zk} \int_0^k e^{(z^* - z)y} \ln y\, dy - \frac{1}{z - z_3}\, e^{z_3 k} \int_0^k e^{(z^* - z_3)y} \ln y\, dy \right.$$
$$\left. - \frac{1}{z^* - z_3}\, e^{z^* k} \int_0^k e^{(z - z^*)y} \ln y\, dy + \frac{1}{z^* - z_3}\, e^{z_3 k} \int_0^k e^{(z - z_3)y} \ln y\, dy \right).$$

Three unknown coefficients C_1, C_2 and C_3 are determined from the properties of Fourier transform and because $\varphi(k)$ is the odd function

$$\lim_{k \to \infty} \varphi\,(k) = 0, \quad \varphi\,(0) = 0, \quad \varphi''\,(0) = 0.$$

Using these conditions in equation (2.75) we arrive at

$$\begin{aligned} &C_1 + C_2 + C_3 = 0, \\ &C_1 z^2 + C_2 z^{*2} + C_3 z_3^2 = 0, \\ &C_3 = \frac{|z|^2}{\gamma\,(z - z^*)} \left(\frac{1}{z - z_3} \int_0^\infty e^{(z^* - z_3)y} \ln y\, dy - \frac{1}{z^* - z_3} \int_0^\infty e^{(z - z_3)y} \ln y\, dy \right). \end{aligned} \tag{2.76}$$

From equation (2.75) we find the first derivative of the function $\varphi(k)$ at the zero point

$$\varphi'(0) = C_1 z + C_2 z^* + C_3 z_3. \tag{2.77}$$

According to the definition of cumulants, we can calculate the variance from equation (2.62) as

$$\langle x, x \rangle_{st} = - \left. \frac{d^2 \ln \vartheta_{st}(k)}{dk^2} \right|_{k=0^+} = |z|^2\,. \tag{2.78}$$

A detailed solution of the equation (2.71) is described in Appendix A.

From equations (2.76)-(2.78) and formula (2.28), after some rearrangements, we obtain the following expression for the correlation time of the particle position in a steady state

$$\tau_c = \frac{1}{\gamma\,(z^2 - z^{*2})}\left[(z - z_3)\int_0^\infty e^{(z-z_3)y}\ln y\,dy - (z^* - z_3)\int_0^\infty e^{(z^*-z_3)y}\ln y\,dy\right].$$

After integrating the expression in the parentheses by parts we arrive at

$$\tau_c = \frac{1}{\gamma\,(z^2 - z^{*2})}\int_0^\infty \frac{e^{z^*y} - e^{zy}}{y}\,e^{-z_3y}\,dy. \tag{2.79}$$

Expressing the roots of the cubic equation z, z^* and z_3 in equation (2.79) in terms of the parameters p and q, we get

$$\tau_c = \frac{2}{\sqrt{3}\,\gamma\,(p^2 - q^2)}\int_0^\infty e^{-\frac{3}{2}(p-q)y}\,\frac{\sin\frac{\sqrt{3}}{2}(p+q)y}{y}\,dy. \tag{2.80}$$

Finally, from equation (2.80) we obtain the exact analytical formula for the correlation time of confined Cauchy-Lévy flights in the symmetric bistable quartic potential

$$\tau_c = \frac{2}{\sqrt{3}\,\gamma\,(p^2 - q^2)}\,\mathrm{arctg}\left(\frac{1}{\sqrt{3}}\,\frac{p+q}{p-q}\right). \tag{2.81}$$

Discussion. It is interesting to analyze the dependence of the correlation time on the height of potential barrier and positions of potential wells. In the limit of sufficiently high potential barrier (or small noise intensity parameter D_1) at fixed positions $\pm a$ of the potential wells

$$\frac{\Delta U}{aD_1} \gg 1,$$

from equations (2.73) and (2.81) we find

$$\tau_c \simeq \frac{\pi a}{2D_1}, \tag{2.82}$$

i. e. the correlation time does not depend on the height of potential barrier.

We try to explain this result using the analogy between the escape time from a metastable state and the correlation time of steady-state diffusion in a bistable potential. Indeed, the correlation time of confined diffusion in a symmetric double-well potential is determined by the fast intrawell motion and slow transitions through a potential barrier. For a sufficiently high barriers a contribution of rare crossing events to the correlation time becomes dominant and we get some temporal characteristic like that of the escape time from a deep potential well. The results of the paper [102], where the characteristic exponential Kramers' factor $e^{\Delta U/D}$ (see [43]) was found in the dependence of the correlation time of steady-state Brownian diffusion in a bistable potential, confirm this analogy. To cross a very high potential barrier, a particle must have a large activation energy D, which is essentially the intensity of the white Gaussian noise. Conversely, a stable Lévy process $\xi_\alpha(t)$ has infinite intensity of jumps and, as a result, a particle can overcome any barrier height by a single flight. A formal substitution of $D = \infty$ into Kramers' factor indicates the independence of the correlation time from the height of a potential barrier for Lévy flights.

Also we should mentioned the result for the mean transition time of Lévy particle from one potential well to another in the symmetric quartic potential with $\gamma = 1$, obtained in [36], in the limit of small noise intensity parameter D_α for arbitrary Lévy index α. The authors of paper [36] have found the expression

$$\langle \tau_{tr} \rangle \simeq \frac{\alpha a^\alpha}{D_\alpha}. \tag{2.83}$$

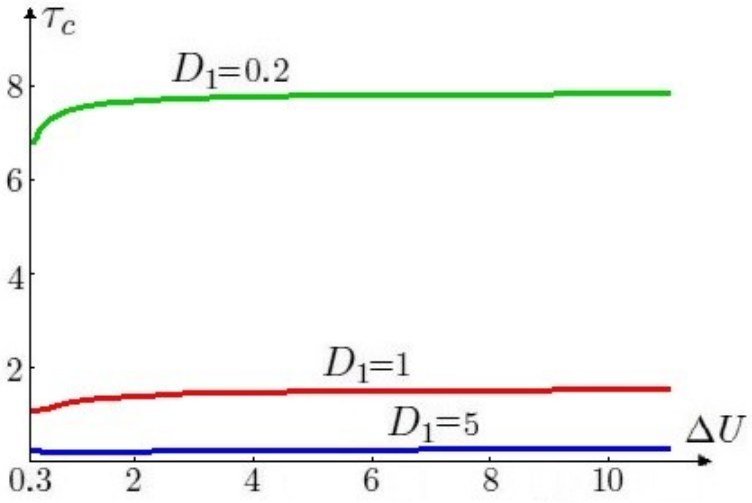

Figure 2.7: The dependence of the correlation time on the height of potential barrier ΔU at fixed positions of potential wells ($a = 1$) for different values of noise intensity parameter D_1.

Equation (2.83) is similar to equation (2.82) in the case $\alpha = 1$.

The dependence of the correlation time on the height of potential barrier ΔU at fixed positions of potential wells for different values of noise intensity parameter D_1, is shown in figure 2.7. This figure confirms a weak dependence of the correlation time on the height of potential barrier and shows a saturation value given by equation (2.82). Thus, we can introduce new Kramers' law for anomalous diffusion in the form of Lévy flights in polynomial potentials, starting by the fractional Fokker-Planck equation (2.37).

The dependence of the correlation time on the distance a between potential wells and potential barrier, at fixed height of a barrier and for different values of noise intensity parameter D_1, is shown in figure 2.8.

As seen from figure 2.8, for sufficiently large distances a we have power-law dependence. Let us find the exponent of this law. Indeed, for sufficiently large a

$$a \gg \frac{\Delta U}{D_1}$$

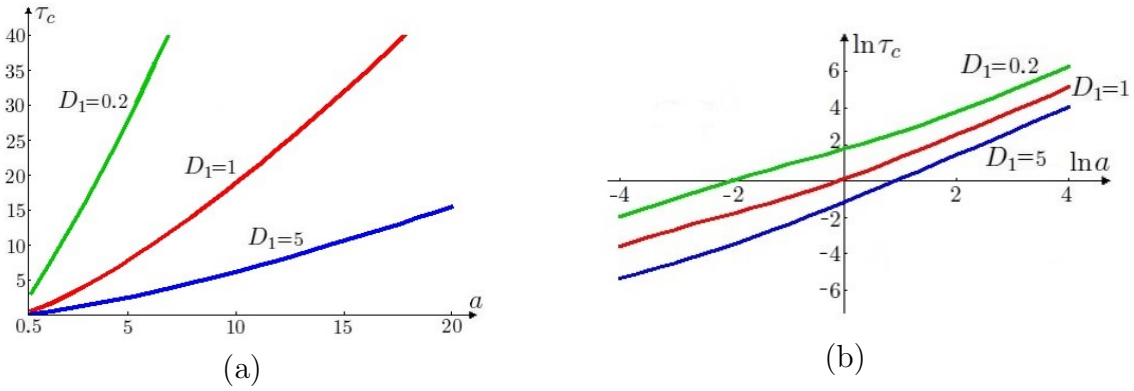

Figure 2.8: The correlation time versus the position of potential wells a in the normal (a) and log-log scale (b) at the fixed height of potential barrier $\Delta U = 0.1$ for different values of the noise intensity parameter D_1.

from equations (2.73) and (2.81) we obtain for the correlation time

$$\tau_c \simeq \frac{\pi}{3\sqrt{3}} \sqrt[3]{\frac{a^4}{4\,\Delta U D_1^2}} \sim a^{4/3}. \tag{2.84}$$

Thus, the correlation time of the particle position increases with the distance of potential wells from a barrier, according to a power law with the exponent 4/3. To explain this behavior we note that, as follows from equation (2.68), with increasing the parameter a at the fixed height of potential barrier, the potential wells move away from the origin simultaneously with decreasing their steepness. As a result, the intrawell motion of a particle becomes slower and the correlation time increases.

As expected, figure 2.9 shows that the correlation time decreases with increasing the noise intensity parameter, but the form of this dependence at the fixed height of potential barrier varies from the hyperbolic (2.82) (see also equation (2.83)), for very small D_1, to a power law $D_1^{-2/3}$ for large D_1, in accordance with equation (2.84). At last, in the absence of a barrier ($\Delta U \to 0$, $a \to 0$, $\gamma = 4\Delta U/a^4$) and from (2.73) we have $p = (D_1/\gamma)^{1/3}$, $q = 0$ and equation (2.81)

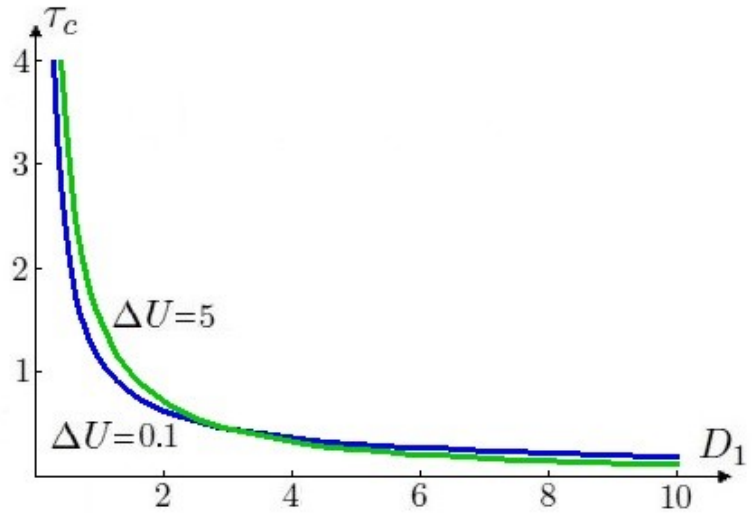

Figure 2.9: The correlation time versus the noise intensity parameter D_1 for different heights of potential barrier ΔU. The positions of potential wells are fixed: $a = 1$.

gives

$$\tau_c \simeq \frac{\pi}{3\sqrt{3}\sqrt[3]{\gamma D_1^2}}. \tag{2.85}$$

Expression (2.85) coincides with the result recently obtained in [31] for the monostable symmetric quartic potential that proves the correctness of these calculations.

Finally, we have to note that the proposed method can be applied, in principle, to analytical calculations of time characteristics of confined Lévy flights in more steep potentials.

2.4 Spectral characteristics of steady-state Lévy flights in monostable confined potential

In this section we consider Lévy flights in the symmetric steep potential well of the following type

$$U(x) = \frac{\gamma}{2m}\left(\frac{x}{L}\right)^{2m}, \tag{2.86}$$

where L is the width of the potential well.

For this potential profile, as shown in [27], the stationary probability distribution of the particle displacement for anomalous diffusion in the form of Lévy flights with index $\alpha = 1$ has the following expressions for odd $m = 2n + 1$

$$P_{st}(x) = \frac{\beta^{4n+1}}{\pi(x^2+\beta^2)} \prod_{l=0}^{n-1} \frac{1}{x^4 - 2\beta^2 x^2 \cos\left[\pi(4l+1)/(4n+1)\right] + \beta^4} \tag{2.87}$$

and for even $m = 2n$

$$P_{st}(x) = \frac{\beta^{4n-1}}{\pi} \prod_{l=0}^{n-1} \frac{1}{x^4 - 2\beta^2 x^2 \cos\left[\pi(4l+1)/(4n-1)\right] + \beta^4}, \tag{2.88}$$

where $\beta = L\sqrt[2m-1]{D_1 L/\gamma}$ and D_1 is the intensity parameter of the noise with stable Cauchy distribution.

In the limit of very large exponent m, the potential (2.86) transforms to an infinitely deep rectangular potential well (see figure 2.10)

$$U(x) = \begin{cases} 0, & |x| \le L, \\ \infty, & |x| > L. \end{cases} \tag{2.89}$$

To make this limit in equations (2.87) and (2.88) we need to rearrange them into

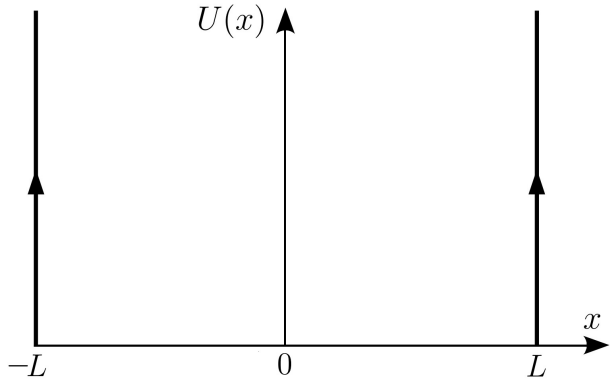

Figure 2.10: Infinitely deep rectangular potential well.

a more convenient form (see Appendix B)

$$P_{st}(x) = \begin{cases} \frac{1}{\pi\beta} \exp\left\{ \sum\limits_{k=1}^{\infty} \frac{1}{2k \cos\frac{\pi k}{2m-1}} \left(\frac{x}{\beta}\right)^{2k} \right\}, & |x| \le \beta, \\ \frac{1}{\pi\beta} \left(\frac{\beta}{x}\right)^{2m} \exp\left\{ \sum\limits_{k=1}^{\infty} \frac{1}{2k \cos\frac{\pi k}{2m-1}} \left(\frac{\beta}{x}\right)^{2k} \right\}, & |x| > \beta. \end{cases} \tag{2.90}$$

In the limit $m \to \infty$, the steady-state probability distribution (2.90) transforms to the arcsine distribution (see the curve with $\alpha = 1$ in figure (2.11))

$$P_{st}(x) = \begin{cases} \frac{1}{\pi} \frac{1}{\sqrt{L^2 - x^2}}, & |x| \le L, \\ 0, & |x| > L. \end{cases} \tag{2.91}$$

The validity of this transformation can be confirmed by comparing equation (2.91) with the exact results obtained in [29] for arbitrary Lévy index α

$$P_{st}(x) = \frac{(2L)^{1-\alpha}\,\Gamma(\alpha)}{\Gamma^2(\alpha/2)(L^2 - x^2)^{1-\alpha/2}}, \tag{2.92}$$

Note that formula (2.92) was derived by using the special conditions for impermeable boundaries at $x = \pm L$.

The stationary probability densities (2.92) for different values of the Lévy index α, are depicted in figure 2.11. Points in the figure have been obtained

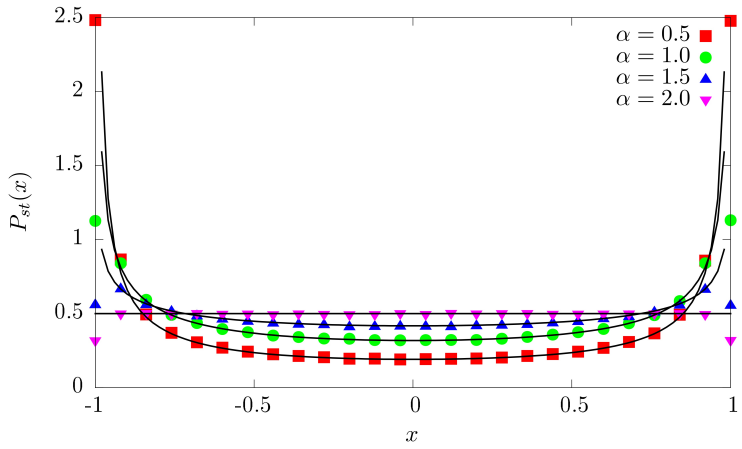

Figure 2.11: Stationary probability densities $P_{st}(x)$ for different values of the Lévy index α. The value of the parameters are: $\gamma = 1$, $D_\alpha = 1$ and $L = 1$.

by numerically integration of the stochastic differential equation (2.34), with Lévy noise source, and applying the Euler-Maruyama method within the Ito scheme [115; 116]. More precisely, a large number of very long realizations of the stochastic process $x(t)$ is generated. From these realizations the time dependent densities $P(x,t)$ are estimated. Finally, the stationary density $P_{st}(x)$ is approximated.

The case $\alpha = 2$ corresponds to usual Brownian motion. In such a case the steady-state probability distribution of particle position

$$P_{st}(x) = C_0\, e^{-U(x)/D}, \tag{2.93}$$

is of the Boltzmann-Gibbs type and for the infinitely deep rectangular potential well becomes uniform (C_0 is the normalization constant). As noted above, the infinitely deep rectangular potential well can be achieved from equation (2.86) in the limit of $m \to \infty$. Practically, such a convergence is quite fast and with $m = 800$ we obtain a very good agreement between numerical simulations and exact formula (2.92), except the points close to the boundaries (see figure 2.11).

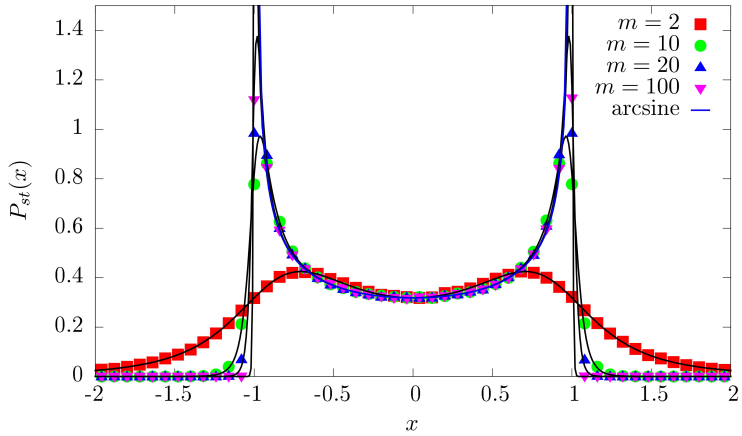

Figure 2.12: Stationary probability distributions $P_{st}(x)$ for $\alpha = 1$ and increasing exponent m (see (2.86)–(2.88)). The values of the other system parameters are the same as those of figure 2.11.

In figure 2.12 we show the stationary probability density functions for $\alpha = 1$, obtained with increasing exponent m. Exact results, which are given by equation (2.88), are represented by solid lines. Points correspond to results of Monte Carlo simulations of the Langevin equation (2.34) with the potential (2.86). In the limit of $m \to \infty$, the stationary probability density function tends to the arcsine distribution of equation (2.91). Figure 2.12 demonstrates how we can obtain the stationary probability distributions in the infinitely deep rectangular potential well, starting from a steep potential and without considering the problem of the boundary conditions.

The steady-state spectral characteristics of Lévy flights with potential profile (2.86) can not be obtained analytically for arbitrary Lévy index α, in contrast to asymptotic expression of the spectral power density of steady-state Lévy flights. From equations (2.18), (2.37), (2.86) and (2.90) for $\alpha = 1$ we get the first derivative of the steady-state correlation function at zero point

$$K'\left[0^{+}\right] = \left\langle x\hat{L}^{+}\left(x\right)x\right\rangle = -\left\langle xU'(x)\right\rangle = -\gamma\left\langle\left(\frac{x}{L}\right)^{2m}\right\rangle = -\infty. \tag{2.94}$$

This result differs from the result for ordinary Brownian motion ($\alpha = 2$), for which from equations (2.18), (2.36) and (2.93) we have

$$K'[0^+] = -D.$$

Figure 2.13 demonstrates the normalized autocorrelation functions $K[\tau]$ for different values of the exponent m (see (2.86)) at a fixed Lévy index α. As seen, the decay of the correlation function accelerates as the value of Lévy index α decreases, i. e. its derivative decreases rapidly when approaching the point $\tau = 0$. Furthermore, figure 2.13(c) shows that for the symmetric power potential $K'[0^+] = -\infty$, as predicted by the formula (2.94). This asymptotic behavior becomes more noticeable for small Lévy index α.

In accordance with formula (2.94), we can assume a non-analytical dependence of the correlation function on τ near the point $\tau = 0^+$ in the form of stretched exponent

$$K\left[\tau\right] \simeq \sigma^2 \exp\left\{-\left(\frac{\tau}{\tau_0}\right)^{\nu}\right\} \simeq \sigma^2 \left[1 - \left(\frac{\tau}{\tau_0}\right)^{\nu}\right], \qquad 0 < \nu < 1. \tag{2.95}$$

Applying the Laplace transform to equation (2.95), we arrive at

$$\tilde{K}[p] \simeq \sigma^2 \left[\frac{1}{p} - \frac{\Gamma(1+\nu)}{\tau_0^{\nu}\, p^{1+\nu}}\right], \qquad p \to \infty. \tag{2.96}$$

Substitution of equation (2.96) into equation (2.30) gives the following asymptotic expression of the spectral power density

$$S(\omega) \sim \frac{1}{\omega^{1+\nu}}, \qquad \omega \to \infty. \tag{2.97}$$

The exponent ν is a function of the potential exponent m, noise intensity parameter D_α, Lévy index α, steepness of potential γ and size of the potential well

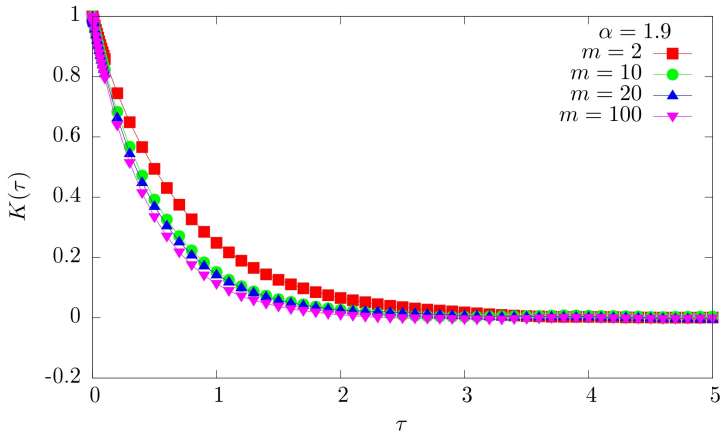

(a)

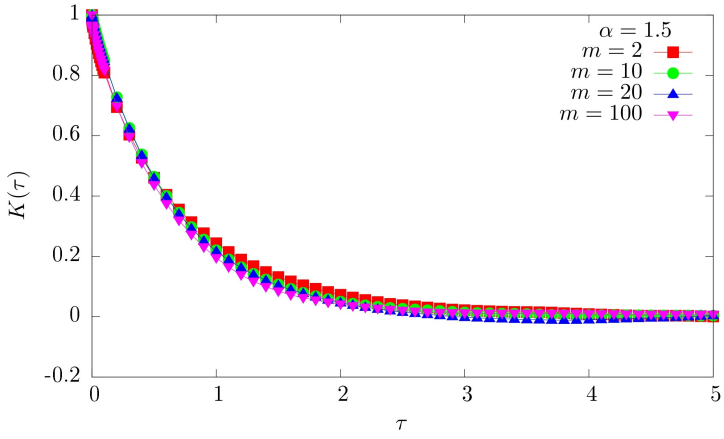

(b)

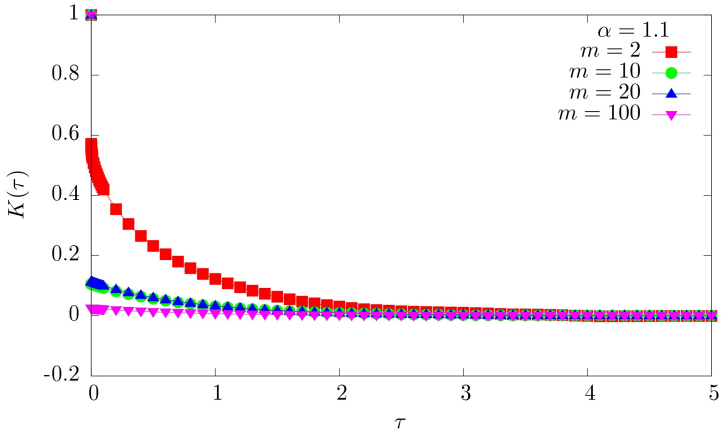

(c)

Figure 2.13: The correlation function for $\alpha = 1.9$ (a), $\alpha = 1.5$ (b) and $\alpha = 1.1$ (c). Various curves correspond to different values of the exponent m of potential (2.86). The values of the other system parameters are the same as those of figure 2.11.

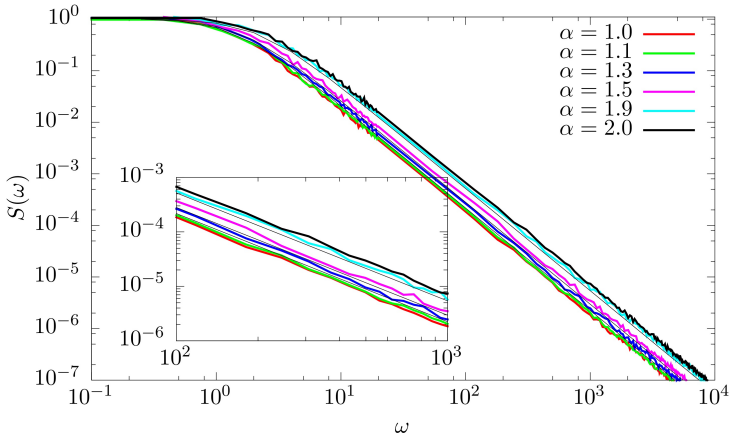

Figure 2.14: The spectral power density for $m = 100$ and for different values of the Lévy index α in log-log scale.

L.

In figure 2.13 one can see the best fitting of the normalized correlation function $K[\tau]$ to the stretched exponential function (2.95), obtained by numerical simulation of the Langevin equation (2.34) with the potential profile (2.86) and calculated at different values of the exponent m. The values of σ^2, τ_0, and ν derived from the fitting procedures are given in table 2.1.

α	σ^2	τ_0	ν
1.0	0.342 ± 0.008	0.608 ± 0.062	0.686 ± 0.057
1.1	$0.025 \pm 3\times10^{-5}$	0.790 ± 0.003	0.975 ± 0.005
1.3	0.950 ± 0.001	0.702 ± 0.003	0.987 ± 0.006
1.5	0.967 ± 0.001	0.622 ± 0.002	0.980 ± 0.004
1.9	0.999 ± 0.001	0.452 ± 0.002	0.984 ± 0.005

Table 2.1: Values of stretched exponential parameters fitted to the normalized correlation function.

Figure 2.14 displays the spectral power density obtained by numerical simulation of Langevin equation (2.34) with the potential profile of equation (2.86) for $m = 100$ and for different values of the Lévy index α. Thin black lines re-

fer to spectral power densities for $\alpha = 1.3$, 1.5 and 1.9 estimated, starting from the fitted stretched exponent given in equation (2.96) and calculating its Fourier transform. Trajectories have been constructed by the Langevin dynamics with the integration step $\Delta t = 10^{-6}$. Every trajectory $x(t)$ consists of 2^{24} elements. Spectral power densities has been averaged over 300 realizations. In all simulations we fixed a noise intensity parameter to $D_\alpha = 1$. The agreement between these curves and those calculated by direct simulation of the corresponding Langevin equation is very good.

2.5 Probabilistic characteristics of diffusion in 2D potentials

As it has been emphasized above, the analytical analysis of the temporal, spectral and correlation characteristics of anomalous diffusion in the form of Lévy flights still remains a complex problem even for the one-dimensional case. Here, we study the probabilistic characteristics of diffusion in two-dimensional potentials.

According to Newton's dynamics, the motion of a particle in a viscous medium in the potential profile $U(x, y)$ under the action of random external forces in a two-dimensional plane can be described by a system of equations

$$\begin{aligned} m\ddot{x} + \nu\dot{x} &= -U_x^{'}(x, y) + \xi_1(t), \\ m\ddot{y} + \nu\dot{y} &= -U_y^{'}(x, y) + \xi_2(t), \end{aligned} \tag{2.98}$$

where $x(t)$ and $y(t)$ are the particle coordinates on the plane (x, y), m is a particle mass, ν is a coefficient of viscosity, and $\xi_1(t)$ and $\xi_2(t)$ are external random forces. The particle acceleration (inertial effects) can be neglected if the viscosity coefficient is large enough. In such a case, we arrive at the following system of overdamped Langevin equations describing the diffusion of the particle in an arbitrary two-dimensional potential $U(x, y)$

$$\begin{aligned} \dot{x} &= -U_x^{'}(x, y) + \xi_1(t), \\ \dot{y} &= -U_y^{'}(x, y) + \xi_2(t), \end{aligned} \tag{2.99}$$

where $\xi_1(t)$ and $\xi_2(t)$ are arbitrary statistically independent white noise sources with zero means $\langle \xi_1(t) \rangle = \langle \xi_2(t) \rangle = 0$, and we put $\nu = 1$.

To obtain a closed equation for the joint probability density function of random Markovian processes $x(t)$ and $y(t)$ which can be written in the form of the

average

$$P(x,y,t) = \langle \delta(x - x(t))\delta(y - y(t)) \rangle, \tag{2.100}$$

we apply the functional method developed in [3].

Differentiating both sides of equation (2.100) with respect to time and using equations (2.99), we arrive at

$$\begin{aligned}
\frac{\partial P}{\partial t} &= \frac{\partial}{\partial t} \langle \delta(x - x(t))\delta(y - y(t)) \rangle \\
&= -\left\langle \frac{\partial}{\partial x}\delta(x - x(t))\dot{x}(t)\delta(y - y(t)) \right\rangle - \left\langle \frac{\partial}{\partial y}\delta(y - y(t))\dot{y}(t)\delta(x - x(t)) \right\rangle \\
&= -\frac{\partial}{\partial x}\left\langle \left[-U_x^{'} + \xi_1(t)\right] \delta(x - x(t))\delta(y - y(t)) \right\rangle \\
&- \frac{\partial}{\partial y}\left\langle \left[-U_y^{'} + \xi_2(t)\right] \delta(y - y(t))\delta(x - x(t)) \right\rangle \\
&= \frac{\partial}{\partial x}\left(\frac{\partial U}{\partial x}P\right) + \frac{\partial}{\partial y}\left(\frac{\partial U}{\partial y}P\right) - \frac{\partial}{\partial x}\langle \xi_1(t)\delta(x - x(t))\delta(y - y(t)) \rangle \\
&- \frac{\partial}{\partial y}\langle \xi_2(t)\delta(x - x(t))\delta(y - y(t)) \rangle .
\end{aligned}$$

To split a correlation between a stochastic functional and the processes $\xi_i(t)$ $(i = 1, 2)$ we use the following formula (see equation (10) in the paper [3])

$$\begin{aligned}
&\langle \xi_i(t)\delta(x - x(t))\delta(y - y(t)) \rangle \\
&= \int_{-\infty}^{+\infty} \frac{\rho_i(z)}{z^2}\ dz \int_0^z \left\langle \left(e^{k\frac{\delta}{\delta\xi_i(t)}} - 1\right) \delta(x - x(t))\delta(y - y(t)) \right\rangle dk,
\end{aligned}$$

where $\rho_i(z)$ are the kernel functions determining the statistics of white noises $\xi_i(t)$.

Using the equivalence of operators $\dfrac{\delta}{\delta\xi_1(t)}$ and $\left(-\dfrac{\partial}{\partial x}\right)$, $\dfrac{\delta}{\delta\xi_2(t)}$ and $\left(-\dfrac{\partial}{\partial y}\right)$ with respect to the product $\delta(x - x(t))\delta(y - y(t))$, which follows from Langevin

equations (2.98) we get the general Kolmogorov equation for the joint PDF

$$\begin{aligned}\frac{\partial P(x,y,t)}{\partial t} &= \frac{\partial}{\partial x}\left(\frac{\partial U}{\partial x}P(x,y,t)\right) + \frac{\partial}{\partial y}\left(\frac{\partial U}{\partial y}P(x,y,t)\right) \\ &+ \int_{-\infty}^{+\infty}\frac{\rho_1(z)}{z^2}\left(e^{-z\frac{\partial}{\partial x}} - 1 + z\frac{\partial}{\partial x}\right)P(x,y,t)dz \\ &+ \int_{-\infty}^{+\infty}\frac{\rho_2(z)}{z^2}\left(e^{-z\frac{\partial}{\partial y}} - 1 + z\frac{\partial}{\partial y}\right)P(x,y,t)dz. \end{aligned} \tag{2.101}$$

Further we find the steady-state joint probability distribution in the potential with radial symmetry $U(r)$ ($r = \sqrt{x^2+y^2}$) in the case of two identical noises $\xi_1(t)$ and $\xi_2(t)$.

2.5.1 Gaussian white noise sources

In the case of two Gaussian white noises with equal intensities: $\rho_1(z) = \rho_2(z) = 2D\delta(z)$ equation (2.101) transforms into usual Fokker-Planck equation

$$\frac{\partial P}{\partial t} = \mathrm{div}(P\mathrm{grad}U) + D\Delta P, \tag{2.102}$$

which can be written in polar coordinates as

$$\frac{\partial P}{\partial t} = \frac{1}{r}\frac{\partial}{\partial r}\left(rU_r^{'}P\right) + \frac{1}{r^2}\frac{\partial}{\partial \varphi}\left(U_\varphi^{'}P\right) + \frac{D}{r}\frac{\partial}{\partial r}\left(r\frac{\partial P}{\partial r}\right) + \frac{D}{r^2}\frac{\partial^2 P}{\partial \varphi^2}. \tag{2.103}$$

In the steady-state regime ($t \to \infty$), for potential $U(r)$ with radial symmetry, the steady-state distribution does not depend on the angle φ, therefore equation (2.103) gives

$$\frac{1}{r}\frac{d}{dr}\left(rU_r^{'}P_{st}\right) + \frac{D}{r}\frac{d}{dr}\left(r\frac{dP_{st}}{dr}\right) = 0. \tag{2.104}$$

Thus, the steady-state distribution for additive Gaussian noises is of the Boltzmann-Gibbs type

$$P_{st}(x,y) = Ce^{-\frac{U(r)}{D}}, \tag{2.105}$$

where the normalization constant C can be calculated as

$$C = \left(2\pi \int_0^\infty r\, e^{-\frac{U(r)}{D}} dr\right)^{-1},$$

and $r = \sqrt{x^2+y^2}$.

As an example of a potential with radial symmetry, we consider the parabolic potential $U(x,y) = \gamma(x^2+y^2)/2 = \gamma r^2/2$. In this case the joint steady-state probability distribution (2.105) takes the form

$$P_{st}(x,y) = \frac{\gamma}{2\pi D}\, e^{-\frac{\gamma(x^2+y^2)}{2D}}. \tag{2.106}$$

Figure 2.15 shows the 2D-plot of the steady-state joint PDF (2.106) in the parabolic potential $U(x,y) = \gamma(x^2+y^2)/2$ and illustrates its radial symmetry property in the case of two-dimensional Brownian diffusion.

2.5.2 Lévy noise sources

For the case of two identical Lévy noise sources with kernel function $\rho(z) = K|z|^{1-\alpha}$ equation (2.101) takes the following form

$$\begin{aligned}\frac{\partial P}{\partial t} &= \frac{\partial}{\partial x}\left(\frac{\partial U}{\partial x}P\right) + \frac{\partial}{\partial y}\left(\frac{\partial U}{\partial y}P\right) \\ &\quad + K\int_{-\infty}^{+\infty} \frac{1}{|z|^{\alpha+1}}\left(P(x-z,y,t) + P(x,y-z,t)\ -2P(x,y,t)\right) dz \\ &= \mathrm{div}(P\mathrm{grad}U) + D_\alpha \nabla^\alpha P(x,y,t),\end{aligned} \tag{2.107}$$

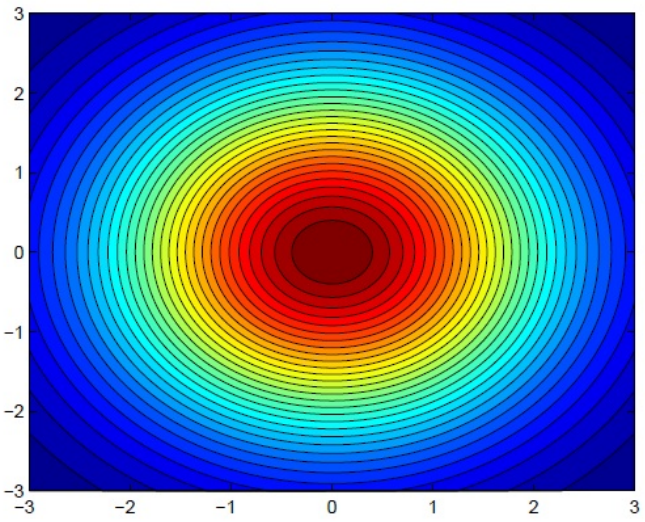

Figure 2.15: 2D-plot of steady-state joint PDF for the harmonic potential $U(x,y) = \gamma(x^2+y^2)/2$ in the case of white Gaussian driving noises. The values of parameters are $D = 5$, $\gamma = 2$.

where $D_\alpha = \dfrac{K\pi}{\Gamma(\alpha+1)\sin(\pi\alpha/2)}$ and $\nabla^\alpha = \dfrac{\partial^\alpha}{\partial|x|^\alpha} + \dfrac{\partial^\alpha}{\partial|y|^\alpha}$ is the fractional Laplacian.

After two-dimensional Fourier transform of equation (2.107) (see Appendix C) we arrive at the following equation for the joint characteristic function of coordinates $\Theta(k,q,t)$

$$\frac{\partial\Theta(k,q,t)}{\partial t} = -ikU_x'\left(-i\frac{\partial}{\partial k}, -i\frac{\partial}{\partial q}\right)\Theta(k,q,t) - iqU_y'\left(-i\frac{\partial}{\partial k}, -i\frac{\partial}{\partial q}\right)\Theta(k,q,t) - D_\alpha\left(|k|^\alpha + |q|^\alpha\right)\Theta(k,q,t). \tag{2.108}$$

Equation (2.108) generalizes the results obtained in [117] for 2D harmonic potential and the bivariate α-stable noise.

Equation for stationary characteristic function has the following form

$$ikU_x^{'}\left(-i\frac{\partial}{\partial k},-i\frac{\partial}{\partial q}\right)\Theta_{st}(k,q)+iqU_y^{'}\left(-i\frac{\partial}{\partial k},-i\frac{\partial}{\partial q}\right)\Theta_{st}(k,q)$$
$$+D_\alpha\left(|k|^\alpha+|q|^\alpha\right)\Theta_{st}(k,q)=0. \tag{2.109}$$

In the case of the parabolic potential $U(x,y)=\gamma(x^2+y^2)/2$ Langevin equations (2.98) become

$$\begin{aligned}\dot{x}&=-\gamma x+\xi_1(t),\\ \dot{y}&=-\gamma y+\xi_2(t)\end{aligned} \tag{2.110}$$

and are independent.

The joint PDF splits into the product of separate probability density functions due to statistical independence of random processes $x(t)$ and $y(t)$, and, as a consequence, the joint characteristic function also splits into the product of separate characteristic functions. Thereby, we seek a solution of equation (2.109) in the following form

$$\Theta_{st}(k,q)=\vartheta_{st}(k)\cdot\vartheta_{st}(q)$$

and obtain the following differential equation

$$k\gamma\vartheta_{st}(q)\frac{d\vartheta_{st}(k)}{dk}+q\gamma\vartheta_{st}(k)\frac{d\vartheta_{st}(q)}{dq}+D_\alpha\left(|k|^\alpha+|q|^\alpha\right)\vartheta_{st}(k)\cdot\vartheta_{st}(q)=0.$$

Applying the standard method of separation of variables with condition $\vartheta_{st}(0)=1$, we finally arrive at

$$\Theta_{st}(k,q)=\exp\left\{-\frac{D_\alpha}{\gamma\alpha}\left(|k|^\alpha+|q|^\alpha\right)\right\}. \tag{2.111}$$

As well known [6], the entire class of stable probability distribution $P_{\alpha,\beta}(x)$

has the following characteristic function

$$\vartheta_{\alpha,\beta}(k) = \exp\{-|k|^{\alpha} e^{\frac{i\pi\beta}{2}\mathrm{sgn}k}\}, \tag{2.112}$$

where α is Lévy index ($0 < \alpha < 2$), β is the parameter of asymmetry ($|\beta| \leq 1 - |\alpha - 1|$). In the symmetry case ($\beta = 0$) the corresponding stable probability distribution can be calculate by inverse Fourier transform of characteristic function (2.112)

$$P_{\alpha,0}(z) = \frac{1}{2\pi} \int_{-\infty}^{+\infty} e^{-|k|^{\alpha} - ikz} dk. \tag{2.113}$$

Therefore, from equation (2.111) the steady-state joint PDF can be written in the following form

$$\begin{aligned} P_{st}(x,y) &= \frac{1}{4\pi^2} \int_{-\infty}^{+\infty} \int_{-\infty}^{+\infty} \Theta_{st}(k,q) e^{-ikx - iqy} dk dq \\ &= \frac{1}{2\pi} \int_{-\infty}^{+\infty} e^{-\frac{D_\alpha}{\gamma\alpha}|k|^{\alpha} - ikx} dk \cdot \frac{1}{2\pi} \int_{-\infty}^{+\infty} e^{-\frac{D_\alpha}{\gamma\alpha}|q|^{\alpha} - iqy} dq. \end{aligned}$$

Using (2.113), we finally obtain the following expression for arbitrary α

$$P_{st}(x,y) = \left(\frac{\gamma\alpha}{D_\alpha}\right)^{2/\alpha} \cdot P_{\alpha,0}\left(\left(\frac{\gamma\alpha}{D_\alpha}\right)^{1/\alpha} x\right) \cdot P_{\alpha,0}\left(\left(\frac{\gamma\alpha}{D_\alpha}\right)^{1/\alpha} y\right). \tag{2.114}$$

According to equation (2.113), for the Cauchy noise ($\alpha = 1$)

$$P_{1,0}(z) = \frac{1}{2\pi} \int_{-\infty}^{+\infty} e^{-|k| - ikz} dk \tag{2.115}$$

and from equation (2.114), we arrive at

$$P_{st}(x,y) = \left(\frac{\gamma D_1}{\pi}\right)^2 \frac{1}{(D_1^2 + \gamma^2 x^2)(D_1^2 + \gamma^2 y^2)}. \tag{2.116}$$

The 2D-plots of steady-state joint PDF (2.116) in the parabolic potential

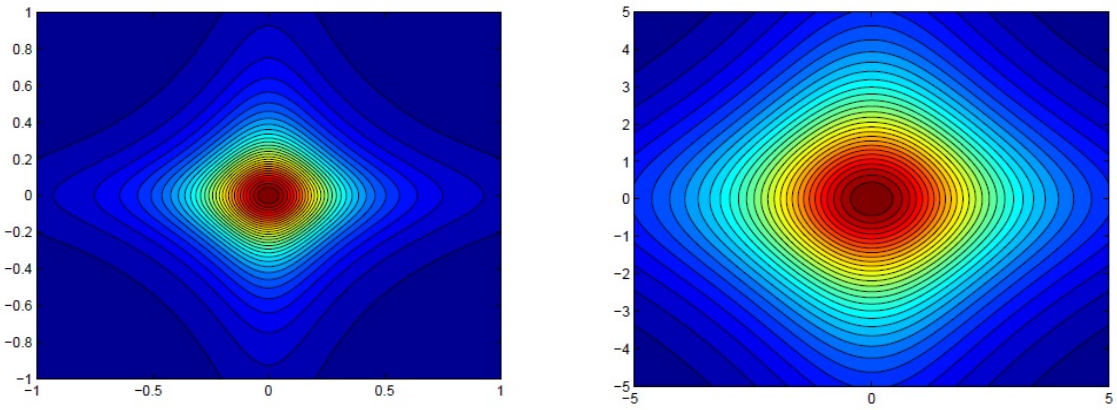

(a) $D_1 = 0.5$ (b) $D_1 = 5$

Figure 2.16: 2D-plot of steady-state joint PDF for the harmonic potential $U(x, y) = \gamma(x^2 + y^2)/2$ subject to the Cauchy stable noises with (a) $D_1 = 0.5$ and (b) $D_1 = 5$. The value of parameter γ is 2.

$U(x, y) = \gamma(x^2 + y^2)/2$ for different values D_1 are shown in figure 2.16. Unlike the steady-state joint PDF for Gaussian noises (2.106), two-dimensional Lévy flights do not possess property of radial symmetry due to independence of flights in perpendicular directions. It should be noted that if we consider the quartic potential $U(x, y) = \gamma(x^2 + y^2)^2/4$ as a potential with radial symmetry, the system of Langevin equations (2.98) does not decay into independent equations as in the case of the harmonic potential. This is a natural consequence of the fact that the motion along the axes is no longer independent, despite the independence of the noise components.

The violation of the radial symmetry of the probability distribution was first discovered by the authors of [117] for a noise source with a discrete spectral measure by means of numerical simulations. The authors also showed that if the sources are correlated in a special way, the particle flights will be isotropic and the distribution will retain the radial symmetry inherent in the potential under consideration.

Chapter 3

Stochastic approach to the description of memristors

Summary

This chapter presents the study of stochastic models of memristor. In section 3.1 the simplest model of resistive switching is considered. In section 3.2 the models of the charge-controlled and the current-controlled ideal memristors are presented. Finally, in section 3.3 we propose a stochastic model of a memristive system based on a generalization of known approaches and experimental results.

3.1 Resistive switching model

First of all, we study the macro model of the resistive switching. All two-terminal non-volatile memory devices based on resistive switching (or resistance change) are memristors, regardless of the device material and physical operating mechanisms. They all are characterized by a pinched hysteresis loop confined to the first and the third quadrants of the current-voltage plane, whose contour shape

in general changes with both the amplitude and frequency of any periodic input voltage or current source.

For the simplest resistive switching model the current $I(t)$ and the voltage $U(t)$ are connected by the following relation [118]

$$I(t) = \frac{U(t)}{R(U(t))} = G(U(t))\,U(t), \tag{3.1}$$

where $R(t)$ and $G(t)$ are the resistance and the conductivity respectively. We propose to construct a model in which the resistance depends only on the voltage derivative $U'(t)$. In this case the resistance change can be specified by the sign function, which corresponds to the two states of the memristor with high $R_H = a + b$ and low $R_L = a - b$ resistance $(a > b)$

$$R(U'(t)) = a + b\,\mathrm{sgn}(U'(t)), \quad |U(t)| \le U_{th}, \tag{3.2}$$

where U_{th} is the threshold voltage of memristor.

In this case, equation (3.1)

$$\begin{aligned} I(t) &= \frac{a}{a^2 - b^2}U(t) - \frac{b}{a^2 - b^2}\mathrm{sgn}(U^{'}(t))U(t) \\ &= \frac{A}{2}(G_H + G_L)U(t) - \frac{A}{2}(G_H - G_L)\,\mathrm{sgn}(U^{'}(t))U(t), \quad |I(t)| \le G_H U_{th} \end{aligned} \tag{3.3}$$

where we introduce new variables – high and low conductivities

$$\begin{aligned} \frac{a}{a^2 - b^2} &= \frac{1}{2}\left(G_H + G_L\right), \\ \frac{b}{a^2 - b^2} &= \frac{1}{2}\left(G_H - G_L\right). \end{aligned}$$

The current-voltage characteristic is depicted on figure 3.1 and can be considered as an approximation of the $I - V$ curve of a real memristor.

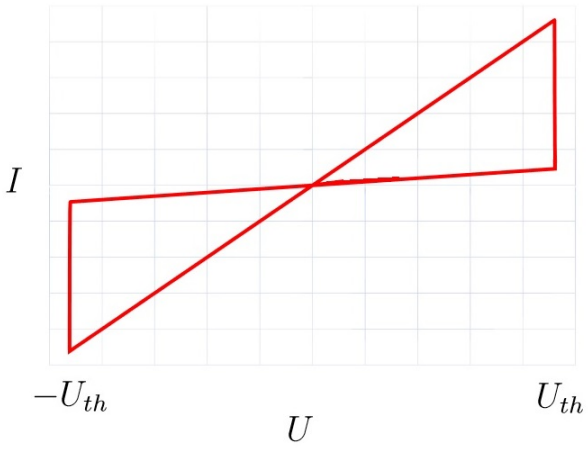

Figure 3.1: Current-voltage characteristic of the resistive switching model.

Harmonic signal.– Firstly, we choose the harmonic signal as the input

$$U(t) = A \sin \omega t, \tag{3.4}$$

where $A = U_{th}$ and observe how the spectral composition of the current changes at the output of the resistor.

Based on trigonometric Fourier series expansion, we obtain the following expression for the current

$$I(t) = \frac{A}{2}(G_H + G_L) \sin \omega t - \frac{A}{2}(G_H - G_L) \sum_{k=0}^{\infty} (-1)^{k+1} \frac{8k}{\pi(4k^2 - 1)} \sin 2k\omega t. \tag{3.5}$$

Figure 3.2 demonstrates the plots of the applied sinusoidal voltage (3.4) and resulting current (3.5). As one can note, there are the basic harmonic and even harmonics of the basic frequency at the output.

Sawtooth signal.– Secondly, we consider a sawtooth signal with a period $T = \frac{2\pi}{\omega}$ and an amplitude U_0 (see figure 3.3(a)). In this case we have to decompose in the Fourier series both the signal and its product on the sign function. The

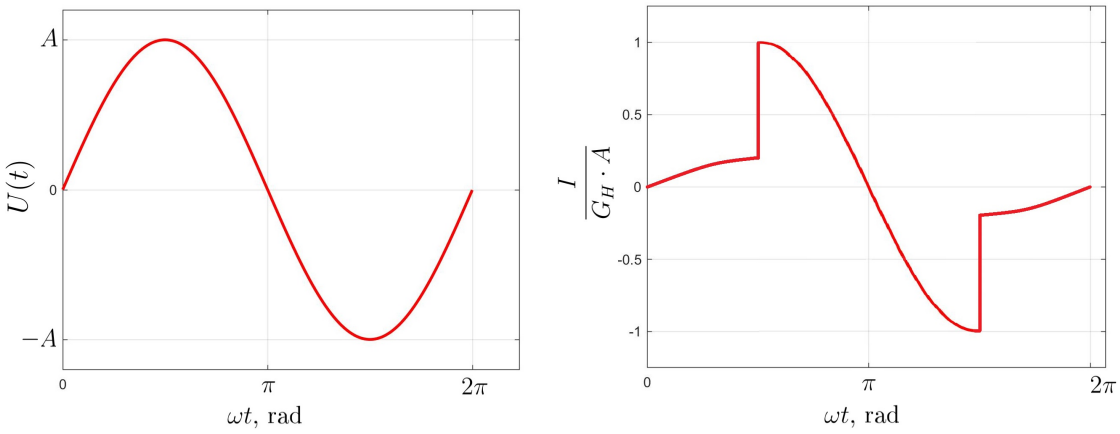

Figure 3.2: The applied sinusoidal voltage (a) and resulting current (b) as a function of ωt.

final expression reads as

$$I(t) = \frac{1}{2}(G_H + G_L)\sum_{k=0}^{\infty}\frac{8U_0}{\pi^2(2k+1)^2}(-1)^{k+1}\sin(2k+1)\omega t$$
$$-\frac{1}{2}(G_H - G_L)\sum_{k=1}^{\infty}\frac{2U_0}{\pi k}(-1)^{k+1}\sin 2k\omega t. \tag{3.6}$$

The applied sawtooth voltage and resulting current (3.6) are shown in figure 3.3. In this case the current includes both even and odd harmonics of the basic frequency. The main limitation of the considered model is the monotonic variation of the applied voltage between the lower and upper thresholds values.

We can conclude that the appearance of even harmonics regardless of the signal type illustrates the properties of the considered nonlinear device.

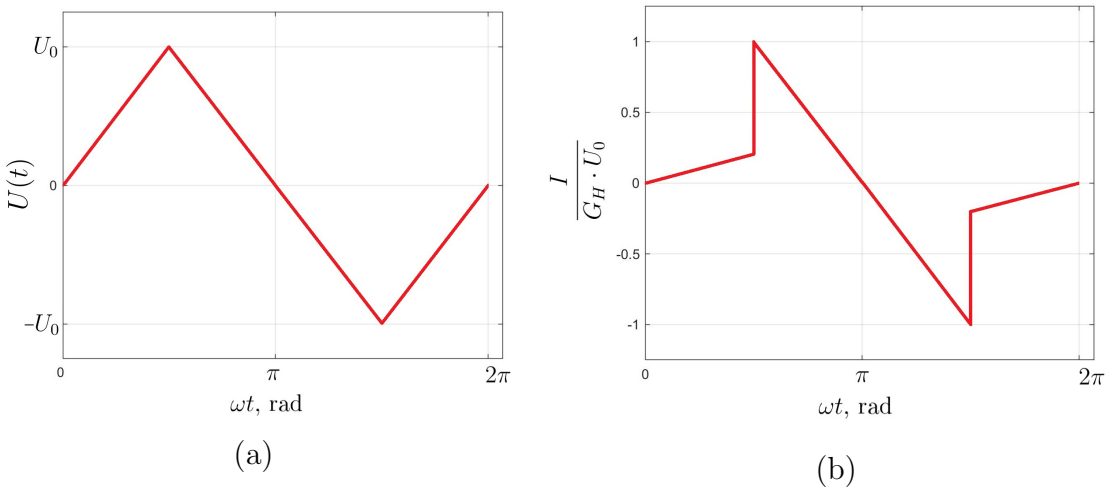

Figure 3.3: The applied sawtooth voltage (a) and resulting current (b) as a function of ωt.

3.2 Ideal memristor model under Gaussian noise

In this section we demonstrate how the Gaussian fluctuations of the applied voltage or current may change the memristors state. These changes are indicated on an example of the ideal memristor using the probability characteristics of its resistance.

The simplest model of a memory device is the so-called ideal memristor proposed by Leon Chua in [48; 76]. For this nonlinear element of electrical circuit the Ohm's law and the associated equations of state are written as follows

$$U(t) = R(q)I(t), \quad I(t) = \frac{dq}{dt}, \tag{3.7}$$

where $U(t)$, $I(t)$ and $q(t)$ are the voltage, the current and the charge on the memristor respectively. Equations (3.7) describe the charge-controlled memristor which resistance $R(q)$ depends on the charge. As follows from equation (3.7), the ideal memristor is an integrable model and, hence, can be defined by an equivalent

algebraic relation

$$w(t) = \int_0^t U(t)dt = \int_0^{q(t)} R(q)dq = \Phi(q(t)). \tag{3.8}$$

First of all, we apply to the memristor a stochastic voltage $U(t)$ in the form of a stationary Gaussian noise with non-zero mean U_0 and the correlation function $K(\tau)$. According to equation (3.8), the random process $w(t)$ is again a Gaussian random process with the following probability distribution

$$P_w(y,t) = \frac{1}{\sqrt{4\pi D(t)}} \cdot \exp\left\{-\frac{(y-U_0t)^2}{4D(t)}\right\}, \tag{3.9}$$

where

$$D(t) = \int_0^t (t-\tau)K(\tau)d\tau. \tag{3.10}$$

Then we can apply the theorem of the probability theory to calculate from equations (3.8)-(3.9) the probability density function (PDF) of the charge flowing through a memristor

$$P_q(z,t) = \frac{\Phi'(z)}{\sqrt{4\pi D(t)}} \cdot \exp\left\{-\frac{(\Phi(z)-U_0t)^2}{4D(t)}\right\} \tag{3.11}$$

and, as a consequence, the PDF of the resistance

$$P_R(r,t) = \frac{r}{\sqrt{4\pi D(t)}} \sum_k \frac{1}{|\Phi''(q_k(r))|} \cdot \exp\left\{-\frac{(\Phi(q_k(r))-U_0t)^2}{4D(t)}\right\}, \tag{3.12}$$

where $q_k(R)$ is the k-th branch of uniqueness of the function $R = \Phi'(q)$.

Further, we consider the monotonic exponential dependence of the resistance on charge [119]

$$R(q) = R_{ON} + \frac{\Delta R}{e^{-(q+q_1)/q_0}+1}, \tag{3.13}$$

where $\Delta R = R_{OFF} - R_{ON}$ ($R_{ON} \ll R_{OFF}$), q_0 specifies the steepness of the transition between the low resistance state (LRS) R_{ON} and the high resistance state (HRS) R_{OFF}, q_1 is a parameter determining the memristance at the initial time moment. In this case the exact expression for PDF of the reristance $R(t)$ has the following form

$$P_R(r,t) = \frac{q_o \Delta R}{\sqrt{4\pi D(t)}} \frac{r}{(R_{OFF}-r)(r-R_{ON})} \cdot \exp\left\{-\frac{(\Phi(q(r)) - U_0 t)^2}{4D(t)}\right\}, \quad (3.14)$$

where

$$\Phi(q(r)) = -q_1 R_{ON} - q_0 \Delta R \ln\left(e^{q_1/q_0}+1\right) + q_0 R_{OFF} \ln\left(\frac{\Delta R}{R_{OFF}-r}\right) - q_0 R_{ON} \ln\left(\frac{\Delta R}{r-R_{ON}}\right), \quad R_{ON} < r < R_{OFF}. \quad (3.15)$$

For white Gaussian noise $U(t)$ with the correlation function

$$K(\tau) = 2D\delta(\tau), \quad (3.16)$$

where $2D$ is the noise intensity, we have to substitute $D(t) = Dt$ in equation (3.14) in accordance with equation (3.10). Figure 3.4 demonstrates the plots of PDF of the resistance (3.14) for the case of white Gaussian noise. As seen, the noise causes the memristor to switch to high resistance state. In the case of the noise with zero mean one can observe both states.

For the case of colored Gaussian noise $U(t)$ with the exponential correlation function

$$K(\tau) = \sigma^2 e^{-|\tau|/\tau_c}, \quad (3.17)$$

where σ^2 and τ_c are the variance and the correlation time respectively, expres-

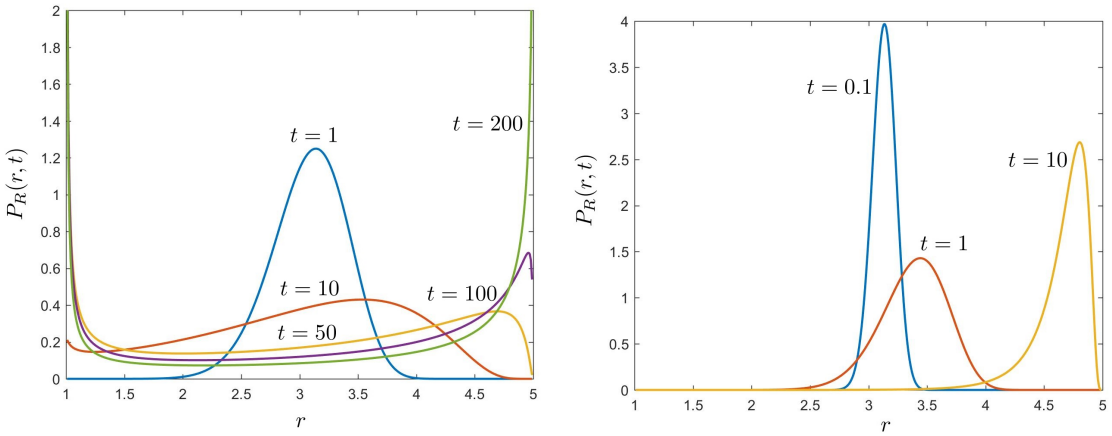

(a) (b)

Figure 3.4: Evolution of PDF of the resistance (3.14) for white Gaussian noise for (a) $U_0 = 0$ and (b) $U_0 = 1$. The values of the parameters are $q_0 = 1$, $q_1 = 0.1$, $R_{ON} = 1$, $R_{OFF} = 5$, $D = 0.5$.

sion (3.10) gives

$$D(t) = \sigma^2 \tau_c \left[t - \tau_c \left(1 - e^{-t/\tau_c} \right) \right]. \tag{3.18}$$

The plots of corresponding PDF of the memristance (3.14) in the case of colored Gaussian noise are shown in figure 3.5. One can observe in figure 3.5 the same tendencies as in figure 3.4.

For comparison, we apply to memristor the current $I(t)$ in the form of a stationary Gaussian noise with zero mean and the correlation function $K(\tau)$. In accordance with equation (3.7), the charge $q(t)$ is a Gaussian process with the following probability distribution

$$P_q(r,t) = \frac{1}{\sqrt{4\pi D(t)}} \cdot \exp\left\{ -\frac{z^2}{4D(t)} \right\}. \tag{3.19}$$

Corresponding to equation (3.19) the PDF of the memristance in this case reads

$$P_R(r,t) = \frac{1}{\sqrt{4\pi D(t)}} \sum_k \frac{1}{|R'(q_k(r))|} \cdot \exp\left\{ -\frac{q_k^2(r)}{4D(t)} \right\}, \tag{3.20}$$

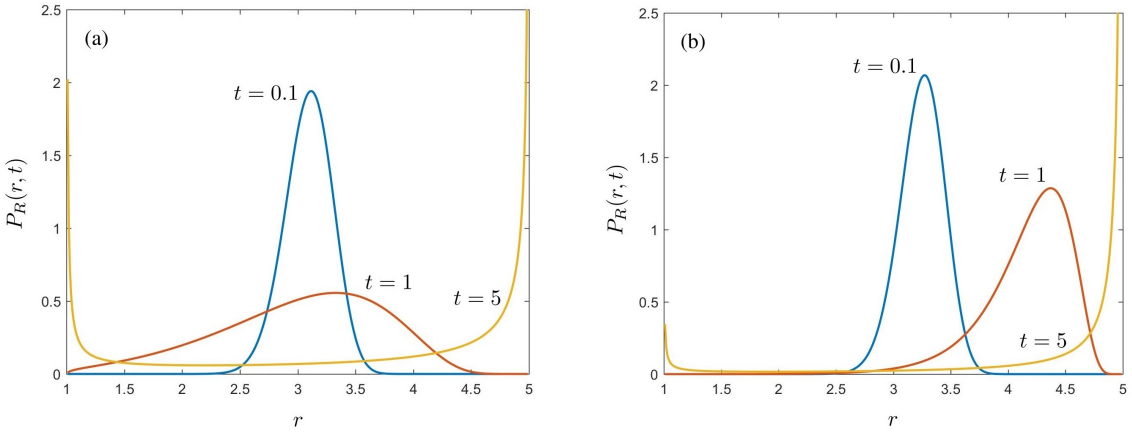

(a) (b)

Figure 3.5: Evolution of PDF of the resistance (3.14) for colored Gaussian noise for (a) $U_0 = 0$ and (b) $U_0 = 5$. The values of the parameters are $q_0 = 1$, $q_1 = 0.1$, $R_{ON} = 1$, $R_{OFF} = 5$, $\sigma^2 = 1$, $\tau_c = 1$.

Here we use the same notations as in equation (3.12). For the case of an exponential dependence (3.13) we obtain

$$P_R(r,t) = \frac{1}{\sqrt{4\pi D(t)}} \frac{q_o \Delta R}{(R_{OFF} - r)(r - R_{ON})} \cdot \\ \cdot \exp\left\{ -\frac{1}{4D(t)} \left(q_1 + q_0 \ln \frac{R_{OFF} - r}{r - R_{ON}} \right)^2 \right\}, \tag{3.21}$$

The 2D-plot of PDF of the memristance (3.21) for the case of white Gaussian fluctuations of the current is depicted in figure 3.6. As seen, the initial unimodal probability distribution of the resistance becomes bimodal with increasing the time of observation. Two peaks correspond to LRS and HRS and manifest switching between them caused by fluctuations of the current.

Further, we study a current-controlled ideal memristor. Based on the proposition that the hysteresis in the current-voltage characteristic requires some sort of atomic rearrangement, modulating the electronic current, we consider a thin

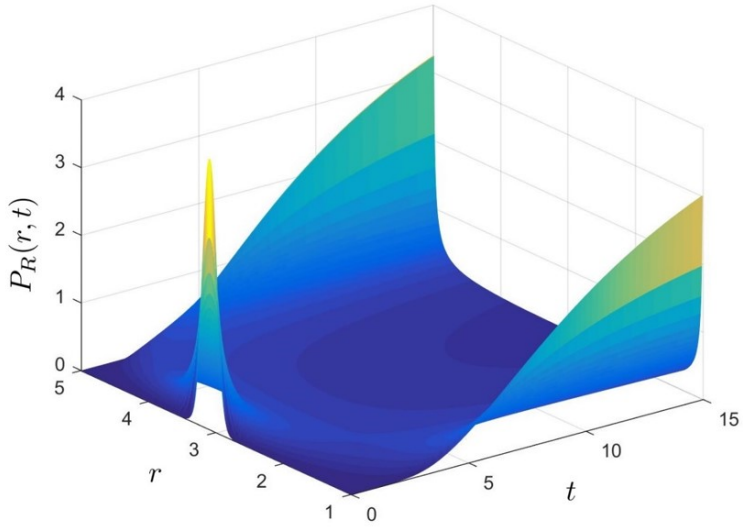

Figure 3.6: 2D-plot of PDF of resistance for the case of white Gaussian noise excitation as a function of resistance and time. The values of the parameters are $q_0 = 1$, $q_1 = 0.1$, $R_{ON} = 1$, $R_{OFF} = 5$, $D = 0.5$.

semiconductor film of thickness L sandwiched between two metal contacts, as shown in figure 3.7. The total resistance of the device is determined by two variable resistors connected in series

$$R_m = R_{ON} w(t) + R_{OFF} \left(1 - w(t)\right), \tag{3.22}$$

where $w(t) = l(t)/L$ is the normalized size of the doped region ($w(t) \in [0; 1]$, see figure 3.7), R_{ON} is the resistance of the memristor if it is completely doped (LRS) and R_{OFF} is its resistance if it is undoped (HRS).

Based on the theoretical model recently described in [49], we analyze the same characteristics as for the charge-controlled memristor considered above. Specifi-

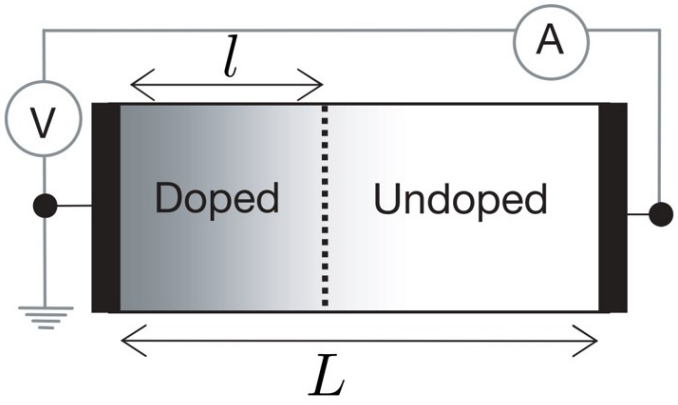

Figure 3.7: Schematic image of a memristor of length L, made of a doped and an undoped region. The doped region of normalized length $w(t)$ has resistance $w(t)R_{ON}$ and the undoped region has resistance $[1 - w(t)]R_{OFF}$.

cally, we have the following system of equations

$$\begin{aligned} U(t) &= R_m I(t), \\ \frac{dw(t)}{dt} &= \frac{\mu_V R_{ON}}{L^2} I(t), \end{aligned} \tag{3.23}$$

where μ_V is the average ion mobility and L is the full length of the device.

We study the case of the applied current $I(t)$ in the form of white Gaussian noise with non-zero mean I_0 and the intensity $2D_1$. The charge $q(t)$ is again Gaussian process, but according to the second equation of system (3.23), the PDF of the bounded random process $w(t)$ is non-Gaussian and contains two delta functions

$$P_w(y,t) = p_1(t)\delta(y) + p_2(t)\delta(1-y) + \frac{1}{\sqrt{4\pi D_1 c_0^2 t}} \cdot \exp\left\{-\frac{(y - c_0 I_0 t)^2}{4D_1 c_0^2 t}\right\} 1_{(0,1)}(y), \tag{3.24}$$

where $c_0 = \mu_V R_{ON}/L^2$, $1_A(y)$ is the indicator of set A and

$$p_1(t) = \int_{-\infty}^{0} \frac{1}{\sqrt{4\pi D_1 c_0^2 t}} \cdot \exp\left\{-\frac{(y - c_0 I_0 t)^2}{4 D_1 c_0^2 t}\right\} dy,$$
$$p_2(t) = \int_{1}^{\infty} \frac{1}{\sqrt{4\pi D_1 c_0^2 t}} \cdot \exp\left\{-\frac{(y - c_0 I_0 t)^2}{4 D_1 c_0^2 t}\right\} dy.$$

From equations (3.23) and (3.24) the PDF of the resistance has the following form

$$P_R(r,t) = \frac{1}{\Delta R} \cdot P_w\left(\frac{R_{OFF} - r}{\Delta R}, t\right). \tag{3.25}$$

Analysis of time evolution of the PDF gives results similar to the figure 3.6.

3.3 Stochastic model of memristor

The main physical parameter describing the state of a memristor is its resistance. Among a wide variety of resistive-switching memory devices implemented with different materials, a significant part is based on the formation and destruction of the CF in a thin dielectric film by applying an external voltage. The stochasticity of the memristors is mainly attributed to this process [51; 64; 68]. The process of conductive filament (CF) formation and destruction is based on a random hopping of the metal ions or dielectric structural defects (oxygen vacancies), which are positively charged, between the trapping sites within the structure of dielectric material. Let us call these ions or vacancies as diffusing particles. This diffusion process leads eventually to the formation or destruction of CF, depending on the direction of the external electric field, which defines the average drift direction. A conducting path is thus formed through the areas where the concentration of the particles is high enough.

3.3.1 Description of model

Following [91], we describe the motion of diffusing particles by Langevin equation

$$\eta \frac{dx}{dt} = -\frac{\partial U(x,V)}{\partial x} + \xi(t), \tag{3.26}$$

where x is the coordinate of a particle, η is the coefficient of viscosity, $U(x,V)$ is the potential profile defining the regular force acting on the particles, which depends on the voltage V of the electrodes of the memristor, and $\xi(t)$ is delta-correlated white Gaussian noise with zero mean and the noise intensity 2θ. When the fluctuations have only thermal nature, according to the Sutherland-Einstein relation, the intensity is proportional to the temperature of the thermal bath T: $\theta = k_B T$, where k_B is the Boltzmann constant. The average concentration of randomly walking particles as a function of time and space coordinate is used as internal state parameter defining the state of the memristor. Following [94; 120; 121], for simplicity of analysis, we consider the one-dimensional model, which can be generalized to threedimensional if necessary. Let the top electrode (TE) be positioned at $x = 0$ and the bottom electrode (BE) at $x = L$. The uncertainty provided by the model itself and the inevitable uncertainties in the calculation of macrophysical parameters (such as electrical and thermal conductivity of the material, viscosity, variations in activation energies for defect and electron transport, etc.), inaccurate control of the structure and boundary conditions, imprecise control of the initial conditions (such as the initial concentration of the defects, the inhomogeneity of the initial states, etc.) and the presence of thermal fluctuations are described by the stochastic force $\xi(t)$ (see equation (3.26)), whose intensity is proportional to the temperature in the presence of only thermal fluctuations.

The potential profile $U(x)$ for hopping particles is represented by the potential

wells separated by the barriers and is depicted on figure 3.8. The height of the barriers is the activation energy E_a which must be provided to the hopping particle to surmount the barrier and move to the neighboring well in a random direction. Besides the periodic component $\Phi(x)$ of the function $U(x)$, the external field provides the slope F of potential profile directed to one or another electrode depending on the polarity of the applied voltage as it is shown in figure 3.8 (a, b, c)

$$U(x, V) = \Phi(x) - Fx, \tag{3.27}$$

where $F = qV/\varepsilon L$, q is the charge of the particle and ε is the dielectric constant.

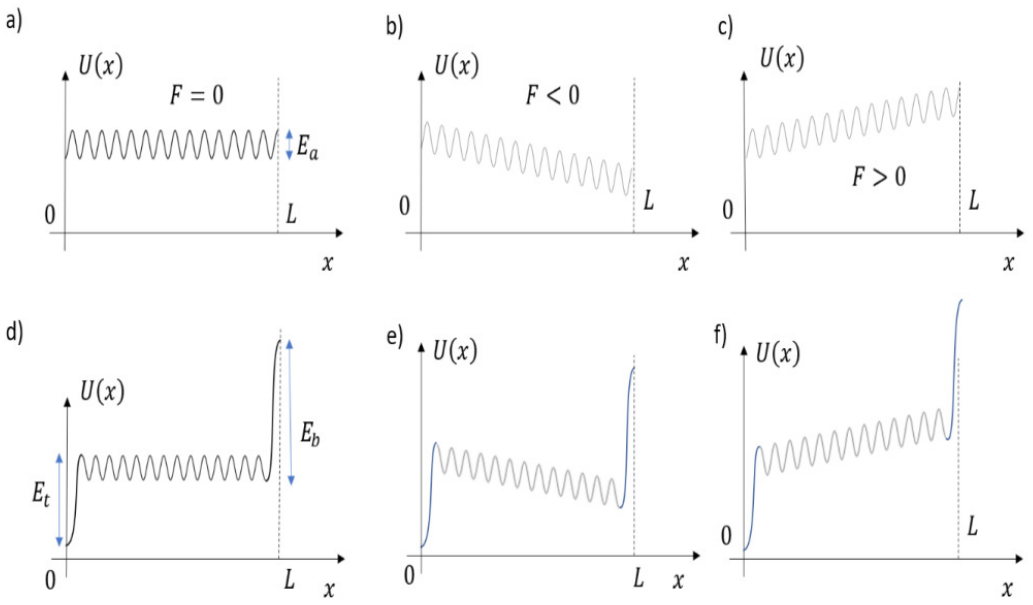

Figure 3.8: The potential profile $U(x)$ defining the regular force acting on diffusing particles under zero external bias $F = 0$ (a, d), negative $F < 0$ corresponding to ON set (b, e) and positive $F > 0$ corresponding to OFF set (c, f). The view of potential profile taking into account the influence of the top electrode (TE) and the bottom electrode (BE) materials (d, e, f) in a general case.

Using various electrode materials, we can modify the energy properties of the

interface that influence the shape of the potential profile near the boundaries $x = 0$ and $x = L$. The role of these changes can be important as it can influence the resistance values in LRS and HRS as well as the properties of the switching dynamics [122; 123]. Usually, TE has a low and easily oxidizable work function (WF) and BE has a higher WF. In general, it can be taken into consideration by the potential additional well with the depth E_t near the TE and the potential barrier with the height E_b near BE, as shown in the figure 3.8 (d, e, f). In this paper we consider only two special cases, when $E_t = E_b = E_a$ and when $E_b \to \infty$ under $E_t = E_a$. The latter case corresponds to the ideally inert material of BE.

The Langevin equation (3.26) corresponds to the Fokker-Planck equation (FPE) for the concentration of particles $n(x, t)$

$$\frac{\partial n}{\partial t} = \frac{1}{\eta}\frac{\partial}{\partial x}\left[\frac{\partial U(x,V)}{\partial x}n\right] + D\frac{\partial^2 n}{\partial x^2}, \tag{3.28}$$

where $D = \theta/\eta^2$ is the diffusion coefficient. The Brownian diffusion in tilted periodic potential (3.27), described by equation (3.28), can be replaced by the diffusion in the flat tilted potential U_1 without barriers [3; 123; 124; 125; 126; 127]

$$U_1(x, V) = -v_{eff}x, \tag{3.29}$$

with effective drift coefficient v_{eff} and the effective diffusion coefficient D_{eff}. As a result, equation (3.28) for the coarse-grained concentration of particles $n_1(x, t)$ takes the following form

$$\frac{\partial}{\partial t}n_1(x,t) = \frac{\partial}{\partial x}\left[n_1(x,t)\frac{\partial U_1(x,V)}{\partial x}\right] + D_{eff}\frac{\partial^2}{\partial x^2}n_1(x,t) \tag{3.30}$$

and the exact expression for the effective drift and diffusion coefficients, valid for

arbitrary values of F and θ, are the following [126; 127]

$$v_{eff} = \frac{l}{T_1(x_0, x_0 + l)}, \tag{3.31}$$

$$D_{eff} = \frac{l^2}{2} \frac{\Delta T_2(x_0, x_0 + l)}{[T_1(x_0, x_0 + l)]^3}, \tag{3.32}$$

where l is the period of periodic component $\Phi(x)$ of potential (3.27), T_1 is the mean first passage time (FPT) of the particle through the boundary $x_0 + l$, when it starts from the point x_0, and ΔT_2 is the variance of this FPT. If for any value of external voltage V we can consider that the resulting energy of activation is much greater than the intensity of fluctuations, $E \approx E_a - Fl/2 \gg \theta$, then we can use the following approximate expressions for (3.31) and (3.32)

$$v_{eff} = \frac{2l}{\tau_{kr}} \sinh \frac{Fl}{2\theta}, \tag{3.33}$$

$$D_{eff} = \frac{l^2}{\tau_{kr}} \cosh \frac{Fl}{2\theta}, \tag{3.34}$$

where

$$\tau_{kr} = \tau_0 \exp\{E_a/\theta\}. \tag{3.35}$$

is the Kramers time. Here E_a is the activation energy for zero bias and $\tau_0(\theta)$ is defined by the specific shape of periodic potential $\Phi(x)$. For thermal fluctuations, $\theta = k_B T$, the expressions (3.33) and (3.34) satisfy the following relation [128]

$$D_{eff} = \theta \frac{d}{dF} v_{eff}. \tag{3.36}$$

The approximate expressions for effective drift (3.33) and diffusion (3.34) coefficients provide a monotonic dependence on the parameters θ and F and were obtained under some specific assumption about the shape of the periodic potential profile $\Phi(x)$. Namely, the width of the barriers is about the width of the

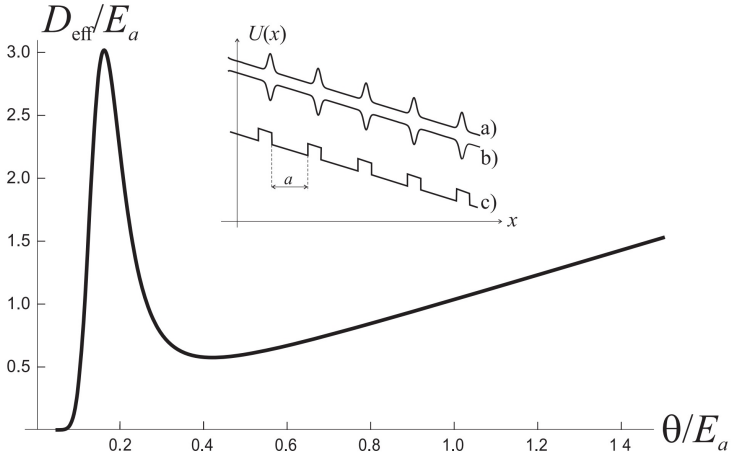

Figure 3.9: Effective diffusion coefficient as a function of dimensionless fluctuation intensity θ/E_a for potential profile (c) shown in the inset with the value $a = 0.8$. Inset: examples of tilted periodic potentials for which the acceleration of diffusion can be observed. E_a is the activation energy or the barrier height at $V = 0$.

wells and the top of each barrier is in the middle between two nearby wells for any value of F. The real shape of the potential profile is defined by the specific structure of the dielectric material and can be different. It was shown in [3; 127; 129; 130] that the functions $D_{eff}(\theta)$ and $D_{eff}(F)$ can be nonmonotonic for some particular shapes of potential wells and barriers. For example, these functions will have a maximum if the potential profile $\Phi(x)$ has wide wells and narrow barriers or vice versa, as it is shown in the inset a) and b) of figure 3.9. A similar potential profile can be created by inserting rows of metallic nanoparticles into the dielectric layer [131]. This nonmonotonicity with a maximum is a signature of the phenomenon of acceleration of diffusion in subcritically tilted periodic potentials. To take it into account, we should use the exact expressions for the effective drift and diffusion coefficients (3.31) and (3.32).

The complete memristor model, in addition to the drift-diffusion equation (3.30) and Ohmic type relationship, should also include the equations that connect the coarse-grained concentration of the defects $n_1(x, t)$ with the resistance

R, taking into account that the current I flowing between the electrodes heats the material locally and therefore contributes to the increase of the noise intensity. It can also be taken into account that the electric field inside the memristor can be distorted since there are areas with different conductivity depending on the $n_1(x,t)$ distribution. Therefore, in a general case one can consider the potential field as a function of a larger number of parameters $U_1(x,V,I,n_1)$ obeying the additional equations and then the FPE (3.30) can become nonlinear in n_1. Note that the drift term in (3.30) can be represented as the following sum

$$\frac{\partial}{\partial x}\left[\frac{\partial U_1(x,V,I,n_1)}{\partial x}n_1\right] = \frac{\partial U_1(x,V,I,n_1)}{\partial x}\frac{\partial n_1}{\partial x} + \frac{\partial^2 U_1(x,V,I,n_1)}{\partial x^2}n_1. \quad (3.37)$$

The case $U_1 = U_1(x,n_1)$ was investigated in [120] for one-dimensional case with the assumption that the second term in (3.37) can be neglected. This is true when $U_1(x)$ is a linear function. The influence of Joule heating was investigated numerically in [66; 83; 84; 85] for the three-dimensional case. We consider the most simple case, when Joule heating and nonlinear effects are not taken into account. The specific form of $R(n_1)$ is not crucial for the model considered here and depends on the properties of specific materials. Further we investigate the case when a low value of n_1 leads to high resistance and vice versa [132]. Let this dependence is strongly nonlinear and threshold-like: the resistance is drastically reduced when n_1 becomes greater than the threshold value $n_1 = n_{th}$. In this simplified case, the total resistance of the memristor can be calculated by formula (3.22).

3.3.2 Comparison with the experiment

To validate the stochastic model of a memristive device described in the previous subsection, we verify the fundamental properties of resistive switching such

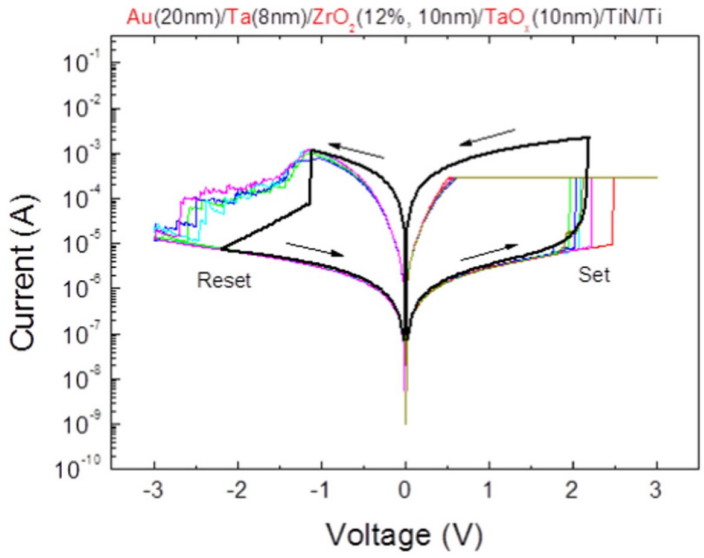

Figure 3.10: $I-V$ characteristic of the memristive device. Color lines: experimental, measured on the device based on Au/Ta/ZrO_2(Y)/Ta_2O_5/TiN/Ti structure (different colors correspond to different switching cycles). Black line: theoretical, based on numerical solution of equations (3.29), (3.30), (3.33), (3.34), (3.35) and (3.22) with boundary conditions (3.38). Voltage sweeping period is 4s. Other parameters are $E_a/\theta = 23$, $\Delta E/\theta = 4.23$, $l^2/\tau_0 = 6 \cdot 10^{-13}$ cm^2 s^{-1}, $L = 10$ nm, $N_1 = 100\%$, $N_2 = 25\%$ and $n_{th} = 50\%$.

as the $I - V$ characteristic and its dependence on the driving frequency. The experimental memristive device used for validation was fabricated on the basis of a newly engineered Au/Ta/ZrO_2(Y)/Ta_2O_5/TiN/Ti multilayer structure, which is described in more details in [133]. $I - V$ sweep measurements were carried out at room temperature in atmospheric conditions by using the Agilent B1500A semiconductor device analyzer. The measured $I-V$ characteristics are presented in figure 3.10 by color lines, where the colors correspond to the different cycles.

The sweeping period is 4s and sweeping amplitude is 3 V. The sign of bias on the device corresponds to the potential of the Au electrode relative to the grounded TiN/Ti electrode. The experimental memristive device demonstrates typical bipolar switching of anionic type related to reconstruction and destruction

of the CF composed of oxygen vacancies [134]. The SET process at positive bias corresponds to the transition from the HRS to the LRS. The backward transition at negative bias is denoted as the RESET process in figure 3.10.

The results of numerical solution of equations (3.29), (3.30), (3.33), (3.34), (3.35) and (3.22) are shown by the black line at the figure 3.10. For the model test we use the following parameters: The dimensionless activation energy in the equations (3.33, 3.34, 3.35) is $E_a/\theta = 23$, which becomes $E_a = 0.6$ eV at room temperature, when fluctuations have the thermal nature. This fact is in agreement with recent measurements of activation energy based on the analysis of flicker noise generated by a memristive device [135]. The maximum dimensionless variation of activation energy corresponding to the maximal value of the sweeping voltage $V = 2.2$ V is $\Delta E/\theta = 4.23$. The other parameter values are $l^2/\tau_0 = 6 \cdot 10^{-13}$ cm^2 s^{-1} and $L = 10$ nm (the length of the structure). The sweeping period is 4s and the sweeping amplitude 2.2 V. For modeling we used the following boundary conditions

$$n_1(0,t) = N_1, \quad n_1(L,t) = N_2, \tag{3.38}$$

where 0 and L are the coordinates of the TE and BE made of different materials. For the relative concentration of defects at the boundaries, we consider $N_1 = 100\%$ for the easily oxidizable TiN/Ti electrode and $N_2 = 25\%$ for the opposite Au electrode, which assumes that its ability to provide defects is 4 times lower. Such an assumption may be appropriate for a non-ideal inert material of BE. In the case of the ideal inert material we should use at the BE the reflective boundary conditions, which could be more appropriate for Au in the case of high material purity. The threshold value of the concentration for resistance switching is $n_{th} = 50\%$.

Comparing the experimental and simulated results shown in the figure 3.10

we can see that the analytic model describes the experiment with a quite good qualitatively agreement and captures the key fundamental properties of the real $I - V$ characteristic. There is a hysteresis on the characteristic $I - V$ and its area and shape correspond to that observed in the experiment. During the SET process, the sharp switching from HRS to LRS appears at approximately the same voltage around 2 V. The SET value of the current is different because the current through the experimental sample is limited by the compliance current $I_c = 300$ μA. The analytic equations introduced in subsection 3.3.1 do not model the circuits for current restriction at the SET regime. Therefore the value of the resistance in LRS reached in the model is less comparable to that in the experiment. Additional conditions that model the limitation of the current can be added to the analytic model, if necessary, while it is not crucial for the model verification.

In the RESET regime we can see that the switching process from LRS to HRS starts approximately at the same value of driving voltage $V = 1.1$ V, but the model switches to the HRS state slightly faster. This difference may be due to the particular choice of boundary conditions. Conditions (3.38), used for the test of the model, allow to reduce the concentration of the defects at $V < 0$ by two ways: by inverse flow of the defects back to the TE located at $x = 0$ and through the BE boundary at $x = L$, which works as the sink of defects, when $n_1(L, t) > N_2$. If we consider the reflecting boundary condition at $x = L$, suitable for a material ideally inert of the electrode, the dispersion of the defects through the electrode will become impossible and we will observe a slowing down of the switching process. On the other hand, in the literature we can find the experimental data with $I - V$ characteristics that show a faster RESET process appropriate to the result of the above simulation with boundary conditions (3.38) (see, for example, paper [136]).

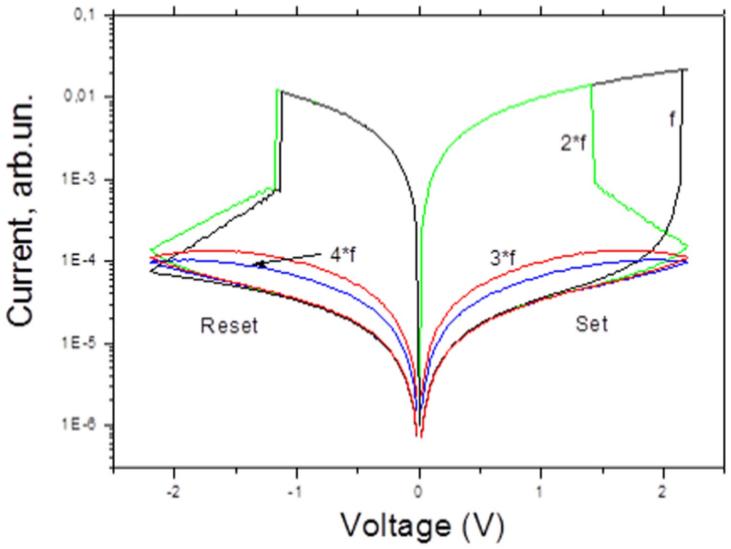

Figure 3.11: Theoretical $I - V$ characteristic for different driving frequencies: black is for $f = 0.25$ Hz, the same frequency as for the black plot in figure 3.10, green – $2f$, red – $3f$ and blue – $4f$. The other parameters of the model are equal to those used for figure 3.10.

Another fundamental property of real memristive devices is the shrinking of the hysteresis loop with the driving frequency [137]. This basic property is captured by the proposed model, as we can see from figure 3.11, where the theoretical $I - V$ characteristic, with the same parameters but for different values of driving frequencies, is shown. This dependence of hysteresis of the $I - V$ characteristic on the driving frequency is in agreement with experimental results shown in [137] and references therein. In the next subsection, we show that the proposed model is not only able to capture the key properties of real memristive systems, but allows to obtain the exact analytical solutions, which implies the qualitative and quantitative improvement of the theoretical techniques to analyze such systems in different physical conditions.

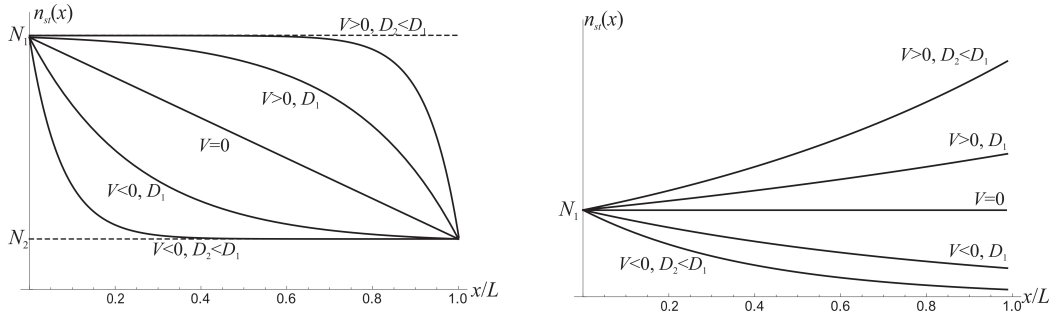

(a) (b)

Figure 3.12: Steady-state concentration $n_{st}(x)$ for different values of external force $F = qV/L$ and diffusion coefficient D_{eff} equal to D_1 and D_2, where $D_2 < D_1$: (a) for boundary conditions (3.38); (b) for boundary conditions (3.42) corresponding to the ideally inert material of the BE.

3.3.3 Exact solution and analysis

The stationary solution $n_{st}(x)$ of the FPE (3.28) is

$$\left[\frac{\partial}{\partial x}\frac{\partial U_1(x,V)}{\partial x} + D_{eff}\frac{\partial^2}{\partial x^2}\right] n_{st}(x) = 0. \tag{3.39}$$

For the linear potential profile (3.27) equation (3.39) reads

$$D_{eff}\frac{d^2 n_{st}(x)}{dx^2} - v_{eff}\frac{dn_{st}(x)}{dx} = 0. \tag{3.40}$$

Taking the boundary conditions (3.38), one may obtain the following stationary solution (shown in figure 3.12(a))

$$n_{st}(x) = \frac{N_2 - N_1}{\exp\left(\frac{v_{eff}L}{D_{eff}}\right) - 1}\left[\exp\left(\frac{v_{eff}x}{D_{eff}}\right) - 1\right] + N_1. \tag{3.41}$$

As was mentioned before, if BE is made of inert material with a very high WF, it can be modelled as a reflecting boundary, that is infinitely high barrier,

for the defects at the point $x = L$. Replacing boundary conditions (3.38) with the following ones

$$n_{st}(0) = N_1,\ G_{st}(L) = v_{eff} n_{st}(L) - D_{eff} \left. \frac{dn_{st}(x)}{dx} \right|_{x=L} = 0, \tag{3.42}$$

where $G_{st}(L)$ is the stationary flux of the diffusing defects at the point $x = L$, we can repeat all the procedure and obtain the following equilibrium concentration which is shown in figure 3.10b

$$n_{st}(x) = N_1 \exp\left(\frac{v_{eff} x}{D_{eff}}\right). \tag{3.43}$$

We can see that for the reflecting boundary condition (3.42), the variations of $n_{st}(L)$ with external bias F is much wider than that obtained with the boundary conditions (3.38). It means that the amplitude of the resistive switching between LRS and HRS will be greater when the BE material is inert. The same conclusion based on experimental results was realized in [122]. An exponential dependence of the resistance value from the maximum reset voltage has been experimentally observed also in memristive devices with inert BE [123]. The concentration (3.43) corresponds to the equilibrium state of the system described by (3.28), while the concentration (3.41) appears in the nonequilibrium steady state, because there is the constant flow of defects between the electrodes in this steady state.

Further we obtain the non-stationary solution of equation (3.28) and see how the concentration of defects is changed with time under arbitrary values of external voltage, noise intensity, effective diffusion coefficient and other parameters. Let us consider first the boundary conditions (3.38) and write the general solution $n(x,t)$ of equation (3.28) as a sum of two terms

$$n_{st}(x,t) = n_{st}(x) + n_{nst}(x,t), \tag{3.44}$$

where $n_{st}(x)$ is the stationary part (3.41) satisfying the boundary conditions (3.38) and $n_{nst}(x)$ the non-stationary part with zero boundary conditions

$$n_{nst}(0,t) = n_{nst}(L,t) = 0.$$

Taking the non-stationary part as a function with separable variables

$$n_{nst}(x,t) = T(t)S(x), \tag{3.45}$$

we transform equation (3.28) into the following form

$$S(x)\frac{dT(t)}{dt} = -T(t)v_{eff}\frac{dS(x)}{dx} + T(t)D_{eff}\frac{d^2S(x)}{dx^2}. \tag{3.46}$$

Now, by grouping terms with spatial and temporal variables, we finally obtain the equations for the functions $S(x)$ and $T(t)$

$$\frac{dT(t)}{dt} = CT(t), \tag{3.47}$$

$$\frac{d^2S(x)}{dx^2} - \frac{v_{eff}}{D_{eff}}\frac{dS(x)}{dx} - \frac{C}{D_{eff}}S(x) = 0, \tag{3.48}$$

where C is an arbitrary constant, which should be negative to make solution (3.47) bounded

$$T(t) = C_1 e^{Ct}. \tag{3.49}$$

Linear and homogeneous equation (3.48) has two characteristic roots $\lambda_{1,2}$

$$\lambda_{1,2} = \frac{1}{2}\left(\frac{v_{eff}}{D_{eff}} \pm \sqrt{\left(\frac{v_{eff}}{D_{eff}}\right)^2 + 4\frac{C}{D_{eff}}}\right). \tag{3.50}$$

Since the constant C is negative, the characteristic roots $\lambda_{1,2}$ may be either

real or complex. For real ones, the solutions of the equation (3.48) are

$$\begin{aligned} S(x) &= C_2 \exp\left[\frac{x}{2}\left(\frac{v_{eff}}{D_{eff}} + \sqrt{\left(\frac{v_{eff}}{D_{eff}}\right)^2 + 4\frac{C}{D_{eff}}}\right)\right] \\ &+ C_3 \exp\left[\frac{x}{2}\left(\frac{v_{eff}}{D_{eff}} - \sqrt{\left(\frac{v_{eff}}{D_{eff}}\right)^2 + 4\frac{C}{D_{eff}}}\right)\right], \quad C < 0 \\ S(x) &= C_4 + C_5 \exp\left(\frac{v_{eff}}{D_{eff}}\right), \quad C = 0. \end{aligned} \tag{3.51}$$

However, in this case, according to the boundary conditions $S(0) = S(L) = 0$ both arbitrary constants $C_{2,3}$ are equal to zero. Thus, the constant C should be chosen in such a way that characteristic roots $\lambda_{1,2}$ are complex

$$\lambda_{1,2} = a \pm ib, \tag{3.52}$$

where

$$a = \frac{v_{eff}}{2D_{eff}}, \tag{3.53}$$

$$b = \frac{1}{2}\sqrt{-\left(\frac{v_{eff}}{D_{eff}}\right)^2 - 4\frac{C}{D_{eff}}}. \tag{3.54}$$

and, because the solution $S(x)$ should be real, we consider the constraint $C_3 = C_2^*$ for the complex coefficients C_2 and C_3 of equation (3.51). With this choice of the constants C, C_2, C_3, we obtain the following solution of the equation (3.48)

$$S(x) = e^{ax}\left[\hat{C}_2 \sin(bx) + \hat{C}_3 \cos(bx)\right], \tag{3.55}$$

where $\hat{C}_2$ and $\hat{C}_3$ are new real unknown constants. Finally, using boundary con-

ditions

$$S(0) = \hat{C}_3 = 0, \quad S(L) = \hat{C}_2 \sin(bL) = 0, \tag{3.56}$$

one can find the equation for the constant C

$$\frac{L}{2}\sqrt{-\left(\frac{v_{eff}}{D_{eff}}\right)^2 - 4\frac{C}{D_{eff}}} = \pi n. \tag{3.57}$$

Therefore, the set of possible values of the constant C is the following

$$C(n) = \frac{D_{eff}}{4}\left(-\frac{4(\pi n)^2}{L^2} - \left(\frac{v_{eff}}{D_{eff}}\right)^2\right) < 0, \quad n = 0, 1, 2, ... \tag{3.58}$$

As a result, the non-stationary solution may be written as follows

$$n_{nst}(x,t) = \sum_{n=0}^{\infty} C_1(n) e^{C(n)t} e^{ax} \hat{C}_2(n) \sin\left(\frac{\pi n x}{L}\right). \tag{3.59}$$

Denoting the product of $C_1(n)$ and $\hat{C}_2(n)$ as a new constant $C_0(n)$ we finally obtain

$$n_{nst}(x,t) = \exp\left(\frac{v_{eff}x}{2D_{eff}}\right) \sum_{n=0}^{\infty} C_0(n) \exp\left[C(n)t\right] \sin\left(\frac{\pi n x}{L}\right), \tag{3.60}$$

where the set of arbitrary constants $C_0(n)$ is defined by the initial conditions

$$C_0(n) = \frac{2}{L}\int_0^L \exp\left(-\frac{v_{eff}x}{2D_{eff}}\right) n_{nst}(x,0) \sin\left(\frac{\pi n x}{L}\right) dx. \tag{3.61}$$

Equations (3.60)-(3.61) are the exact non-stationary solution of FPE (3.28) with the boundary conditions (3.38). Figure 3.13(a) shows the nonstationary concentration of the defects $n_1(x,t)$ for different times during the set process under $V > 0$ and constant, when the system is switched from HRS to LRS.

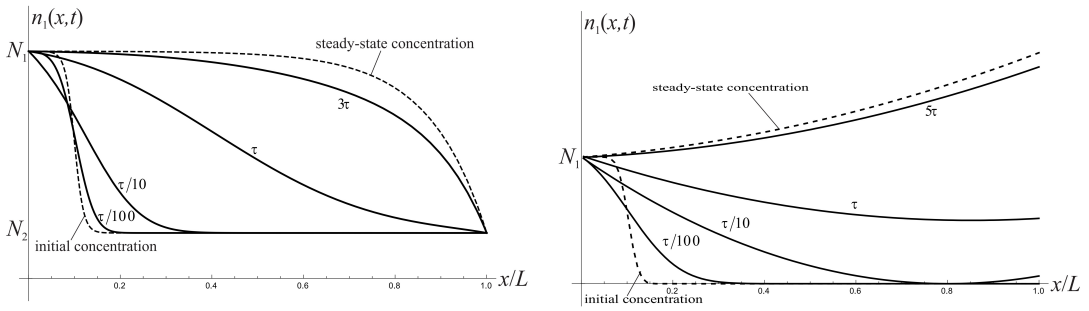

(a) (b)

Figure 3.13: Evolution of non-stationary concentrations (3.60) and (3.62) from initial state to the steady-state ON under $V > 0$ and constant, for times multiple of relaxation time τ: (a) for boundary conditions (3.38); (b) for boundary conditions (3.42) corresponding to the ideally inert material of the BE.

The area of the doped region, initially located only close to TE, it grows and reaches steady state, in which the doped region fills almost all the area from TE to BE. According to equation (3.22) it corresponds to the switching of the resistance value from HRS to LRS. The growth process of the doped region is qualitatively similar to the drift-diffusion model introduced in [94], but in our case we do not need to introduce any additional constrains in the equations of the model, the so-called window functions (see also [77; 78; 79]). The nonstationary concentration (3.60) naturally evolves towards the stationary one under the action of regular and random forces.

The nonstationary concentration $n_1(x,t)$ for the reflecting boundary conditions (3.42) can be obtained with the same theoretical procedure starting from equation (3.44), with the first term given by (3.43). Similarly to the equation (3.60) the non-stationary term reads

$$n_{nst}(x,t) = \exp\left(\frac{v_{eff}x}{D_{eff}}\right)\sum_{n=0}^{\infty} C_0(n)\exp\left(C(n)t\right)\sin b(n)x \tag{3.62}$$

with only difference in the equations for the constants C, a and b. From the

boundary conditions (3.42) it follows

$$S(0) = 0, \tag{3.63}$$

$$v_{eff}S(L) - D_{eff}\frac{dS(x)}{dx}\bigg|_{x=L} = 0. \tag{3.64}$$

Consequently, instead of the equation (3.56) we can obtain

$$\hat{C}_3(n) = 0, \tag{3.65}$$

$$\hat{C}_2(n)\left[\left(\frac{v_{eff}}{D_{eff}} - a\right)\sin(bL) - b\cos(bL)\right] = 0. \tag{3.66}$$

Taking into account equations (3.53) and (3.54), expression (3.66) leads to the following transcendental equation for a, b and C

$$\tan(bL) = \frac{b}{a}, \tag{3.67}$$

which has no analytic solution, but can be solved numerically or graphically. The plot of non-stationary concentration of particles $n(x,t)$ for reflecting boundary (3.42) is shown in figure 3.13(b) for different times during the set process under $V > 0$, when the system is switched from HRS to LRS.

For the understanding of switching variability of resistance values in LRS and HRS it is important to compare the switching time observed in experiment with the relaxation time of the defects concentration towards the stationary state. In other words, for the complete analysis it is necessary to understand if the system under observation has reached the stationary state or it remains far from equilibrium. Now, the information about the relaxation time τ towards the steady-state concentration under the boundary conditions (3.38) can be easily extracted from the equation (3.58). Indeed for every space coordinate x the function $n_{nst}(x,t)$ tends to zero with time as a sum of exponents. The slowest one of them corre-

sponds to $C(1)$

$$C(1) = \frac{D_{eff}}{8}\left(-\frac{4\pi^2}{L^2} - \left(\frac{v_{eff}}{D_{eff}}\right)^2\right). \tag{3.68}$$

Thus, the relaxation time reads

$$\tau = \frac{-1}{C(1)} = \frac{2L}{v_{eff}} \frac{2D_{eff}/v_{eff}L}{1+\pi^2\left(2D_{eff}/v_{eff}L\right)^2}. \tag{3.69}$$

The relaxation time (3.69) as a function of the bias voltage is shown in figure 3.14 for two values of fluctuation intensity. In accordance with known theoretical and experimental results [64; 68; 94], this dependence is close to the Arrhenius law, which is shown by dashed lines in figure 3.14. The exact expression $\tau(V)$ deviates from the Arrhenius law for small voltages, when the switching times become large.

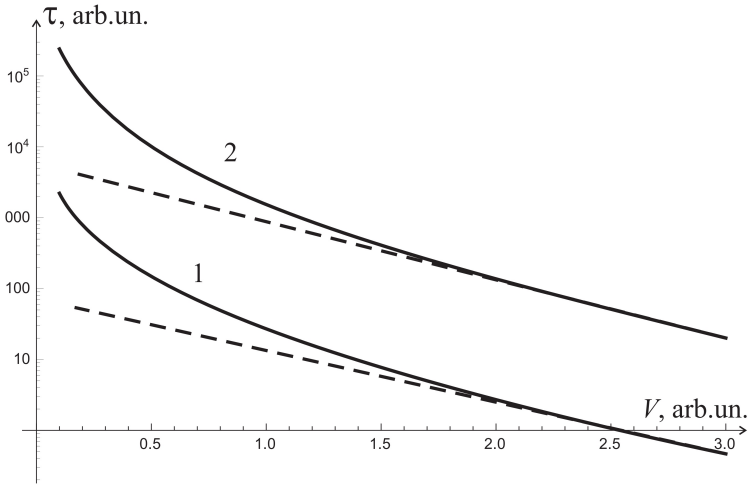

Figure 3.14: Relaxation time as a function of bias voltage for two values of noise intensity θ_1 (curve 1) and θ_2 (curve 2), with $\theta_1 > \theta_2$. Dashed straight lines represent the Arrhenius law.

The relaxation time (3.69) as a function of fluctuations intensity is shown in figure 3.15. The origin of fluctuations can be either thermal or from an external source. For example, the latter can be caused by a voltage driving noise added

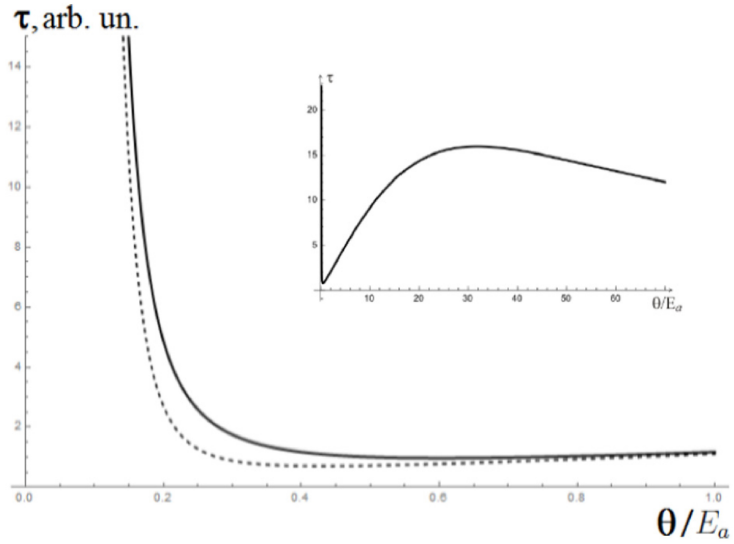

Figure 3.15: Relaxation time as a function of dimensionless noise intensity θ/E_a for potential profile with equal widths of barriers and wells $a = b = 0.5$, where E_a is activation energy at $V = 0$ (solid line). Relaxation time for potential profile with the wide wells $a = 0.8$ and narrow barriers $b = 0.2$ shown in the inset in figure 3.9(c) (dashed line). Inset: the same relaxation time as a function of dimensionless noise intensity but for large values of θ/E_a.

into the system. In a general case $\tau(\theta)$ is a nonmonotonic function (see the inset in figure 3.15). The range in which τ decreases with the intensity of the fluctuations $\theta < E_a$ is the most interesting from practical point of view, since it provides the possibility of accelerating the relaxation process through noise. As can seen from the inset of figure 3.15 there is an optimal value of the noise intensity so that the relaxation time is minimal. In the case of use of the dielectric structures, with the special shapes of potential barriers and wells allowing the acceleration of diffusion (that is the nonmonotonic behavior of $D_{eff}(\theta)$ shown in figure 3.9), the relaxation time will become shorter. In particular, the curve with dashed line refers to a periodic potential profile with wide wells $a = 0.8$ and narrow barriers $b = 0.2$, while the solid line curve refers to a periodic potential profile with $a = b = 0.5$. Therefore, the choice of a particular potential profile gives rise

to a further possibility of accelerating the relaxation process.

Chapter 4

Conclusions

In the foregoing thesis, I have carried out the further development of statistical analysis of nonlinear dynamical systems with both Gaussian and non-Gaussian random perturbations and its application to study the probabilistic, temporal and spectra-correlation characteristics of the anomalous diffusion in the form of Lévy flights. Moreover, the properties of the memristive systems for an ideal memristor and macroscopic model using stochastic approach were investigated. The main results, obtained in the work, are the following:

1. The residence time problem of a particle subject to a non-Gaussian noise source in arbitrary potential profile has been analyzed. We obtain the exact analytical results for the statistical characteristics of the residence time for anomalous diffusion in the form of Lévy flights in the inverse parabolic potential. The noise enhanced stability phenomenon for Lévy flights can be observed in the system investigated, as for usual Brownian diffusion.

2. The exact analytical expression for the correlation time of Lévy flights in the symmetric bistable quartic potential has been first obtained. As it has been shown, the correlation time ceases to depend on the height of potential barrier separating the two stable states for sufficiently high barriers unlike the Kramers' law for Brownian motion. Also, the interesting power-law

dependence with the exponent 4/3 of the correlation time on the position of potential wells has been found. Our findings are in a good agreement with previous exact results and numerical simulation data.

3. The exact analytical result for the stationary PDF of the particle position in the case of confined Lévy flights with the unit Lévy index in the asymmetric bistable quartic potential has been found. The result obtained could be useful for solving the barrier crossing problem for Lévy flights and estimating the nonlinear relaxation time.

4. The new analytical expression of the steady-state probability density function for Cauchy-Lévy flights with index $\alpha = 1$ in the symmetric steep potential well of the type $U(x) \propto x^{2m}$ has been derived. In the limit case $m \to \infty$ our results coincide with those previously obtained for the infinity well of deep rectangular potential profile, without considering the problem of the boundary conditions.

5. The asymptotic expression of the spectral power density for the steady-state superdiffusion in symmetric steep potential profiles, for arbitrary Lévy noise index α, has been found. The theoretical results obtained were compared with those obtained for the normal Brownian diffusion. The results obtained by numerical simulations are in a very good agreement with the analytical ones.

6. For two-dimensional diffusion the general Kolmogorov equation for the joint probability density function of particle coordinates has been obtained by functional methods directly from two Langevin equations with statistically independent noise sources. We compared the properties of Brownian diffusion and Lévy flights in parabolic potential with radial symmetry and

came to the conclusion that the radial symmetry property of the steady-state joint probability distribution available for normal diffusion is broken for Lévy flights.

7. Two models of an ideal Chua memristor with the external Gaussian noise have been investigated. We have shown that for charge-controlled memristor the shape of the probability density function of resistance depends on what is applied in the form of Gaussian noise, the voltage or the current. Also, different noise excitations in the form of white and colored Gaussian noise have been analyzed. In the specific example of an exponential dependence of the resistance on the charge flowing through the memristor the influence of the noise mean value and the type of driven Gaussian noise on the memristors switchings between two states has been found. A stochastic voltage applied to the memristor in the form of a stationary Gaussian noise causes the memristor to switch to high resistance state and one can observe both states for the noise with zero mean. In the case of white Gaussian fluctuations of the current the initial unimodal probability distribution of the memristance becomes bimodal with increasing the time of observation. Two peaks correspond to LRS and HRS and manifest switching between them caused by fluctuations of the current. For the current-controlled memristor we have obtained exact analytical expressions for the PDF of the memristance.

8. A simple stochastic model for memristive systems was proposed. The model is validated experimentally and its ability to reproduce some fundamental properties of resistive switching such as the hysteresis of the $I - V$ characteristic and its dependence on the driving frequency was confirmed. The proposed model takes fluctuation into account and allows to obtain the

exact analytic solutions for the concentration of defects, considered as an internal parameter of the system. This model paves the way to improve the theoretical techniques to deeper investigate the switching dynamics of the memristor devices. The steady states of the model systems are shown to be of equilibrium or nonequilibrium depending on the boundary conditions, which in turn depend on the materials of the electrodes. The relaxation time to the stationary state is obtained in analytic form and it has a non-monotonic dependence on the intensity of the fluctuations for a certain set of values of the external parameters. There is an optimal intensity of external noise so that the relaxation time is minimal. Some specific shapes of potential profiles, that describe the internal structure of the memristive material, have been shown to accelerate the relaxation process. This paves the way to the use of noise as a control parameter for switching dynamics, and provides insight on the interplay between the properties of the dielectric structure and the switching times of the memristive devices.

Appendix A

Solving a third-order inhomogeneous differential equation for calculating the correlation time in steady state

The goal is to to find the solution of the following inhomogeneous differential equation of the third order

$$\frac{d^3\varphi}{dk^3} + a^2\frac{d\varphi}{dk} - \beta_1\varphi = \frac{1}{k\gamma}\frac{d\vartheta_{st}\,(k)}{dk}, \tag{A.1}$$

where $\beta_1 = D_1/\gamma$. The stationary characteristic function $\vartheta_{st}(k)$ was recently found in [28] and is given by the expression (2.62).

For the case $k > 0$ the solution of the homogeneous differential equation corresponding to (A.1) is sought as $\varphi(k) = Ce^{zk}$. In this case, the characteristic equation reads as

$$z^3 + a^2 z - \beta_1 = 0,$$

and has three roots: two of which $z = -(p-q)/2 + i\sqrt{3}(p+q)/2$ and z^* are

complex and one $z_3 = p - q$ is real, where

$$p = \left(\beta_1/2 + \sqrt{(a^2/3)^3 + (\beta_1/(2))^2}\right)^{1/3},$$
$$q = \left(\sqrt{(a^2/3)^3 + (\beta_1/(2))^2} - \beta_1/(2)\right)^{1/3}, \;\; p > q.$$

Then the solution of a homogeneous differential equation corresponding to equation (A.1), has the form

$$\varphi_{gh} = C_1 e^{zk} + C_2 e^{z^* k} + C_3 e^{z_3 k}. \tag{A.2}$$

Denote by D the differentiation operator, i.e. $D = \frac{d}{dx}$. Then, taking into account the expression for the steady-state characteristic function (2.62), the equation (A.1) will be written in operator form as

$$\left(D^3 + a^2 D - \beta_1\right)\varphi = \frac{A}{k}\left(e^{z^* k} - e^{zk}\right), \tag{A.3}$$

where $A = |z|^2/(\gamma(z - z^*))$.

Equation (A.3) can be rewritten in the following form

$$F(D)\varphi = f(k),$$

where $F(D) = D^3 + a^2 D - \beta_1$.

Applying to (A.3) the inverse operator $\frac{1}{F(D)}$, we arrive at

$$\varphi_{pi}(k) = \frac{1}{F(D)} f(k).$$

Using the properties of the inverse operator, we obtain

$$\begin{aligned}
\varphi_{pi}(k) &= \frac{1}{D^3 + a^2 D - \beta_1} \frac{A}{k} \left(e^{z^* k} - e^{zk}\right) \\
&= \frac{1}{(D-z)(D-z^*)(D-z_3)} \frac{A}{k} \left(e^{z^* k} - e^{zk}\right) \\
&= \frac{1}{(D-z)(D-z_3)} A e^{z^* k} \frac{1}{D} \frac{1}{k} - \frac{1}{(D-z^*)(D-z_3)} A e^{zk} \frac{1}{D} \frac{1}{k} \\
&= \frac{A}{z - z_3} \left[\frac{1}{D-z} - \frac{1}{D-z_3}\right] e^{z^* k} \ln k - \frac{A}{z^* - z_3} \left[\frac{1}{D-z^*} - \frac{1}{D-z_3}\right] e^{zk} \ln k \\
&= \frac{A}{z - z_3} e^{zk} \int_0^k e^{(z^*-z)y} \ln y \, dy - \frac{A}{z^* - z_3} e^{z^* k} \int_0^k e^{(z-z^*)y} \ln y \, dy \\
&- \frac{A}{z - z_3} e^{z_3 k} \int_0^k e^{(z^*-z_3)y} \ln y \, dy + \frac{A}{z^* - z_3} e^{z_3 k} \int_0^k e^{(z-z_3)y} \ln y \, dy.
\end{aligned}$$

Finally, the general solution of (A.3) can be written as

$$\begin{aligned}
\varphi(k) &= C_1 e^{zk} + C_2 e^{z^* k} + C_3 e^{z_3 k} + \frac{A}{z - z_3} e^{zk} \int_0^k e^{(z^*-z)y} \ln y \, dy \\
&- \frac{A}{z^* - z_3} e^{z^* k} \int_0^k e^{(z-z^*)y} \ln y \, dy - \frac{A}{z - z_3} e^{z_3 k} \int_0^k e^{(z^*-z_3)y} \ln y \, dy \\
&+ \frac{A}{z^* - z_3} e^{z_3 k} \int_0^k e^{(z-z_3)y} \ln y \, dy. \qquad \text{(A.4)}
\end{aligned}$$

To find the unknown coefficients C_1, C_2 and C_3 in (A.4), we firstly use the condition arising from the properties of the Fourier transform

$$\lim_{k \to +\infty} \varphi(k) = 0.$$

Because of $\mathrm{Re} z < 0$ and $\mathrm{Re} z^* < 0$ for first two terms in (A.4) we have

$$\lim_{k \to +\infty} (C_1 e^{zk} + C_2 e^{z^* k}) = 0.$$

Applying L'Hôpital's rule twice for the fourth and the fifth terms in (A.4), it

easily to show that

$$\lim_{k\to\infty} e^{zk}\int_0^k e^{(z^*-z)y}\ln y\,dy = \lim_{k\to\infty}\frac{\int_0^k e^{(z^*-z)y}\ln y\,dy}{e^{-zk}} = \left(\frac{\infty}{\infty}\right) = \lim_{k\to\infty}\frac{e^{(z^*-z)k}\ln k}{-z\,e^{-zk}}$$
$$= \lim_{k\to\infty}\frac{\ln k}{-z\,e^{-z^*k}} = \left(\frac{\infty}{\infty}\right) = \lim_{k\to\infty}\frac{1}{|z|^2 k e^{-z^*k}} = 0,$$

and

$$\lim_{k\to\infty} e^{z^*k}\int_0^k e^{(z-z^*)y}\ln y\,dy = \lim_{k\to\infty}\frac{\int_0^k e^{(z-z^*)y}\ln y\,dy}{e^{-z^*k}} = \left(\frac{\infty}{\infty}\right) = \lim_{k\to\infty}\frac{e^{(z-z^*)k}\ln k}{-z^*\,e^{-z^*k}}$$
$$= \lim_{k\to\infty}\frac{\ln k}{-z^*\,e^{-zk}} = \left(\frac{\infty}{\infty}\right) = \lim_{k\to\infty}\frac{1}{|z|^2 k e^{-zk}} = 0.$$

From (A.4) we have

$$\lim_{k\to\infty} e^{z_3k}\left(C_3 - \frac{A}{z-z_3}\int_0^k e^{(z^*-z_3)y}\ln y\,dy + \frac{A}{z^*-z_3}\int_0^k e^{(z-z_3)y}\ln y\,dy\right) = 0$$

and find the coefficient C_3

$$C_3 = \frac{A}{z-z_3}\int_0^\infty e^{(z^*-z_3)y}\ln y\,dy - \frac{A}{z^*-z_3}\int_0^\infty e^{(z-z_3)y}\ln y\,dy.$$

Then the first derivative of the function φ in zero point can be written as

$$\varphi'(0) = C_1 z + C_2 z^* - \frac{A\,z_3}{z^*-z_3}\int_0^\infty e^{(z-z_3)y}\ln y\,dy + \frac{A\,z_3}{z-z_3}\int_0^\infty e^{(z^*-z_3)y}\ln y\,dy. \qquad (A.5)$$

The unknown coefficients C_1 and C_2 in (A.5) can be calculated from the conditions $\varphi(0) = 0$ and $\varphi''(0) = 0$, arising from the odd function $\varphi(k)$ (see (2.29)). Finally,

we arrive at

$$\begin{aligned}\varphi'(0) &= \frac{A(z-z_3)}{z+z^*}\int_0^\infty e^{(z-z_3)y}\ln y\,dy - \frac{A(z^*-z_3)}{z+z^*}\int_0^\infty e^{(z^*-z_3)y}\ln y\,dy \\ &= \frac{A}{z+z^*}\left[\int_0^\infty \ln y\ \frac{d}{dy}e^{(z-z_3)y}dy - \int_0^\infty \ln y\ \frac{d}{dy}e^{(z^*-z_3)y}dy\right] \\ &= \frac{A}{z+z^*}\left[\ln y\left[e^{(z-z_3)y}-e^{(z^*-z_3)y}\right]|_0^\infty - \int_0^\infty \left(e^{zy}-e^{z^*y}\right)e^{-z_3y}\frac{dy}{y}\right] \\ &= -\frac{2i|z|^2}{\gamma(z^2-z^{*2})}\int_0^\infty \left(e^{zy}-e^{z^*y}\right)e^{-z_3y}\frac{dy}{y}.\end{aligned}$$

Using the expressions for the roots z, z^* and z_3 through the parameters p and q and taking into account that

$$|z|^2 = p^2+pq+q^2, z^2-z^{*2} = -i\sqrt{3}(p^2-q^2),$$

we arrive at

$$\varphi'(0) = \frac{2}{\sqrt{3}\gamma}\frac{p^2+pq+q^2}{p^2-q^2}\int_0^\infty e^{-3(p-q)y/2}\sin\frac{\sqrt{3}}{2}(p+q)y\,\frac{dy}{y}. \tag{A.6}$$

Thus, it is required to calculate the integral of the form

$$I(\alpha,\beta) = \int_0^\infty e^{-\alpha x}\,\frac{\sin\beta x}{x}\,dx,$$

after differentiating which by β we have

$$I'_\beta(\alpha,\beta) = \int_0^\infty e^{-\alpha x}\cos\beta x\,dx = \mathrm{Re}\left\{\int_0^\infty e^{-\alpha x}\,e^{i\beta x}\,dx\right\} = \mathrm{Re}\left\{\frac{1}{\alpha-i\beta}\right\} = \frac{\alpha}{\alpha^2+\beta^2}.$$

Then

$$I(\alpha,\beta) = \int\frac{\alpha d\beta}{\alpha^2+\beta^2} = \int\frac{d\left(\beta/\alpha\right)}{1+\left(\beta/\alpha\right)^2} = \arctan\frac{\beta}{\alpha}+C(\alpha).$$

Note that $I(\alpha,0)=0=C(\alpha)$. Therefore,

$$\int_0^\infty e^{-\alpha x}\,\frac{\sin\beta x}{x}\,dx = \arctan\frac{\beta}{\alpha}.$$

In the framework of Section 2.2: $\alpha = 3(p-q)/2$ and $\beta = \sqrt{3}(p+q)/2$. Finally,

the first derivative of the function $\varphi(k)$ at zero is

$$\varphi'(0) = \frac{2}{\sqrt{3}\gamma} \frac{p^2 + pq + q^2}{p^2 - q^2} \arctan \frac{1}{\sqrt{3}} \frac{p+q}{p-q}.$$

Appendix B

Modification of formulas for a steady-state probability distribution in a symmetric power monostable potential

Earlier in paper [30] the authors have obtained the general expression for the stationary probability density of the particle coordinate in a smooth symmetric potential of the form

$$U(x) = \gamma \frac{x^{2m}}{2m} \tag{B.1}$$

with anomalous diffusion in the form of Lévy flights with Lévy index $\alpha = 1$. For the odd exponent $m = 2n + 1$ it has the form

$$P_{st}(x) = \frac{\beta^{4n+1}}{\pi(x^2 + \beta^2)} \prod_{l=0}^{n-1} \frac{1}{x^4 - 2\beta^2 x^2 \cos\left[\pi(4l+1)/(4n+1)\right] + \beta^4} \tag{B.2}$$

and respectively for even $m = 2n$

$$P_{st}(x) = \frac{\beta^{4n-1}}{\pi} \prod_{l=0}^{n-1} \frac{1}{x^4 - 2\beta^2 x^2 \cos\left[\pi(4l+1)/(4n-1)\right] + \beta^4}, \tag{B.3}$$

where $\beta = \sqrt[2m-1]{D_1/\gamma}$ and D_1 is the intensity parameter of driven noise with Cauchy stable distribution.

Replacing the steepness γ with γ/L^{2m} in (B.1), we arrive at

$$U(x) = \frac{\gamma}{2m}\left(\frac{x}{L}\right)^{2m} \tag{B.4}$$

For the new potential (B.4) the parameter β is rewritten as $\beta = L\sqrt[2m-1]{DL/\gamma}$.

Further we convert expression (B.2) for the case of an odd exponent m. For convenience, we introduce the notation $A(l) = \frac{4l+1}{4n+1}$. Performing factorization of the denominator of a fraction under the sign of the product

$$x^4 - 2\beta^2 x^2 \cos\pi A + \beta^4 = (\beta^2 - x^2\, e^{-i\pi A})(\beta^2 - x^2\, e^{i\pi A}), \tag{B.5}$$

we obtain the sum instead of the product

$$\begin{aligned} P_{st}(x) &= \frac{\beta^{4n+1}}{\pi(x^2+\beta^2)} \prod_{l=0}^{n-1} \frac{1}{(\beta^2 - x^2\, e^{-i\pi A})(\beta^2 - x^2\, e^{i\pi A})} \\ &= \frac{\beta^{4n+1}}{\pi(x^2+\beta^2)} \exp\left\{ \sum_{l=0}^{n-1} \ln \frac{1}{(\beta^2 - x^2\, e^{-i\pi A})(\beta^2 - x^2\, e^{i\pi A})} \right\} \\ &= \frac{\beta^{4n+1}}{\pi(x^2+\beta^2)} \exp\left\{ -\sum_{l=0}^{n-1} \left[\ln(\beta^2 - x^2\, e^{-i\pi A}) + \ln(\beta^2 - x^2\, e^{i\pi A})\right] \right\}. \end{aligned} \tag{B.6}$$

Let use the Taylor series expansion of the logarithm, which is valid for $|x| < \beta$

$$\begin{aligned} &\ln(\beta^2 - x^2\, e^{-i\pi A}) = \ln\left[\beta^2\left(1 - \frac{x^2 e^{-i\pi A}}{\beta^2}\right)\right] = \ln\beta^2 + \ln\left(1 - \frac{x^2 e^{-i\pi A}}{\beta^2}\right) \\ &= \ln\beta^2 - \sum_{k=1}^{\infty} \frac{1}{k}\left(\frac{x}{\beta}\right)^{2k} e^{-i\pi k A}. \end{aligned}$$

By analogy

$$\ln(\beta^2 - x^2\, e^{i\pi A}) = \ln\beta^2 - \sum_{k=1}^{\infty} \frac{1}{k}\left(\frac{x}{\beta}\right)^{2k} e^{i\pi k A}.$$

Then

$$P_{st}(x) = \frac{\beta^{4n+1}}{\pi(x^2+\beta^2)} \exp\left[\sum_{l=0}^{n-1}\left(\ln\frac{1}{\beta^4} + \sum_{k=1}^{\infty}\frac{1}{k}\left(\frac{x}{\beta}\right)^{2k}\left(e^{i\pi kA}+e^{-i\pi kA}\right)\right)\right]$$
$$= \frac{\beta^{4n+1}}{\pi(x^2+\beta^2)} \exp\left[n\ln\frac{1}{\beta^4} + \sum_{l=0}^{n-1}\left(\sum_{k=1}^{\infty}\frac{1}{k}\left(\frac{x}{\beta}\right)^{2k}\left(e^{i\pi kA}+e^{-i\pi kA}\right)\right)\right]$$
$$= \frac{\beta}{\pi(x^2+\beta^2)} \exp\left[\sum_{k=1}^{\infty}\frac{1}{k}\left(\frac{x}{\beta}\right)^{2k}\sum_{l=0}^{n-1}\left(e^{i\pi k\frac{4l+1}{4n+1}}+e^{-i\pi k\frac{4l+1}{4n+1}}\right)\right]. \qquad \text{(B.7)}$$

To calculate the internal sum of l, use the formula for the sum of the geometric progression

$$\sum_{l=0}^{n-1}\left(e^{i\pi k\frac{4l+1}{4n+1}}+e^{-i\pi k\frac{4l+1}{4n+1}}\right) = \sum_{l=0}^{n-1}\left(e^{\frac{i\pi k}{4n+1}}\right)^{4l+1} + \sum_{l=0}^{n-1}\left(e^{-\frac{i\pi k}{4n+1}}\right)^{4l+1}$$
$$= e^{\frac{i\pi k}{4n+1}}\cdot\frac{1-e^{\frac{4i\pi nk}{4n+1}}}{1-e^{\frac{4i\pi k}{4n+1}}} + e^{-\frac{i\pi k}{4n+1}}\cdot\frac{1-e^{-\frac{4i\pi nk}{4n+1}}}{1-e^{-\frac{4i\pi k}{4n+1}}} = \frac{e^{\frac{i\pi k}{4n+1}}-e^{i\pi k}}{1-e^{\frac{4i\pi k}{4n+1}}} + \frac{e^{\frac{-i\pi k}{4n+1}}-e^{-i\pi k}}{1-e^{-\frac{4i\pi k}{4n+1}}}$$
$$= \frac{e^{\frac{i\pi k}{4n+1}}-(-1)^k}{1-e^{\frac{4i\pi k}{4n+1}}} + \frac{e^{\frac{-i\pi k}{4n+1}}-(-1)^k}{1-e^{-\frac{4i\pi k}{4n+1}}} = \frac{e^{\frac{i\pi k}{4n+1}}-(-1)^k}{1-e^{\frac{4i\pi k}{4n+1}}} + \frac{e^{\frac{3i\pi k}{4n+1}}-(-1)^k e^{\frac{4i\pi k}{4n+1}}}{e^{\frac{4i\pi k}{4n+1}}-1}$$
$$= \frac{e^{\frac{i\pi k}{4n+1}}-(-1)^k-e^{\frac{3i\pi k}{4n+1}}+(-1)^k e^{\frac{4i\pi k}{4n+1}}}{1-e^{\frac{4i\pi k}{4n+1}}} = \frac{e^{\frac{i\pi k}{4n+1}}(1-e^{\frac{2i\pi k}{4n+1}})-(-1)^k\cdot(1-e^{\frac{4i\pi k}{4n+1}})}{1-e^{\frac{4i\pi k}{4n+1}}}$$
$$= \frac{e^{\frac{i\pi k}{4n+1}}}{1+e^{\frac{2i\pi k}{4n+1}}} - (-1)^k = \frac{1}{e^{-\frac{i\pi k}{4n+1}}+e^{\frac{i\pi k}{4n+1}}} - (-1)^k = \frac{1}{2\cos\frac{\pi k}{4n+1}} - (-1)^k.$$

Substituting the obtained result in (B.7), we arrive at

$$P_{st}(x) = \frac{\beta}{\pi(x^2+\beta^2)}\exp\left\{\sum_{k=1}^{\infty}\left[\frac{1}{2\cos\frac{\pi k}{4n+1}}\cdot\frac{1}{k}\left(\frac{x}{\beta}\right)^{2k} + (-1)^{k+1}\frac{1}{k}\left(\frac{x}{\beta}\right)^{2k}\right]\right\}$$
$$= \frac{\beta}{\pi(x^2+\beta^2)}\exp\left\{\sum_{k=1}^{\infty}\left[\frac{1}{2\cos\frac{\pi k}{4n+1}}\cdot\frac{1}{k}\left(\frac{x}{\beta}\right)^{2k} + \ln\left(1+\left(\frac{x}{\beta}\right)^2\right)\right]\right\} \qquad \text{(B.8)}$$
$$= \frac{1}{\pi\beta}\exp\left\{\sum_{k=1}^{\infty}\frac{1}{2\cos\frac{\pi k}{4n+1}}\cdot\frac{1}{k}\left(\frac{x}{\beta}\right)^{2k}\right\} = \frac{1}{\pi\beta}\exp\left\{\sum_{k=1}^{\infty}\frac{1}{2\cos\frac{\pi k}{2m-1}}\cdot\frac{1}{k}\left(\frac{x}{\beta}\right)^{2k}\right\}.$$

The result for the case of even exponent $m = 2n$ is obtained similarly, but the

calculation of the internal sum by l will be different, namely

$$\begin{aligned}
&\sum_{l=0}^{n-1}\left(e^{i\pi k\frac{4l+1}{4n-1}}+e^{-i\pi k\frac{4l+1}{4n-1}}\right)=\sum_{l=0}^{n-1}\left(e^{\frac{i\pi k}{4n-1}}\right)^{4l+1}+\sum_{l=0}^{n-1}\left(e^{\frac{-i\pi k}{4n-1}}\right)^{4l+1}\\
&=e^{\frac{i\pi k}{4n-1}}\cdot\frac{1-e^{\frac{4i\pi nk}{4n-1}}}{1-e^{\frac{4i\pi k}{4n-1}}}+e^{-\frac{i\pi k}{4n-1}}\cdot\frac{1-e^{-\frac{4i\pi nk}{4n-1}}}{1-e^{-\frac{4i\pi k}{4n-1}}}\\
&=e^{\frac{i\pi k}{4n-1}}\cdot\frac{1-e^{i\pi k}\,e^{\frac{i\pi k}{4n-1}}}{1-e^{\frac{4i\pi k}{4n-1}}}+e^{-\frac{i\pi k}{4n-1}}\cdot\frac{1-e^{-i\pi k}\,e^{-\frac{i\pi k}{4n-1}}}{1-e^{-\frac{4i\pi k}{4n-1}}}\\
&=\frac{e^{\frac{i\pi k}{4n-1}}-(-1)^k e^{\frac{2i\pi k}{4n-1}}}{1-e^{\frac{4i\pi k}{4n-1}}}+\frac{e^{\frac{-i\pi k}{4n-1}}-(-1)^k e^{\frac{-2i\pi k}{4n-1}}}{1-e^{-\frac{4i\pi k}{4n-1}}}\\
&=\frac{e^{\frac{i\pi k}{4n-1}}-(-1)^k e^{\frac{2i\pi k}{4n-1}}}{1-e^{\frac{4i\pi k}{4n-1}}}+\frac{e^{\frac{3i\pi k}{4n-1}}-(-1)^k e^{\frac{2i\pi k}{4n-1}}}{e^{\frac{4i\pi k}{4n-1}}-1}\\
&=\frac{e^{\frac{i\pi k}{4n-1}}-(-1)^k\,e^{\frac{2i\pi k}{4n-1}}-e^{\frac{3i\pi k}{4n-1}}+(-1)^k\,e^{\frac{2i\pi k}{4n-1}}}{1-e^{\frac{4i\pi k}{4n-1}}}\\
&=\frac{e^{\frac{i\pi k}{4n-1}}}{1+e^{\frac{2i\pi k}{4n-1}}}=\frac{1}{e^{-\frac{i\pi k}{4n-1}}+e^{\frac{i\pi k}{4n-1}}}=\frac{1}{2\cos\frac{\pi k}{4n-1}}.
\end{aligned}$$

Finally, for $m=2n$ we have

$$\begin{aligned}
P_{st}(x)&=\frac{1}{\pi\beta}\,\exp\left\{\sum_{k=1}^{\infty}\frac{1}{2\cos\frac{\pi k}{4n-1}}\cdot\frac{1}{k}\left(\frac{x}{\beta}\right)^{2k}\right\}\\
&=\frac{1}{\pi\beta}\,\exp\left\{\sum_{k=1}^{\infty}\frac{1}{2\cos\frac{\pi k}{2m-1}}\cdot\frac{1}{k}\left(\frac{x}{\beta}\right)^{2k}\right\}
\end{aligned}\tag{B.9}$$

and obtain complete match with the case (B.8) for the odd exponent m.

Using similar calculations, it is not difficult to obtain the stationary probability distribution for the case of $|x|>\beta$ with even and odd values of the parameter m. The final expression for an arbitrary m reads

$$P_{st}(x)=\frac{1}{\beta\pi}\left(\frac{\beta}{x}\right)^{2m}\exp\left\{\sum_{k=1}^{\infty}\frac{1}{2\cos\frac{\pi k}{2m-1}}\cdot\frac{1}{k}\left(\frac{\beta}{x}\right)^{2k}\right\}.\tag{B.10}$$

Finally we have the following modification of initial relations (B.2)-(B.3)

$$P_{st}(x) = \begin{cases} \frac{1}{\pi\beta}\ \exp\left\{\sum\limits_{k=1}^{\infty} \frac{1}{2\cos\frac{\pi k}{2m-1}} \cdot \frac{1}{k}\left(\frac{x}{\beta}\right)^{2k}\right\}, & |x| < \beta; \\ \frac{1}{\pi\beta}\left(\frac{\beta}{x}\right)^{2m} \exp\left\{\sum\limits_{k=1}^{\infty} \frac{1}{2\cos\frac{\pi k}{2m-1}} \cdot \frac{1}{k}\left(\frac{\beta}{x}\right)^{2k}\right\}, & |x| > \beta. \end{cases} \tag{B.11}$$

Appendix C

Derivation of the formula for the joint characteristic function in the case of diffusion in 2D potential

To obtain an equation with respect to the joint characteristic coordinate function $\Theta(k,q,t)$, we apply double Fourier transform to the following equation

$$\frac{\partial P}{\partial t} = \frac{\partial}{\partial x}\left(\frac{\partial U}{\partial x}P\right) + \frac{\partial}{\partial y}\left(\frac{\partial U}{\partial y}P\right) + K\int_{-\infty}^{+\infty}\frac{1}{|z|^{\alpha+1}}\left(P(x-z,y,t)\right.$$
$$\left.+P(x,y-z,t) - 2P(x,y,t)\right)dz \tag{C.1}$$

Let consider the first term of the right side of equation (C.1) by entering the notation $f = \frac{\partial U}{\partial x}P$. The Fourier transform for it gives

$$\int_{-\infty}^{+\infty}\int_{-\infty}^{+\infty}\frac{\partial f}{\partial x}\cdot e^{ikx+iqy}dxdy = \int_{-\infty}^{+\infty}e^{iqy}dy\int_{-\infty}^{+\infty}\frac{\partial f}{\partial x}\cdot e^{ikx}dx$$
$$= \left|\begin{array}{c} dv = \frac{\partial f}{\partial x}dx \to v = f \\ u = e^{ikx} \to du = ik\cdot e^{ikx}dx \end{array}\right| = \int_{-\infty}^{+\infty}e^{iqy}dy\left(e^{ikx}f\right)\Big|_{-\infty}^{+\infty} \tag{C.2}$$
$$- ik\int_{-\infty}^{+\infty}\int_{-\infty}^{+\infty}fe^{ikx+iqy}dxdy.$$

Due to the fact that the probability distribution P decreases faster than $U_x^{'}$ grows,

the substitution in expression (C.2) turns to zero.

We present the derivative of the smooth potential as the following sum

$$U_x^{'}(x,y) = \sum_{n,m} a_{nm} x^n y^m,$$

then

$$\begin{aligned}
&- ik \int_{-\infty}^{+\infty} \int_{-\infty}^{+\infty} U_x^{'} P \cdot e^{ikx+iqy} dxdy \\
&= -ik \sum_{n,m} \int_{-\infty}^{+\infty} \int_{-\infty}^{+\infty} a_{nm} x^n y^m P \cdot e^{ikx+iqy} dxdy \\
&= -ik \sum_{n,m} \int_{-\infty}^{+\infty} \int_{-\infty}^{+\infty} a_{nm} \left(\frac{\partial}{\partial ik}\right)^n \left(\frac{\partial}{\partial iq}\right)^m P \cdot e^{ikx+iqy} dxdy \\
&= -ikU_x^{'} \left(\frac{\partial}{\partial ik}, \frac{\partial}{\partial iq}\right) \cdot \Theta(k,q,t
\end{aligned} \tag{C.3}$$

For the second term of equation (C.1) we obtain by analogy

$$\int_{-\infty}^{+\infty} \int_{-\infty}^{+\infty} \frac{\partial}{\partial y} \left(\frac{\partial U}{\partial y} P\right) \cdot e^{ikx+iqy} dxdy = -iqU_y^{'} \left(\frac{\partial}{\partial ik}, \frac{\partial}{\partial iq}\right) \cdot \Theta(k,q,t). \tag{C.4}$$

We consider the integral term of equation (C.1). After the double Fourier transform and applying the displacement formula, we arrive to

$$\begin{aligned}
&K \int_{-\infty}^{+\infty} \frac{e^{ikz} + e^{iqz} - 2}{|z|^{\alpha+1}} \; dz \cdot \Theta(k,q,t) = K \int_{-\infty}^{+\infty} \frac{e^{ikz} - 1}{|z|^{\alpha+1}} \; dz \cdot \Theta(k,q,t) \\
&+ K \int_{-\infty}^{+\infty} \frac{e^{iqz} - 1}{|z|^{\alpha+1}} \; dz \cdot \Theta(k,q,t).
\end{aligned} \tag{C.5}$$

Each of the integrals above can be reduced using Euler's formula to the following form

$$\int_{-\infty}^{+\infty} \frac{e^{ikz} - 1}{|z|^{\alpha+1}} \; dz = \int_{-\infty}^{+\infty} \frac{\cos kz + i \sin kz - 1}{|z|^{\alpha+1}} \; dz = 2 \int_0^{+\infty} \frac{\cos kz - 1}{z^{\alpha+1}} \; dz,$$

where

$$\int_0^{+\infty} \frac{1-\cos kz}{z^{\alpha+1}}\ dz = -|k|^{\alpha}\cos\frac{\pi\alpha}{2}\ \Gamma(-\alpha) = \frac{|k|^{\alpha}}{\alpha}\cos\frac{\pi\alpha}{2}\ \Gamma(1-\alpha).$$

If $0 < \alpha < 1$

$$\frac{|k|^{\alpha}}{\alpha}\cos\frac{\pi\alpha}{2}\ \frac{\pi}{\Gamma(\alpha)\sin\pi\alpha} = \frac{|k|^{\alpha}\pi}{\Gamma(\alpha+1)2\sin(\pi\alpha/2)};$$

if $1 < \alpha < 2$

$$\frac{|k|^{\alpha}}{\alpha(1-\alpha)}\cos\frac{\pi\alpha}{2}\ \Gamma(2-\alpha) = \frac{|k|^{\alpha}}{\alpha(1-\alpha)}\cos\frac{\pi\alpha}{2}\ \frac{\pi}{\Gamma(\alpha-1)\sin\pi(\alpha-1)}$$
$$= \frac{|k|^{\alpha}\pi\cos(\pi\alpha/2)}{-\alpha\Gamma(\alpha)\sin\pi\alpha\cos\pi} = \frac{|k|^{\alpha}\pi}{\Gamma(\alpha+1)2\sin(\pi\alpha/2)}.$$

Thus, the right side of (C.5) will take the form

$$-\frac{K\pi}{\Gamma(\alpha+1)\sin(\pi\alpha/2)}\ (|k|^{\alpha}+|q|^{\alpha})\,\Theta(k,q,t).$$

If one enters the notation $D_{\alpha} = \dfrac{K\pi}{\Gamma(\alpha+1)\sin(\pi\alpha/2)}$, the final equation for the joint characteristic function is written as follows

$$\frac{\partial\Theta(k,q,t)}{\partial t} = -ikU_x^{'}\left(-i\frac{\partial}{\partial k}, -i\frac{\partial}{\partial q}\right)\Theta(k,q,t)$$
$$- iqU_y^{'}\left(-i\frac{\partial}{\partial k}, -i\frac{\partial}{\partial q}\right)\Theta(k,q,t) - D_{\alpha}\,(|k|^{\alpha}+|q|^{\alpha})\,\Theta(k,q,t). \quad \text{(C.6)}$$

Appendix D

List of publications

[A1] A.A. Dubkov and A.A. Kharcheva, "Time characteristics of one-dimensional and two-dimensional stationary Lévy flights in different potential profiles," *IEEE 2015 ICNF*, doi: 10.1109/ICNF.2015.7288589, 2015.

[A2] A.A. Dubkov and A.A. Kharcheva, "Features of barrier crossing event for Lévy flights," *EPL*, vol. 113, p. 30009, 2016.

[A3] A.A. Kharcheva, A.A. Dubkov, B. Dybiec, B. Spagnolo and D. Valenti, "Spectral characteristics of steady-state Lévy flights in confinement potential profiles," *JSTAT Mech-Theory E.*, vol. 2016, p. 054039, 2016.

[A4] A.A. Kharcheva, A.A. Dubkov and B. Spagnolo, "Probabilistic analysis of ideal memristor models under Gaussian noise," *Proc. XXIII Sci. Conf. Radiophysics.*, p. 493, 2019.

[A5] A.A. Kharcheva, A.A. Dubkov and B. Spagnolo, "Probabilistic analysis of two models of ideal memristor with external noise," *IEEE 2019 ICNF*, doi: 10.5075/epfl-ICLAB-ICNF-269294, 2019.

[A6] N.V. Agudov, A.V. Safonov, A.V. Krichigin, A.A. Kharcheva, A.A. Dubkov, D. Valenti, D.V. Guseinov, A.I. Belov, A.N. Mikhailov, A. Carollo, B. Spagnolo,

"Nonstationary distributions and relaxation times in a stochastic model of memristor", *JSTAT Mech-Theory E.*, vol. 2020, p. 024003 (1-23), 2020.

[A7] A.A. Dubkov, B. Dybiec, A.A. Kharcheva, B. Spagnolo and D. Valenti, "Statistics of residence time for Lévy flights in inverse parabolic potential," 2020. *Submitted to Phys. Rev. E.*

References

[1] S. Bezrukov and I. Vodyanoy, "Noise-induced enhancement of signal transduction across voltage-dependent ion channels," *Nature*, vol. 378, p. 362, 1995. 1

[2] V. V. Yanovsky, A. V. Chechkin, D. Schertzer, and A. V. Tur, "Lévy anomalous diffusion and fractional Fokker-Planck equation," *Physica A*, vol. 282, p. 13, 2000. 1

[3] A. Dubkov and B. Spagnolo, "Generalized Wiener process and Kolmogorov's equation for diffusion induced by non-Gaussian noise source," *Fluct. Noise Lett.*, vol. 05, p. L267, 2005. 1, 2, 18, 20, 23, 52, 73, 75

[4] S. I. Denisov, W. Horsthemke, and P. Hänggi, "Generalized Fokker-Planck equation: Derivation and exact solutions," *EPJ B*, vol. 68, p. 567, 2009. 1

[5] S. I. Denisov, P. Hänggi, and H. Kantz, "Parameters of the fractional Fokker-Planck equation," *Europhys. Lett.*, vol. 85, p. 40007, 2009. 1

[6] R. Metzler and J. Klafter, "The random walk's guide to anomalous diffusion: A fractional dynamics approach," *Phys. Rep.*, vol. 339, p. 1, 2000. 2, 4, 56

[7] J. H. Cushman, M. Park, and D. O'Malley, "Chaotic dynamics of superdiffusion revisited," *Geophys. Research Lett.*, vol. 36, p. L08812, 1995. 2

[8] E. Barkai, R. Metzler, and J. Klafter, "From continuous time random walks to the fractional Fokker-Planck equation," *Phys. Rev. E*, vol. 61, p. 132, 2000. 2

[9] A. I. Saichev and G. M. Zaslavsky, "Fractional kinetic equations: solutions and applications," *Chaos*, vol. 7, p. 753, 1997. 2

[10] B. J. West, P. Grigolini, R. Metzler, and T. F. Nonnenmacher, "Fractional diffusion and Lévy stable processes," *Phys. Rev. E.*, vol. 55, p. 99, 1997. 2

[11] K. M. Kolwankar and A. D. Gangal, "Local fractional Fokker-Planck equation," *Phys. Rev. Lett.*, vol. 80, p. 214, 1998. 2

[12] A. Chechkin, V. Gonchar, J. Klafter, and R. Metzler, "Fundamentals of Lévy flight processes," *Adv. Chem. Phys.*, vol. 133, p. 439, 2006. 3

[13] A. M. Mohammed, Y. R. Koh, B. Vermeersch, H. Lu, P. G. Burke, A. C. Gossard, and A. Shakouri, "Fractal Lévy heat transport in nanoparticle embedded semiconductor alloys," *Nano Lett.*, vol. 15, p. 4269, 2015. 3

[14] A. Chechkin, V. Gonchar, J. Klafter, R. Metzler, and L. Tanatarov, "Stationary states of non-linear oscillators driven by Lévy noise," *Chem. Phys.*, vol. 284, p. 233, 2002. 3

[15] T. Solomon, E. Weeks, and H. Swinney, "Observation of anomalous diffusion and Lévy flights in a two-dimensional rotating flow," *Phys. Rev. Lett.*, vol. 71, p. 3975, 1993. 3

[16] S. C. Venkataramani, T. M. J. Antonsen, and E. Ott, "Lévy flights in fluid flows with no Kolmogorov-Arnold-Moser surfaces," *Phys. Rev. Lett.*, vol. 78, p. 3864, 1997. 3

[17] H. Katori, S. Schlipf, and H. Walther, "Anomalous dynamics of a single ion in an optical lattice," *Phys. Rev. Lett.*, vol. 79, p. 2221, 1997. 3

[18] P. Barthelemy, J. Bertolotti, and D. S. Wiersma, "A Lévy flight for light," *Nature*, vol. 453, p. 495, 2008. 3

[19] E. P. Raposo and A. S. L. Gomes, "Analytical solution for the Lévy-like steady-state distribution of intensities in random lasers," *Phys. Rev. A*, vol. 91, p. 043827, 2015. 3

[20] G. M. Viswanathan, S. Buldyrev, S. Havlin, and M. G. E. da Luz, "Optimizing the success of random searches," *Nature*, vol. 401, p. 911, 1999. 3

[21] E. P. Raposo, S. V. Buldyrev, M. G. E. da Luz, G. M. Viswanathan, and H. E. Stanley, "Lévy flights and random searches," *J. Phys. A*, vol. 42, p. 434003, 2009. 3

[22] P. D. Ditlevsen, "Observation of α-stable noise induced millennial climate changes from an ice-core record," *Geophys. Res. Lett.*, vol. 26, p. 1441, 1999. 3

[23] D. Brockmann, L. Hufnagel, and T. Geisel, "The scaling laws of human travel," *Nature*, vol. 439, p. 462, 2006. 3

[24] M. C. Gonzalez, C. A. Hidalgo, and A.-L. Barabasi, "Understanding individual human mobility patterns," *Nature*, vol. 453, p. 779, 2008. 3

[25] A. Chechkin, R. Metzler, V. Gonchar, J. Klafter, and L. Tanatarov, "First passage and arrival time densities for Lévy flights and the failure of the method of images," *J. Phys. A: Math. Gen.*, vol. 36, p. L537, 2003. 3, 4

[26] A. Chechkin, J. Klafter, V. Gonchar, R. Metzler, and L. V. Tanatarov, "Bifurcation, bimodality, and finite variance in confined Lévy flights," *Phys. Rev. E*, vol. 67, p. 010102, 2003. 3, 4

[27] A. Dubkov and B. Spagnolo, "Langevin approach to Lévy flights in fixed potentials: Exact results for stationary probability distributions," *Acta Phys. Pol. B*, vol. 38, p. 1745, 2007. 3, 23, 43

[28] O. Sliusarenko, D. Surkov, V. Gonchar, and A. Chechkin, "Stationary states in bistable system driven by Lévy noise," *Eur. Phys. J. Spec. Top.*, vol. 216, p. 133, 2013. 3, 32, 36, 95

[29] S. I. Denisov, W. Horsthemke, and P. Hänggi, "Steady-state Lévy flights in a confined domain," *Phys. Rev. E.*, vol. 77, p. 061112, 2008. 3, 44

[30] A. Dubkov and B. Spagnolo, "Stationary probability characteristics of superdiffusion," *Modern Problems of Statistical Physics*, vol. 5, p. 1, 2006. 3, 101

[31] A. Dubkov and B. Spagnolo, "Time characteristics of Lévy flights in a steep potential well," *Eur. Phys. J. Spec. Top.*, vol. 216, p. 31, 2013. 3, 4, 18, 42

[32] B. Dybiec, E. Gudowska-Nowak, E. Barkai, and A. A. Dubkov, "Lévy flights versus Lévy walks in bounded domains," *Phys. Rev. E*, vol. 95, p. 052102, 2017. 3, 4, 12

[33] A. Chechkin, V. Gonchar, J. Klafter, R. Metzler, and L. Tanatarov, "Lévy flights in a steep potential well," *J. Stat. Phys.*, vol. 115, p. 1505, 2004. 3

[34] K. Capała and B. Dybiec, "Multimodal stationary states in symmetric single-well potentials driven by Cauchy noise," *JSTAT Mech-Theory E*, vol. 99, p. 033206, 2019. 3

[35] M. Ciesla, K. Capała, and B. Dybiec, "Multimodal stationary states under Cauchy noise," *Phys. Rev. E*, vol. 99, p. 052118, 2019. 3

[36] P. Imkeller and I. Pavlyukevich, "Lévy flights: Transitions and meta-stability," *J. Phys. Math. Gen.*, vol. 39, p. L237, 2006. 4, 39

[37] B. Dybiec, E. Gudowska-Nowak, and P. Hänggi, "Lévy-Brownian motion on finite intervals: Mean first passage time analysis," *Phys. Rev. E*, vol. 73, p. 046104, 2006. 4

[38] B. Dybiec, E. Gudowska-Nowak, and P. Hänggi, "Escape driven by α-stable white noises," *Phys. Rev. E*, vol. 75, p. 021109, 2007. 4

[39] J.-D. Bao, H.-Y. Wang, Y. Jia, and Y.-Z. Zhuo, "Cancellation phenomenon of barrier escape driven by a non-Gaussian noise," *Phys. Rev. E*, vol. 72, p. 051105, 2005. 4

[40] A. Chechkin, V. Gonchar, J. Klafter, and R. Metzler, "Barrier crossing of a Lévy flight," *Europhys. Lett.*, vol. 72, p. 348, 2005. 4

[41] A. Chechkin, O. Sliusarenko, R. Metzler, and J. Klafter, "Barrier crossing driven by Lévy noise: Universality and the role of noise intensity," *Phys. Rev. E.*, vol. 75, p. 041101, 2007. 4

[42] A. Padash, A. Chechkin, B. Dybiec, I. Pavlyukevich, B. Shokri, and R. Metzler, "First-passage properties of asymmetric Lévy flights," *J. Phys. A: Math. Theor.*, vol. 52, p. 454004, 2019. 4

[43] H. Kramers, "Brownian motion in a field of force and the diffusion model of chemical reactions," *Physica*, vol. 7, p. 284, 1940. 4, 39

[44] A. Dubkov, A. L. Cognata, and B. Spagnolo, "The problem of analytical calculation of barrier crossing characteristics for Lévy flights," *JSTAT Mech-Theory E*, p. P01002, 2009. 4

[45] A. Chechkin, V. Gonchar, J. Klafter, and R. Metzler, "Barrier crossing of a Lévy flight," *EPL*, vol. 72, p. 348, 2007. 4

[46] A. Dubkov, B. Spagnolo, and V. Uchaikin, "Lévy flight superdiffusion: An introduction," *I. J. Bifurcation and Chaos*, vol. 18, p. 2649, 2008. 4

[47] A. Dubkov, V. N. Ganin, and B. Spagnolo, "Exact results for spectra of overdamped Brownian motion in fixed and randomly switching potentials," *Acta Phys. Pol. B*, vol. 35, p. 1447, 2004. 4

[48] L. O. Chua, "Memristor the missing circuit element," *IEEE Trans. Circ. Theor.*, vol. 18, p. 507, 1971. 5, 63

[49] D. Strukov, G. Snider, D. Stewart, and S. Williams, "The missing memristor found," *Nature*, vol. 453, p. 80, 2008. 5, 6, 68

[50] R. Waser and M. Aono, "Nanoionics-based resistive switching memories," *Nature Mater.*, vol. 8, p. 833, 2007. 5

[51] J. J. Yang, D. B. Strukov, and D. R. Stewart, "Memristive devices for computing," *Nature Nanotech.*, vol. 8, p. 13, 2013. 5, 70

[52] D. Ielmini and R. Waser, "Resistive switching: From fundamentals of nanoionic redox processes to memristive device applications," *(New York: John Wiley & Sons)*, 2015. 5

[53] B. J. Choi, A. Torrezan, J. W. Strachan, P. Kotula, A. Lohn, M. Marinella, Z. Li, S. Williams, and J. J. Yang, "High-speed and low-energy nitride memristors," *Adv. Funct. Mater.*, vol. 26, p. 5290, 2016. 5

[54] C. Li, D. Belkin, Y. Li, P. Yan, M. Hu, N. Ge, H. Jiang, E. Montgomery, P. Lin, Z. Wang, W. Song, J. W. Strachan, M. Barnell, Q. Wu, S. Williams, J. J. Yang, and Q. Xia, "Efficient and self-adaptive in-situ learning in multilayer memristor neural networks," *Nature Comm.*, vol. 9, p. 2385, 2018. 5, 6

[55] E. L. Pankratov and B. Spagnolo, "Optimization of impurity profile for p-n junction in heterostructures," *Eur. Phys. J. B*, vol. 46, p. 15, 2005. 5

[56] C. Cheng, W. Li, T.-L. Wong, K. Ho, K. Fung, and N. Wang, "Zn_2TiO_4ZnO nanowire axial heterostructures formed by unilateral diffusion," *J. Phys. Chem. C*, vol. 115, p. 178, 2011. 5

[57] D. B. Strukov, F. Alibart, and R. S. Williams, "Thermophoresis/diffusion as a plausible mechanism for unipolar resistive switching in metal-oxide-metal memristors," *Appl. Physics A-Mater*, vol. 107, p. 509, 2012. 5

[58] B. Rajendran, M. Breitwisch, M.-H. Lee, G. Burr, Y.-H. Shih, R. Cheek, A. Schrott, C.-F. Chen, E. Joseph, R. Dasaka, H.-L. Lung, and C. Lam, "Dynamic resistance – A metric for variability characterization of phase-change memory," *EDL IEEE*, vol. 30, p. 126, 2009. 5

[59] A. Lacaita, A. Redaelli, D. Ielmini, F. Pellizzer, A. Pirovano, A. Benvenuti, and R. Bez, "Electrothermal and phase-change dynamics in chalcogenide-based memories," *IEDM*, p. 911, 2005. 5

[60] S. Yu, Y. Wu, R. Jeyasingh, D. Kuzum, and H.-S. P. Wong, "An electronic synapse device based on metal oxide resistive switching memory for neuromorphic computation," *IEEE T Electron. Dev.*, vol. 58, p. 2729, 2011. 5, 6

[61] I. Salaoru, A. Khiat, R. Berdan, Q. Li, C. Papavassiliou, and T. Prodromakis, "Origin of the OFF state variability in ReRAM cells," *J. Phys. D: Appl. Phys.*, vol. 47, p. 145102, 2014. 5

[62] S. Menzel and R. Waser, "Analytical analysis of the generic SET and RESET characteristics of electrochemical metallization memory cells," *Nanoscale*, vol. 5, p. 11003, 2013. 5

[63] D. M. Suri, D. Querlioz, O. Bichler, G. Palma, E. Vianello, D. Vuillaume, C. Gamrat, and B. DeSalvo, "Bio-inspired stochastic computing using binary CBRAM synapses," *IEEE T Electron. Dev.*, vol. 60, p. 2402, 2013. 5

[64] S. Jo, K.-H. Kim, and W. Lu, "Programmable resistance switching in nanoscale two-terminal devices," *Nano Letters*, vol. 9, p. 496, 2009. 5, 70, 88

[65] Q. Li, A. Khiat, I. Salaoru, H. Xu, and T. Prodromakis, "Stochastic switching of TiO_2-based memristive devices with identical initial memory states," *Nanoscale Res. Lett.*, vol. 9, p. 293, 2014. 5

[66] D. Ielmini, "Resistive switching memories based on metal oxides: Mechanisms, reliability and scaling," *Semicond. Sci. Technol.*, vol. 31, p. 063002, 2016. 5, 76

[67] T. Hamilton, S. Afshar, A. van Schaik, and J. Tapson, "Stochastic electronics: A neuro-inspired design paradigm for integrated circuits," *Proc. IEEE*, vol. 102, p. 843, 2014. 5

[68] R. Naous, M. Al-Shedivat, and K. Salama, "Stochasticity modeling in memristors," *IEEE Trans Nanotech.*, vol. 15, p. 1, 2016. 5, 7, 70, 88

[69] M. Ventra, "Electrical transport in nanoscale systems," *Cambridge, UK: Cambridge University Press*, 2008. 5

[70] P. Sheridan, F. Cai, C. Du, W. Ma, Z. Zhang, and W. Lu, "Sparse coding with memristor networks," *Nature nanotech.*, vol. 12, p. 8, 2017. 6

[71] P. Yao, H. Wu, B. Gao, S. Eryilmaz, X. Huang, W. Zhang, Q. Zhang, N. Deng, L. Shi, H.-S. P. Wong, and H. Qian, "Face classification using electronic synapses," *Nature Comm.*, vol. 8, p. 15199, 2017. 6

[72] Z. Wang, S. Joshi, S. Savelev, H. Jiang, R. Midya, P. Lin, M. Hu, N. Ge, J. W. Strachan, Z. Li, Q. Wu, M. Barnell, G.-L. Li, H. Xin, S. Williams, Q. Xia, and J. J. Yang, "Memristors with diffusive dynamics as synaptic emulators for neuromorphic computing," *Nature Mat.*, vol. 16, p. 101, 2016. 6

[73] M. Hu, C. Graves, C. Li, Y. Li, N. Ge, E. Montgomery, N. Dvila, H. Jiang, S. Williams, J. J. Yang, Q. Xia, and J. W. Strachan, "Memristorbased analog computation and neural network classification with a dot product engine," *Adv. Mat.*, vol. 30, p. 1705914, 2018. 6

[74] C. Li, M. Hu, Y. Li, H. Jiang, N. Ge, E. Montgomery, J. Zhang, W. Song, N. Dávila, C. Graves, Z. Li, J. W. Strachan, P. Lin, Z. Wang, M. Barnell, Q. Wu, S. Williams, J. J. Yang, and Q. Xia, "Analogue signal and image processing with large memristor crossbars," *Nature Electr.*, vol. 1, p. 52, 2018. 6

[75] L. Chua and S.-M. Kang, "Memristive devices and systems," *Proc. IEEE*, vol. 64, p. 209, 1976. 6

[76] L. Chua, "Five non-volatile memristor enigmas solved," *Appl. Phys. A*, vol. 124, p. 563, 2018. 6, 63

[77] Y. Joglekar and S. Wolf, "The elusive memristor: properties of basic electrical circuits," *EJP*, vol. 30, p. 661, 2008. 6, 86

[78] Y. Shang, W. Fei, and H. Yu, "Analysis and modeling of internal state variables for dynamic effects of nonvolatile memory devices," *IEEE T CIRCUITS-I*, vol. 59, p. 1906, 2012. 6, 86

[79] E. Linn, A. Siemon, R. Waser, and S. Menzel, "Applicability of well-established memristive models for simulations of resistive switching devices," *IEEE T CIRCUITS-I*, vol. 61, p. 2402, 2014. 6, 86

[80] D. Ielmini, "Modeling the universal set/reset characteristics of bipolar RRAM by field and temperature-driven filament growth," *IEEE Trans. Electr. Dev.*, vol. 58, p. 4309, 2011. 6

[81] J. Borghetti, D. Strukov, M. Pickett, J. J. Yang, D. Stewart, and S. Williams, "Electrical transport and thermometry of electroformed titanium dioxide memristive switches," *J. Appl. Phys.*, vol. 106, p. 124504, 2009. 6

[82] M. Pickett, D. Strukov, J. Borghetti, J. J. Yang, G. Snider, D. Stewart, and S. Williams, "Switching dynamics in titanium dioxide memristive devices," *J. Appl. Phys.*, vol. 106, p. 074508, 2009. 6, 7

[83] S. Kim, S.-J. Kim, K. M. Kim, S. Lee, M. Chang, E. Cho, Y.-B. Kim, C. Kim, U.-I. Chung, and I.-K. Yoo, "Physical electro-thermal model of resistive switching in bi-layered resistance-change memory," *Sci. Rep.*, vol. 3, p. 1680, 2013. 6, 76

[84] S. Kim, S. Choi, and W. Lu, "Comprehensive physical model of dynamic resistive switching in an oxide memristor," *ACS nano*, vol. 8, p. 2369, 2014. 6, 76

[85] A. Marchewka, B. Roesgen, K. Skaja, H. Du, C.-L. Jia, J. Mayer, V. Rana, R. Waser, and S. Menzel, "Nanoionic resistive switching memories: On the physical nature of the dynamic reset process," *Adv. Electron. Mater.*, vol. 1, p. 1500233, 2016. 6, 76

[86] A. N. Malakhov and N. V. Agudov, "The kinetics of liquid-gas phase transitions of a Van der Waals substance with fluctuations taken into account," *Chaos*, vol. 4, p. 665, 1994. 7

[87] D. Valenti, A. Carollo, and B. Spagnolo, "Stabilizing effect of driving and dissipation on quantum metastable states," *Phys. Rev. A*, vol. 97, p. 042109, 2018. 7

[88] A. Carollo, B. Spagnolo, and D. Valenti, "Uhlmann curvature in dissipative phase transitions," *Sci. Rep.*, vol. 8, p. 9852, 2018. 7

[89] A. Carollo, B. Spagnolo, and D. Valenti, "Symmetric logarithmic derivative of fermionic Gaussian states," *Entropy*, vol. 20, p. 485, 2018. 7

[90] A. Stotland and M. Di Ventra, "Stochastic memory: Memory enhancement due to noise," *Phys. Rev. E*, vol. 85, p. 011116, 2012. 7

[91] H. Jiang, D. Belkin, S. Savelev, S. Lin, Z. Wang, Y. Li, S. Joshi, R. Midya, C. Li, M. Rao, M. Barnell, Q. Wu, J. J. Yang, and Q. Xia, "A novel true random number generator based on a stochastic diffusive memristor," *Nature Comm.*, vol. 8, p. 882, 2017. 7, 71

[92] R. Naous, M. Al-Shedivat, and K. Salama, "Stochasticity modeling in memristors," *IEEE T Nanotechnol.*, vol. 15, p. 1, 01 2015. 7

[93] S. Jo, K.-H. Kim, and W. Lu, "Programmable resistance switching in nanoscale two-terminal devices," *Nano Lett.*, vol. 9, p. 496, 2009. 7

[94] G. Medeiros-Ribeiro, F. Perner, R. Carter, H. Abdalla, M. Pickett, and S. Williams, "Lognormal switching times for titanium dioxide bipolar memristors: Origin and resolution," *Nanotechnology*, vol. 22, p. 095702, 2011. 7, 71, 86, 88

[95] A. Stotland and M. Di Ventra, "Stochastic memory: Memory enhancement due to noise," *Phys. Rev. E*, vol. 85, p. 011116, 2012. 8

[96] G. A. Patterson, P. I. Fierens, and D. F. Grosz, "On the beneficial role of noise in resistive switching," *App. Phys. Lett.*, vol. 103, p. 074102, 2013. 8

[97] A. La Barbera and B. Spagnolo, "Spatio-temporal patterns in population dynamics," *Physica A*, vol. 314, p. 120, 2002. 8

[98] D. Valenti, A. Fiasconaro, and B. Spagnolo, "Pattern formation and spatial correlation induced by the noise in two competing species," *Acta Phys. Pol. B*, vol. 35, p. 1481, 2004. 8

[99] N. Agudov, A. Krichigin, D. Valenti, and B. Spagnolo, "Stochastic resonance in a trapping overdamped monostable system," *Phys. Rev. E*, vol. 81, p. 051123, 2010. 8

[100] A. N. Malakhov, "Cumulative analysis of random non-Gaussian processes and their transformations," *Sov. Radio*, 1978. 12

[101] S. Medvedev, "Exact expansion for the correlation function of an arbitrary stationary Markovian process," *Izv. vuzov. Radiophysica*, vol. 20, p. 1241, 1977. 16

[102] A. A. Dubkov, A. N. Malahov, and A. I. Saichev, "The correlation time and the structure of the correlation functions of the nonlinear equilibrium

Brownian movements in potential pits of arbitrary shape," *Izv. vuzov. Radiophysica*, vol. 43, p. 369, 2000. 16, 39

[103] H. Risken, "The Fokker-Planck equation," *2nd Ed. (Springer-Verlag, Berlin-Heidelberg-New York)*, p. 441, 1989. 16

[104] A. I. Saichev, "On a certain method for finding the time characteristics of Markovian processes," *Radiophys. Quantum Electron.*, vol. 17, p. 657, 1974. 17

[105] A. Weron, "On the Chambers-Mallows-Stuck method for simulating skewed stable random variables," *Stat. Probab. Lett.*, vol. 28, p. 165, 1996. 26

[106] J. M. Chambers, C. L. Mallows, and B. W. Stuck, "A method for simulating stable random variables," *J. Am. Stat. Assoc.*, vol. 71, p. 340, 1976. 26

[107] N. Agudov, "Noise delayed decay of unstable states," *Phys. Rev. E*, vol. 57, p. 2618, 1998. 28

[108] N. Agudov and A. Malakhov, "Decay of unstable equilibrium and nonequilibrium states with inverse probability current taken into account," *Phys. Rev. E*, vol. 60, p. 6333, 1999. 28

[109] A. Malakhov, "Time scales of overdamped nonlinear Brownian motion in arbitrary potential profiles," *Chaos*, vol. 7, p. 488, 1997. 28

[110] N. Agudov and B. Spagnolo, "Noise-enhanced stability of periodically driven metastable states," *Phys. Rev. E*, vol. 64, p. 035102(R), 2001. 28

[111] N. Agudov, A. Dubkov, and B. Spagnolo, "Escape from a metastable state with fluctuating barrier," *Physica A*, vol. 325, p. 144, 2003. 28

[112] A. Dubkov, N. Agudov, and B. Spagnolo, "Noise-enhanced stability in fluctuating metastable states," *Phys. Rev. E*, vol. 69, p. 061103, 2004. 28

[113] G. Augello, D. Valenti, and B. Spagnolo, "Non-Gaussian noise effects in the dynamics of a short overdamped Josephson junction," *Eur. Phys. J. B*, vol. 78, p. 225, 2010. 28

[114] D. Valenti, C. Guarcello, and B. Spagnolo, "Switching times in long-overlap Josephson junctions subject to thermal fluctuations and non-Gaussian noise sources," *Phys. Rev. B*, vol. 89, p. 214510, 2014. 28

[115] A. Janicki and A. Weron, "Simulation and chaotic behavior of α-stable stochastic processes," *Marcel Dekker, New York*, 1994. 45

[116] D. J. Higham, "An algorithmic introduction to numerical simulation of stochastic differential equations," *SIAM Rev.*, vol. 43, p. 525, 2001. 45

[117] K. Szczepaniec and B. Dybiec, "Stationary states in two-dimensional systems driven by bivariate Lévy noises," *Phys. Rev. E.*, vol. 90, p. 032128, 2014. 55, 58

[118] L. Chua, "Resistance switching memories are memristors," *Appl. Phys. A*, vol. 102, p. 765, 2011. 60

[119] V. Slipko, Y. Pershin, and M. Di Ventra, "Changing the state of a memristive system with white noise," *Phys. Rev. E*, vol. 87, p. 042103, 2013. 64

[120] S. Tang, F. Tesler, F. Gomez Marlasca, P. Levy, V. Dobrosavljevic, and M. Rozenberg, "Shock waves and commutation speed of memristor," *Phys. Rev. X*, vol. 6, p. 011028, 2016. 71, 76

[121] M. Rozenberg, M. Sanchez, R. Weht, C. Acha, F. Gomez Marlasca, and P. Levy, "Mechanism for bipolar resistive switching in transition metal oxides," *Phys. Rev. B*, vol. 81, p. 115101, 2010. 71

[122] W. Kim, S. Menzel, D. Wouters, Y. Guo, J. Robertson, B. Roesgen, and V. Rana, "Impact of oxygen exchange reaction at the ohmic interface in Ta_2O_5-based ReRAM devices," *Nanoscale*, vol. 8, p. 17774, 2016. 73, 82

[123] E. Ambrosi, A. Bricalli, M. Laudato, and D. Ielmini, "Impact of oxide and electrode materials on the switching characteristics of oxide ReRAM devices," *Faraday Discussions*, vol. 213, p. 6, 2018. 73, 82

[124] H. Risken, "The Fokker-Planck equation: Methods of solution and applications," *Springer-Verlag Berlin Heidelberg New York*, 1984. 73

[125] R. L. Stratonovich, "Conditional Markov processes and their application to the theory of optimal control," *Elsevier, N. Y.*, 1968. 73

[126] P. Reinmann, C. Van den Broeck, H. Linke, P. Hänggi, J. M. Rubi, and A. Perez Madrid, "Giant acceleration of free diffusion by use of tilted periodic potentials," vol. 87, p. 010602, 2001. 73, 74

[127] B. Linder, M. Kotstur, and L. Shimansky-Geier, "Optimal diffusive transport in a tilted periodic potential," vol. 1, p. R25, 2001. 73, 74, 75

[128] G. Costantini and F. Marchesoni, "Threshold diffusion in a tilted washboard potential," *Europhys. Lett.*, vol. 48, p. 491, 1999. 74

[129] P. Reinmann, C. Van den Broeck, H. Linke, P. Hänggi, J. M. Rubi, and A. Perez Madrid, "Diffusion in tilted periodic potentials: Enhancement, universality, and scaling," vol. 165, p. 031104, 2002. 75

[130] N. Agudov and A. Safonov, "Acceleration of diffusion in subcritically tilted periodic potentials," *Fluct. Noise Lett.*, vol. 5, p. L283, 2005. 75

[131] D. Filatov, I. Kazantseva, D. Antonov, I. Antonov, M. Shenina, D. Pavlov, and O. Gorshkov, "Conductive atomic force microscopy study of the resistive switching in yttria-stabilized zirconia films with au nanoparticles," *Scanning*, vol. 2018, p. 5489596, 2018. 75

[132] S. Larentis, F. Nardi, S. Balatti, D. C. Gilmer, and D. Ielmini, "Resistive switching by voltage-driven ion migration in bipolar RRAM – Part II: Modeling," *IEEE Trans. Electr. Dev.*, vol. 59, p. 2468, 2012. 76

[133] S. Tikhov, O. Gorshkov, A. Belov, I. Antonov, M. Koryazhkina, and A. Mikhaylov, "Electrophysical characteristics of multilayer memristive nanostructures based on yttrium-stabilized zirconium dioxide and tantalum oxide," *Tech. Phys.*, vol. 90, p. 298, 2020. 77

[134] A. Mikhaylov, E. Gryaznov, A. Belov, D. Korolev, A. Sharapov, D. Guseinov, D. Tetelbaum, S. Tikhov, N. Malekhonova, A. Bobrov, D. Pavlov, S. Gerasimova, V. Kazantsev, N. Agudov, A. Dubkov, C. Rosrio, N. Sobolev, and B. Spagnolo, "Field- and irradiation-induced phenomena in memristive nanomaterials," *Phys. Status Solidi*, vol. 13, p. 870, 2016. 78

[135] A. Yakimov, D. Filatov, O. Gorshkov, D. Antonov, D. Liskin, I. Antonov, A. Belyakov, A. Klyuev, A. Carollo, and B. Spagnolo, "Measurement of the activation energies of oxygen ion diffusion in yttria-stabilized zirconia by flicker noise spectroscopy," *Appl. Phys. Lett.*, vol. 114, p. 253506, 2019. 78

[136] A. Ascoli, R. Tetzlaff, L. Chua, J. Strachan, and R. Williams, "History erase effect in a non-volatile memristor," *IEEE Trans. Circuits Syst.*, vol. 63, p. 389, 2016. 79

[137] R. Tetzlaff, "Memristors and memristive systems," *(New York: Springer)*, 2014. 80